Understanding the performance of bifacial PV windows with integrated blinds: a PV modelling approach

TNO innovation for life

TU Delft

PVMD Delft University of Technology

Understanding the performance of bifacial PV windows with integrated blinds: a PV modelling approach

MSc. Thesis Report

by

Martin Hurtado Ellmann

In order to obtain the degree of

Master of Science

in

Sustainable Energy Technology

At the Delft University of Technology

To be publicly defended on Tuesday October 29th, 2024 at 15:00

Daily supervisor:	Ir. Simona Villa
Supervisor:	Dr.ir. Rudi Santbergen

Thesis Committee:

Dr.ir. Rudi Santbergen	Assistant professor, PVMD group
Prof.dr Arthur Weeber	Full professor, PVMD group
Dr.ir. Gautham Ram Chandra Mouli	Assistant professor, DCE&S group
Ir. Simona Villa	Solar Applications Scientist, TNO

This MSc. thesis report is confidential and cannot be made public until December 31st, 2025.
An electronic version of this report is available at: https://repository.tudelft.nl/

TNO innovation for life

TU Delft

PVMD Delft University of Technology

"All models are wrong, but some are useful."

George E. P. Box (1919-2013), British statistician.

Preface

This MSc. thesis report is the final work of my MSc. Sustainable Energy Technology studies at the Delft University of Technology. During the last 10 months I have had the honor of being part of both, TNO (the Applied Research Institute of the Netherlands) and the PVMD Research Group at the Delft University of Technology, where I was able to apply my acquired knowledge into a challenging and exciting project regarding bifacial photovoltaic windows with integrated blinds. This achievement would not have been possible without the help and support of many people to whom I would like to thank.

First and foremost, I would like to deeply thank my daily supervisor, Ir. Simona Villa, for letting me be part of the Solar Technology and Applications team and carry out this work at TNO as part of my graduation project. I am also deeply thankful for her valuable guidance throughout this project; the achieved outcomes would not have been possible without her constant feedback, commitment and support. Thank you Simona for believing in me and for encouraging me to always seek constant improvement and give my very best, it has definitely been an amazing journey.

I would also like to express my gratitude to my TU Delft supervisor, Dr.ir. Rudi Santbergen, for his continuous support, his willingness to discuss insights about this project and his supervision through the writing process of this MSc. thesis report. I am also very thankful with Prof.dr. Arthur Weeber and Dr.ir. Gautham Ram Chandra Mouli for being part of the thesis committee. Thank you all for making me critically reflect on my work.

I am also very thankful with all my colleagues at the Solar Technology and Applications department of TNO for their constant feedback and support and for making me feel so welcome at the company. I am especially grateful with Ir. Ashish Binani, Dr.ir. Teun Burgers, Ir. Nicolas Guillevin and Dr.ir. Roland M. E. Valckenborg for their constant input and feedback during my modelling process. I am also grateful for all the amazing friends I made along the way; sharing lunch breaks, chats and laughs with you has definitely made everyday work even more enjoyable. I will deeply cherish this research experience as I move forward in my career.

A big thanks goes to my friends back home, in the Netherlands and in Europe: Rali, Joanna, Janna, Andy, Brandon. Thank you all for your advice, your teachings and for encouraging me to keep on pushing forward when times were getting hard. Your unconditional support has definitely been key for the culmination of my studies.

My deepest gratitude goes to my family: *mama, Rodrigo y Neto. Gracias por ser mi guía, mi fortaleza y por siempre darme su amor y apoyo incondicional. Gracias por siempre estar conmigo sin importar la distancia o las circunstancias. Gracias por creer en mí e impulsarme a alcanzar mis sueños. Sin ustedes, nada de esto hubiera sido posible.*

Dreams do really come true.

Martin Hurtado Ellmann
Delft, October 2024.

Abstract

This research investigates the performance of a novel building-integrated photovoltaic (BIPV) window solution equipped with bifacial photovoltaic (bPV) cells and reflective Venetian blinds through a PV modelling approach. By modelling this PV window solution in *BIGEYE*, the study aims to evaluate how different types of blinds and tilt angles can help to boost the overall performance of the bPV window and to quantify the potential energy gains under varying weather conditions. First, the optical model was validated against experimental data to ensure it could accurately simulate the irradiance received at the front side of the window plane. The optical properties of the Venetian blinds were also defined to quantify the irradiance gain at the rear side of the bPV window. Then, the electrical model was also validated to make sure the model could accurately simulate the electrical behavior of the bPV window demonstrators in real operational conditions. The validated models were then used to test the effect of using different blind configurations in the bPV window's performance.

In this way, three different types of Venetian blinds were tested: S157 (grey colored), S102 (white colored) and V95 (silver colored). The analysis revealed that, when deployed at a tilt angle of 60°, these types of blinds can help to boost the irradiance gain at the rear side of the bPV window by up to 16%, 20% and 25%, respectively, on a fully sunny day. The study also demonstrated that blinds positioned at 60° consistently achieved the greatest absolute boost in temperature-corrected performance ratio (TCPR) of the bPV window over a typical meteorological year (TMY) in Eindhoven, The Netherlands. In this way, the V95 blind type at a tilt angle of 60° demonstrated to be the optimal blind configuration for boosting the performance of this bPV window. Furthermore, an in-depth analysis was conducted to examine the influence of additional factors on the performance of this bPV window, such as the angle of incidence (AOI) between the sun and the blinds' surface normal, which showed to have an inverse correlation with the bPV window's TCPR, highlighting that the performance of the window tends to decrease as this AOI increases.

Furthermore, the study quantified the Yearly Specific Yield (YSY) boost achievable with the optimal blind configuration, finding that a maximum boost of 19% can be attained on a TMY in Eindhoven, 18% in Stockholm, and 17% in Valencia. The difference in performance across locations is attributed to variations in meteorological and geographical factors, such as diffuse fraction and AOI. Overall, the findings provide valuable insights into how different blind configurations can enhance the performance of this bPV window and contribute to enhance the energy performance of high-rise residential towers and office buildings.

Table of contents

List of figures

List of tables

Acronyms

BAPV	Building-Applied Photovoltaics
BIGEYE	Bifacial Gain in Energy Yield
BIPV:	Building-Integrated Photovoltaics
bPV:	Bifacial photovoltaic
BSF	Back surface field
CR:	Coverage Ratio
c-Si	Crystalline silicone
DHI	Diffuse Horizontal Irradiance
DNI	Direct Normal Irradiance
DSSC	Dye-sensitized solar cell
EIPV	Environment-Integrated Photovoltaics
EU:	European Union.
GHG:	Greenhouse gases
GHI	Global Horizontal Irradiance
GUI	Graphical User Interface
IBC	Interdigitated Back Contact
IGU	Insulating glazing unit
LCOE	Levelized cost of energy
mPV	Monofacial photovoltaic
NIR	Near-infrared
NZEB:	Nearly-zero energy building
OPV	Organic photovoltaic
PCE	Power conversion efficiency
PERC	Passivated emitter and rear cell
POA	Plane of array
PV:	Photovoltaic
SHG	Solar heat gain
SolarBEAT:	Solar Building Elements Application Testing
STPV	Semi-transparent photovoltaic
TCPR	Temperature-corrected performance ratio
TMY	Typical meteorological year
TNO:	*Nederlandse Organisatie voor Toegepast Natuurwetenschappelijk Onderzoek* or The Netherlands Organization for Applied Scientific Research
TPV	Transparent photovoltaic
TU/e:	Eindhoven University of Technology
UV	Ultraviolet
VIPV	Vehicle-Integrated Photovoltaic
WWR:	Window-to-wall ratio
XIPV	X-Integrated Photovoltaics
YSY	Yearly specific yield
ZIEZO	*Zonwering Inclusief Elektriciteitsopwekkend Zonneraam* or Shading Including Electricity-Generating Solar Window

1. Introduction

The purpose of this chapter is to introduce the TNO's *ZIEZO* research project, which is the main core of this MSc. thesis work. By the end of this chapter, the reader will have a comprehensive understanding of the project's motivation, its main goal and objectives, key research questions and scope. Additionally, the overall structure of this thesis report will be outlined, providing in this way the necessary context for the topics addressed in subsequent chapters.

To this end, section 1.1 presents the relevance for the development of this project, whereas in section 1.2, a brief description of it is given. In Section 1.3, the main goal, the research questions, the objectives and the scope of this MSc. thesis project are presented. Finally, the outline of this MSc. thesis report is detailed in section 1.4.

1.1. Relevance of the project

As the world population keeps growing, the demand for housing, commercial spaces, offices and building infrastructure in urban areas is escalating at an unprecedent rate. Despite this, 85% of EU buildings were constructed before year 2000, and it is estimated that around 75% of them have a poor energy performance [1]. This has led to buildings consuming around 40% of the total energy consumption in the EU and being responsible for more than one-third of energy-related GHG emission. Consequently, there is an urgent need for improving the energy efficiency of currently existing buildings and newly designed ones to reduce their environmental impact and achieve a fully decarbonized building stock by 2050, as aimed by the EU's Energy Performance of Buildings Directive (EU/2024/1275) [1].

The previous statistics position buildings as the single largest energy consumer in Europe. It is therefore not a coincidence that a strong focus has been set in their energy performance in order to achieve the EU's energy and climate targets. As a result, energy performance standards for buildings are becoming increasingly stricter, and this trend is only expected to continue growing as the building sector transitions to a nearly-zero energy building (NZEB) stock in the following decades.

Although this transition presents huge technical, policy and market challenges, it has also opened up new attractive market opportunities for Building-Integrated Photovoltaic (BIPV) solutions, especially for photovoltaic (PV) windows. PV windows are BIPV elements essentially consisting of conventional windows with embedded solar cells. In this way, this architectural component that otherwise would be a passive building element can be upgraded to generate electricity, which may be directly consumed by the building they are part from. As a result, these devices can help to reduce the off-site electricity demand of a building yet allowing daylight to be transmitted, which also enhances occupant's visual comfort [2].

In particular, PV windows hold a significant potential for improving the energy performance of buildings with a high window-to-wall ratio (WWR), such as high-rise residential towers and office buildings. These types of buildings are abundant in densely populated urban areas and their facades are usually covered with passive glass panes. It is estimated that if all the buildings

with 90% glass on their surface used PV windows, around 40% of that building's energy consumption could be satisfied [3], and this percentage could be even higher if smart-integrated PV window solutions are used instead. These solutions not only can lead to an increased energy yield and an improved visual comfort, but also can provide other benefits, like helping to reduce the overall solar heat gain (SHG) of the building, hence decreasing its heating/cooling demand without compromising its occupant's thermal and visual comfort.

In order to be widely implemented, an important part of ongoing research regarding PV windows for BIPV applications is focused on exploring a range of innovative solutions aimed to create intrinsically transparent PV devices, (the so called transparent PV technologies, or TPV). These solutions aim to create color neutral and visually homogenous PV cells and modules using technologies that include, for example, reducing the thickness of otherwise opaque PV thin-films or using UV/NIR wavelength-selective PV materials for absorbing the unwanted UV and NIR light and letting the visible light to pass through [4-7]. Based on these concepts, several emerging solar cell technologies are being investigated, such as screen-printing dye-sensitized solar cells, NIR organic photovoltaics, polymer solar cells, transparent luminescent solar concentrator, perovskite, tandem perovskite, electrophoretic technique or quantum dot solar cells [5], [6].

Although promising, most of these technologies are not yet close to commercialization due to several technological challenges, including durability, stability, scalability, degradation and, most importantly, low power conversion efficiencies [6]. This is why research efforts have also been tailored to explore other alternatives, such as semi-transparent PV (STPV) technologies. The most straightforward and commercially widespread approach of STPV technologies for BIPV window applications involves separating opaque solar cells to reduce the PV active area to create semi-transparent PV modules. In this way, solar cells with different shapes and patterns may be used to make STPV windows as aesthetically appealing as possible. For example, square solar cells can be spatially spaced on a glass substrate or thin PV cell stripes may be used. Unfortunately, low power conversion efficiencies is the main challenge to overcome by these solutions in order to become a truly viable alternative in the market.

This is why research efforts should be focused on increasing the electricity output of such STPV products. It is commonly recognized that in order to be competitive and achieve a reasonable levelized cost of energy (LCOE), STPV windows for BIPV applications should have at least a minimum efficiency of 7-10% [5]. Additionally, these solutions should provide sufficient transparency levels (usually above 50% [6]) to ensure occupant's visual comfort, which presents a real challenge as these two variables are inversely proportional to each other. Moreover, an ideal STPV window should be visually appealing if a broad adoption in the built environment is desired. To address all these challenges, an integrated STPV window solution is needed; and to this aim, the *ZIEZO* research project was created.

1.2. The ZIEZO research project

With the goal of developing an integrated BIPV window solution capable of coping with the challenges mentioned in the previous section, the *ZIEZO* research project was launched in July 2022. This project funded by the Government of the Netherlands has four partners involved: *Pilkington Nederland B.V.* (a glass provider and manufacturer), *Technische Universiteit*

Eindhoven (TU/e), *W/E Adviseurs Duurzaam Bouwen* (an advisory firm specialized in sustainable buildings) and TNO (the National Applied Research Institute of The Netherlands). These partners have worked together to create an innovative and multifunctional STPV window solution based on bifacial photovoltaic (bPV) technology and reflective Venetian blinds to boost the energy yield of the window while providing over-heating protection and shading for a better indoor thermal and visual comfort [8].

The proposed solution (referred to as the *ZIEZO* window) consists of an insulating glazing unit (IGU) with embedded reflective Venetian blinds that are situated behind a pair of glass panes, which contain several rows of laminated bPV cell stripes. This solution was inspired by two already-existing and commercialized window products: *Pilkington Insulight™ with Screenline®* [9], which integrates Venetian blinds into the insulating glazing unit (IGU), but has no PV cells, and *Pilkington Sunplus™ BIPV (PV Vision)* [10], a BIPV IGU with mono-facial photovoltaic (mPV) cells with no Venetian blinds. The unique IGU composition of the *ZIEZO* window gives the product its thermal properties, while the incorporation of Venetian blinds with a reflective coating has a dual purpose. On the one hand they provide visual comfort to its users by blocking direct sunlight. On the other hand and along with the use of bPV cell technology, additional power can be extracted from a window occupying the same area. The working principle of the *ZIEZO* window is described in more detail in section *3.3 The innovative bPV window concept*.

The performed market study analysis shows that no bPV window for building integration exists in the market yet. Furthermore, although several studies have explored the integration of PV cells as shading elements themselves, there is limited literature on products that use blinds as reflectors to achieve a boost in power output, as in this particular case [11] [12]. Therefore, the innovation behind this newly developed PV window concept lies not only in the use of bPV cell technology, but also in the use of reflective blinds as power boosting elements.

In order to be able to successfully introduce the *ZIEZO* window to the market and to potential customers, a deeper understanding of its performance is needed. Moreover, a more detailed analysis of the optical effects taking place between sunlight and the reflective Venetian blinds is necessary, since these non-trivial interactions are complex in nature due to blind's curvature and coating. With a deeper understanding and quantification of these phenomena, it is possible to explain differences in performance due to different types of blinds, simulate their potential to improve the energy performance of window systems and whole building complexes and to further optimize the product's design or any of its components for particular cases, as for different locations or facade orientations.

To this aim, 12 small-scale bPV window demonstrators with different design features have been manufactured by the partners in this project. Their performance in real outdoor conditions has been measured for one full year by means of different measurement campaigns, which consisted of several experiments in which the position of the blinds was changed in terms of height and tilt angle to see the effect on the electrical performance. These small-scale window demonstrators have been installed in a dummy building at the *SolarBEAT* [13] outdoor research facility at the TU/e campus in Eindhoven, The Netherlands. More information regarding the *SolarBEAT* outdoor research facility will follow up in section *3.1 The SolarBEAT outdoor research facility*.

1.3. Main goal, research questions, project objectives and scope

Along with the analysis of the experimental data that was collected on-site, PV simulation models can also be used to get a more in-depth understanding of the performance of these bPV window demonstrators. For instance, it is possible to create models to determine the effect that combining bPV technology and different types of reflective blinds has on the window performance, or simulate the behavior of the windows under different operation scenarios, such as with different blind positions, in different seasons or weather conditions. These models can also be used to simulate the power output of this BIPV window product if it was deployed in a different location or in a building with a different orientation. Ultimately, PV simulation models can be a powerful tool to provide additional information that cannot be directly measured from the experimental setup.

In this way, the main goal of this project is to create a set of PV simulation models that can help to further understand the performance of this BIPV window solution. In particular, the models will be used to assess how using bPV cell technology and different types of reflective Venetian blinds play a role in boosting the electrical performance of this bPV window product.

In particular, the research questions that will help to meet the primary goal are the following:

- RQ1: How do different types of Venetian blinds affect the electric performance of the bPV windows? What other factors influence its behavior?
- RQ2: How does the position of the Venetian blinds affect the overall performance of the bPV windows? Can we quantify the boosting effect given by the different blind configurations and find the optimal one?
- RQ3: Which other factors have an influence on the bPV window performance? Does it also depends on meteorological or geographical conditions?
- RQ4: Can we quantify the boost in yearly specific yield (YSY) given by the different blind configurations? How much can it be in other locations when the optimal blind configuration is used?

To this extent, the objectives of this project are the following:

- O1: Create a set of PV simulation models that describe the performance of this BIPV window when different types of reflective Venetian blinds are used.
- O2: Validate the created models with experimental data to test their accuracy and reliability.
- O3: Use the created models to perform different simulations to assess the performance of this bPV window when different blind configurations are used.

Regarding the project scope, the bPV window demonstrators will only be assessed in terms of their electrical performance, as the main motivation behind this project is to maximize their power output. Therefore, other aspects that in practice are also relevant for BIPV window applications, such as the indoor thermal performance, the improvement in the heating/cooling demand of a building, the provided illumination level and visual comfort of its users, among others, will not be part of the scope of this project.

1.4. Thesis report outline

This MSc. thesis report is structured as follows:

Chapter *1. Introduction* introduces the reader to the general context of the *ZIEZO* project, presenting the motivation for its development and a general description of it. It also includes the main goal of this MSc. thesis work, as well as the research questions it aims to answer in order to achieve it. The project objectives and scope can also be found in this chapter.

Chapter *2. Literature review* presents a comprehensive review of BIPV and bPV technology, as well as a review of STPV technology with a focus on PV window applications. Furthermore, this chapter also explores the performance ratio (PR) and the temperature-corrected performance ratio (TCPR) metric, which will later be used in Chapter *5. Results and* discussion to evaluate the performance of the bPV window with different blind configurations. Finally, a description of the bPV simulation software *BIGEYE* is provided, which was used to create the bPV window models of this research project.

Chapter *3. The ZIEZO testbed: facility overview and experimental* setup provides a detailed description of the experimental setup used to test the performance of these bPV windows in real outdoor conditions. A description of the research facility, the working principle of this bPV window concept, the experimental setup, the design features and the measured parameters can also be found in this chapter.

Chapter *4. bPV window modelling methodology* describes the approach used to model the bPV windows. In particular, this chapter presents a description of the different components that comprise the bPV window simulation models, along with the assumptions and simplifications that were made. The input parameters that were used in the models are also described in detail. Finally, the optical and electrical validation process of the bPV window models is presented in the last sections of this chapter.

Chapter *5. Results and* discussion presents the results of the simulation experiments conducted with the created bPV window models to test the performance of the bPV window with different blind configurations and under different operation conditions and locations. A detailed discussion and analysis accompanies these findings.

Finally, *6. Conclusions and* recommendations presents the conclusions drawn from this research project. It also offers recommendations for further research work regarding this bPV window solution, that could lead to a better understanding of the optical effects taking place. Furthermore, additional research questions which aim is directed toward assessing the energy enhancement and market potentials of this bPV window solution are proposed.

2. Literature review

The purpose of this chapter is to provide a comprehensive review of literature that is relevant to understand and dimension the topics addressed in the following chapters of this MSc. thesis report. By the end of the chapter, the reader will gain a better understanding on the current state of development and challenges of BIPV solutions, bPV technology and STPV devices, with a particular focus on semi-transparent photovoltaic (STPV) windows. In addition, metrics to quantify their performance will also be discussed. This background knowledge will help to contextualize the innovative aspects of the TNO's *ZIEZO* research project and establish a solid foundation for the subsequent analysis and discussion presented in chapter *5. Results and* discussion.

2.1. Building-Integrated Photovoltaics (BIPV)

In recent decades, integrating PV devices into various structures has emerged as an important strategy in advancing towards sustainable energy solutions. This approach has led to the development of X-Integrated Photovoltaics (XIPV), a broad concept that encompasses the integration of PV devices across different structures and contexts, including vehicles (Vehicle-Integrated Photovoltaics, or VIPV), the environment (Environment-Integrated Photovoltaics, or EIVP), or infrastructure, particularly, the built environment (BIPV). The core principle of XIPV is to embed PV technology into every available surface and not only in flat and regular ones, which are often limited especially in densely populated urban areas. This approach makes XIPV a viable and straightforward solution for reducing the high land area cost of PV and make it more competitive compared to other sustainable energy generation technologies.

Among the various applications of XIPV, BIPV has gained particular attention due to its potential to significantly improve the energy performance of buildings and address the increasing demand for an energy-efficient building stock. Specifically, BIPV integrates PV devices into building elements, such as in facades, walls, roofs, sunshades, skylights, windows and other structural elements [14]. Some examples of BIPV solutions include PV facades that integrate PV modules into building exteriors, PV roof tiles that replace conventional roofing materials with electricity generating tiles or PV sunshades that provide solar protection while generating electricity at the same time. BIPV is therefore a way to enhance passive building components to perform as renewable energy generating sources in addition to being an integrated part of the architecture of a building [10].

One of the key distinctions of BIPV compared to Building-Applied Photovoltaics (BAPV), is that, unlike BAPV —where PV devices are added externally to an already existing building— BIPV solutions form an integral part of the architectural design and structure of a building. This distinction highlights the intrinsic multifunctionality of BIPV elements, which are not only an integral part the structure of a building, but also provide renewable energy. As a result, building proprietors and developers can transform buildings into power-generating assets [10] and substantially improve their energy performance by producing and consuming their own electricity on-site, reducing their dependence on the grid (and therefore, helping to decrease grid congestion) or other energy sources. This is why multifunctionality is an intrinsic characteristic of BIPV solutions, as they serve at least both, a structural and a power-generation purpose.

In some cases, BIPV elements can provide additional benefits to these two. A good example of this increased multifunctionality can be found in integrated PV window systems, which also stand out as one of the most promising BIPV solutions for innovation. These systems do not only play a structural role in a building while generating electricity at the same time, but also can be a crucial component to achieve an efficient building insulation and shading mechanism. An improved insulation has several benefits, such as reducing the heating and cooling demands of a building, thus further improving its energy performance. Shading mechanisms, on the other hand, can enhance the visual comfort of its users. These benefits can be achieved, for example, by integrating low-emission coatings, vacuum double glazing [11] [14] or shading blinds to conventional PV windows, showing how modern BIPV solutions are increasingly incorporating more sophisticated components as this technology matures, and demonstrating a clear evolution towards more seamless and multifunctional designs. In this way, BIPV have had a growing importance in contributing to energy-efficient building designs and to the pursuit for achieving NZEBs.

BIPV solutions, and in particular PV windows, find a great opportunity for widespread installation in densely populated urban areas, where modern high-rise buildings with a high window-to-wall ratio (WWR) are common and regular flat roof spaces suitable for conventional PV installation are limited. In such environments, traditional PV modules may not always be aesthetically desirable [16], which also makes PV windows and attractive alternative for the wide installation of PV devices in metropolitan areas. However, achieving the right balance between visual transparency and energy conversion efficiency still remains as one of the key technical challenges of PV windows, as these two variables are inversely proportional to each other, meaning that higher energy yields typically come at the cost of reduced transparency, and vice versa. Many efforts have been conducted by industry and research institutes to develop innovative designs that can optimize both aspects at the same time, often through sophisticated light management techniques.

Although BIPV has gained increasing interest from architects, building developers and property owners as an attractive alternative to conventional passive architectural elements, it currently still remains a niche market. In fact, BIPV solutions only accounted for 1% of the total world's PV market in 2017 [17]. This limited adoption can be attributed to several key challenges that need to be addressed for a widely adoption into the built environment, which including system design optimization, aesthetic integration improvement, cost reduction, and most importantly, power conversion efficiency enhancement. Without an improved power conversion efficiency, PV windows can hardly compete with conventional building materials in terms of const-

effectiveness. It is commonly recognized that in order to be competitive and achieve a reasonable levelized cost of energy (LCOE), STPV windows for BIPV applications should have at least a minimum efficiency of 7-10% [5]. Therefore, research efforts should mainly be directed toward enhancing the power conversion efficiency of these devices, while maintaining reasonable production and operation costs.

Another important challenge for the widespread implementation of BIPV solutions lies in the accurate modeling and performance simulation of these systems, particularly in complex environments. Modern BIPV product designs incorporate several components which properties and mutual interactions are hard to model. In addition, modeling their performance in urban settings, where shading from surrounding buildings, trees and other obstructions is common, present a major obstacle in accurately calculating their energy yield and determining their energy performance enhancement potential. All these characteristics can lead to less predictable performance, which is key to assess the viability of their implementation. Therefore, effective modeling tools and simulation methodologies are crucial for predicting the real-world performance of these systems under complex and varying conditions.

In summary, while BIPV solutions, including PV windows, present a promising solution for enhancing the energy performance of buildings and advancing toward neutral-energy buildings, there are still several technical, economic and design challenges that must still be overcome for their widespread implementation, such as optimizing their power conversion efficiency, ensuring an accurate performance modelling or achieving a seamless integration into the building environment, just to name a few. However, as technology progresses and important advancements in material science, light management and simulation tools are achieved, BIPV solutions are on their way for becoming a standard feature in modern architecture, transforming buildings from passive energy consumers to active and aesthetically appealing integrated power generators.

2.2. Bifacial Photovoltaic (bPV) technology

Bifacial photovoltaic (bPV) technology is regarded as a promising alternative for solar power production, as it can generate more power than conventional mPV devices by absorbing sunlight from both of its sides, instead of just from one of them [18]. Sun et al. [19] estimates the power output of bPV technology to be between 5% and 30% higher than that of mPV when the albedo is 0.5 and the facility elevation is 1 m above ground level. Not only is the power output higher, but also the LCOE can be between 2-6% lower when bPV systems are installed at high latitudes, typically greater than 30° [20]. All these merits explain the rapidly switching interest from mPV to bPV technology from the market and academic circles, as the bPV market share was less than 20% in 2019 and is expected to grow up to 70% by 2030 [21].

In outdoor facilities, a high albedo has proven to be beneficial to get a high power output gain due to a substantial increase in the rear-side irradiance [22]. In addition, bPV cells with glass-glass structure require a lower cleaning frequency and usually have a longer lifetime than that of mPV cells due to lower cell operation temperatures [21] [22]. All these characteristics turn bPV into a promising alternative with a new wide range of applications and possibilities.

The working principle of bPV is the same as that of mPV, that is, the photoelectric effect. The main difference of bPV technology can be found in the cell layer structure, which adds an anti-reflection coating (ARC) layer and back contacts at the rear side of the PV cell instead of the back surface field (BSF) layer used in mPV cells. This structural difference allows light to be transmitted through both ARC layers (front and back) and absorbed within the emitter layer, leading to a higher carrier generation rate and ultimately, a higher power production.

IBC and PERC solar cell structures are two of the main bPV cell fabrication technologies currently available in the market. Although both PV cell structures involve modifications to the rear side of the cell compared to traditional PV cells, PERC cells are not considered as rear-contact cells in the way IBC cells are. The main difference relies on the fact that PERC cells still have metal contacts on the front side, whereas IBC cells have all of them at the rear side. *Figure 1* shows a diagram of the cell structure of both PV cell technologies. The cell structure in bPV cells plays an important role in the bifaciality coefficient, ranging between 70-80% for both IBC and PERC bPV cell structures [18].

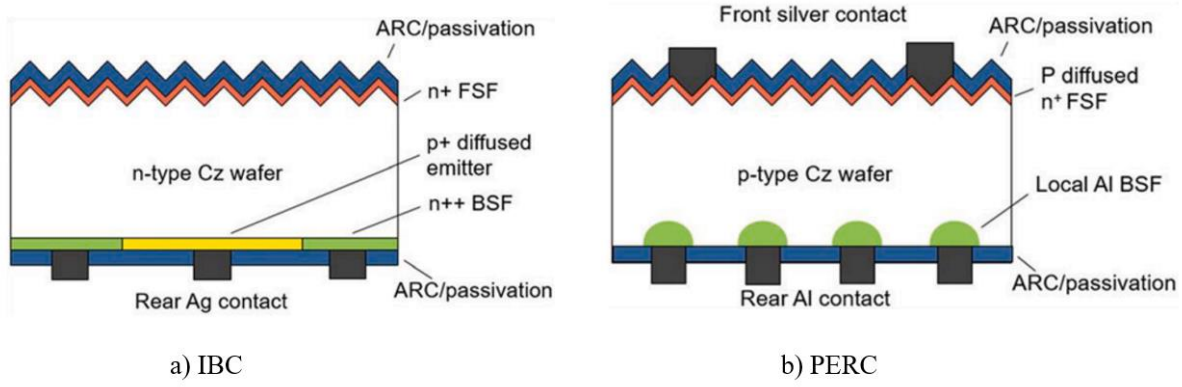

Figure 1: structure diagrams of (left) IBC and (right) PERC bPV cell structures [18].

IBC PV cells are one type of rear contact solar cells which can potentially achieve higher power conversion efficiencies by moving all or part of the front contact grids to the rear side of the device. This feature does not only helps to substantially reduce the shading losses at the front side of the cell, but also simplifies the cell interconnection. In this way, IBC PV cells can be placed closer to each other, giving a PV module a more homogenous appearance and potentially increasing its produced power per unit area. This type of PV cells find an interesting use in BIPV applications and other ones in which the aesthetic appearance is important.

PERC PV cells presents important improvements on the rear side of the PV cell through the addition of a reflective passivation layer and sometimes the implementation of small and localized rear contacts, but these ones are not necessarily present in every case. The passivation layer is used to improve the internal light reflectance and together with the small rear contacts (if present) it is possible to reduce recombination losses and achieve a higher power conversion efficiency (PCE). Thanks to a better light management, PERC PV cells usually perform better in low-light or diffused light conditions, such as early morning, late afternoon or in cloudy days.

Many factors influence the performance of bPV modules, such as the albedo, the number of module rows and the distance between them, the module's tilt angle, their elevation and orientation, their soiling and shading effects, among others [18]. Regarding the tilt angle, it has been noticed that the optimal tilt angle of bPV modules is typically higher than that of mPV under the same deployment conditions [17] [18]. However, this parameter has less effect on the back-side energy yield than that in the front-side. A large tilt angle usually leads to a high bifacial gain. This explains the fact of why bPV technology is more recommended for certain type of applications, such as covering the façade of a building, as a PV window or as noise barrier structures.

Nowadays, bPV devices are used in both space and terrestrial applications. Applications on Earth range from large-scale bPV plants to the integration of bPV devices into building structures, namely BIPV applications. bPV devices can be employed as vertical façade covering structures, shading elements, fences, windows and other building structures, not only serving its main architectural function but also generating electricity, which is their main added value. In addition, bPV devices tend to stay cleaner than mPV ones due to its outer structure that makes them less sensitive to snow, dust or bird drops, achieving overall lower soiling rates and leading to a huge reduction in cleaning costs. Moreover, their orientation is not as critical as in the case of conventional mPV, meaning they can face any orientation including east and west, which was unimaginable in the past [25]. All these features make bPV devices an attractive structural addition to be incorporated in buildings.

Overall, the widespread application of bPV technology is still constrained by many challenges it has still to overcome in order to be widely implemented, which have gradually emerged out as the market share of this PV technology expanded. Besides electrical mismatch due to uneven rear-side irradiance and significant losses caused by system components, another important challenge of bPV technology is to accurately calculate performance estimations. This results especially challenging since several multi-physical processes are involved in bPV generation, such as optical, electrical and thermal processes, which simultaneous interaction makes it complicated to accurately estimate their real performance. Furthermore, the models that describe their optical, electrical and thermal properties are usually considered as individual phenomena, and the complex interactions are usually not taken into account when simulation models are being created. Therefore, a significant portion of research towards bPV is focused on understanding these complex interactions and be able to model them, considering both, simplification and accuracy [18]. In addition, modelling of bPV devices should be complemented with long-term experiments to evaluate model accuracy and the impact of simplifications in real-life performance.

2.3. Semi-transparent Photovoltaic (STPV) technology

Several different types of glazing cooling technologies are currently being under intensive research and development with the aim of creating products that can substantially reduce the SHG in buildings. Besides this approach, the use of STPV technology has emerged as a promising alternative, since this approach allows not only to block incident sunlight and prevent

over-heating in buildings, but also generates power that can be self-consumed within the building, reducing its energy dependence.

STPV technology is a type of PV technology that combines the benefits of visible light transparency and light-to-electricity conversion [17]. Due to this feature, STPV devices are usually employed in buildings as windows or skylights, not only constituting the facade through which sunlight enters a building, but also enabling radiant heat to be transmitted and convective heat to be controlled. In this way, they act as one of the major factors influencing the heating/cooling demand of modern buildings [17]. To achieve this thermal function, STPV cells used in PV windows are usually placed within single or double glazed glass panes to control heat transfer toward the inner space and decrease the cell operation temperature at the same time, which has a beneficial effect in the cell's power conversion efficiency, enhancing the power output of the device.

Semi-transparent (ST) devices for BIPV applications have historically been dominated by crystalline silicon (c-Si) or amorphous silicon (a-Si) PV technologies [26]. Devices based on c-Si technology are strictly considered as 'semi-opaque' PV technology, instead of STPV, as they are fabricated from opaque c-Si cells spatially spaced between each other to achieve a certain level of transparency. On the other hand, devices based on a-Si PV technology are considered as one type of STPV technology only if they enable visible light to be transmitted through the active PV material. This is last requirement is only possible if i) the cells are fabricated on transparent substrates, ii) they have transparent electrodes, and iii) they are molecularly and/or structurally engineered to permit sufficient visible light transmission. Currently, the technology readiness level (TRL) of semi-opaque PV devices is more advanced than that of STPV devices [25] [26], which explains why this technology is mostly used in commercially available STPV products for BIPV applications. *Figure 2* depicts the idea behind this conceptual difference.

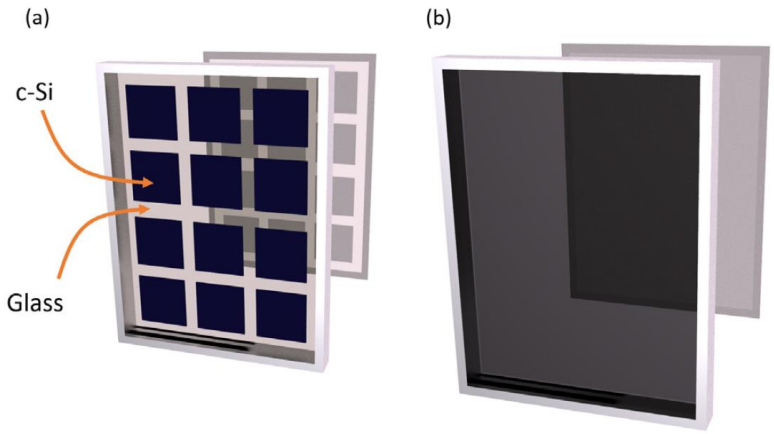

Figure 2: a schematic depiction of a) semi-opaque and b) semi-transparent solar cell device architectures. Source: [17].

Despite less common, other PV technologies can also be integrated into STPV devices, such as inorganic [28], organic [28]-[30], dye-sensitized [32] and more recently, perovskite [33] technologies. Although each of them has different benefits and drawbacks, major gains in power conversion efficiency of inorganic and perovskite solar cells has pushed energy conversion efficiency of these technologies close to the best levels achieved by STPV technologies based on c-Si technology. As research efforts push the conversion efficiency of these PV technologies further, STPV cells for window applications will most likely experiment a transition in the future towards non-silicon based technologies.

A balanced solution between transparency and efficiency is needed for balancing visual comfort with electricity generation. The greatest challenges currently faced by STPV technology in order to be widely implemented are related to cost reduction and efficiency improvement. In addition, having a long-term stability and an aesthetic appearance are also desirable characteristics [34].

2.4. The Performance Ratio (PR) and Temperature-Corrected Performance Ratio (TCPR) metrics

The Performance Ratio (PR) is a performance metric defined in IEC 61724 [35] which is widely used in the PV industry to measure the performance of a PV device, a PV system or a PV power plant. It is a metric that measures the degree of utilization of a PV generation unit [36] and indicates the overall effect of losses in the overall performance of the unit, including effects such as the cell operating temperature, the incomplete utilization of irradiation, the efficiency of the system components, and other failure [36]. In other words, it indicates how well a PV generation unit is performing over a specific time period (typically of one full year). In this way, this performance metric is defined as the ratio between the total electricity actually produced by the PV generation unit to the theoretical total electricity this unit would generate if would continuously operate under (ideal) standard test conditions (STC) and without any further losses. This metric is then scaled to account for the difference between the actual irradiance conditions at the facility's location and the irradiance level under STC.

It is also possible to define the PR in terms of the instantaneous power being produced by a PV generation unit, instead of defining it based on the electricity output over a time period. With this consideration, the (monofacial) PR equation can be defined as follows:

$$PR_{monofacial} = \frac{P_{meas,front}}{P_{STC,front}} \cdot \frac{G_{STC}}{G_{meas,front}} \cdot 100\%$$

where P_{meas} is the instantaneous power being produced by the PV generation unit, $P_{STC,front}$ is the power that would be generated by the front-side of the PV generation unit at ideal STC,

G_{STC} is the standard irradiance at STC (1000 W/m^2) and $G_{meas,front}$ is the real irradiance measured at the front side of the PV generation unit.

The performance of a PV generation unit is dependent on both, the quality of the PV device (its power conversion efficiency) and the meteorological conditions at which the device operates (thus it varies through the year) [37]. It is typically used as a straightforward indicator to compare systems with different designs, same systems installed at different locations, or the performance of a same system over the years. In the case of new PV systems, PR values typically range from 0.6 to 0.9, even exceeding 0.9 at some cool climates, for example in Germany, as reported in [38]. These values already take into account the overall effect of different loss mechanisms, such as the inverter conversion efficiency, wiring, cell mismatch, elevated PV module temperature, reflection from the modules' front surface, soiling, shading, among others. This is due to the fact that this metric usually accounts for the total electricity production at the AC side in the case of PV systems. However, this metric can also be applied considering the electricity production at the DC side, which will lead to higher PR values, as many of these loss mechanisms are not present at the DC side. If further power boosting techniques are applied, such as when bPV or solar concentrator devices are used, higher PR values can be obtained, in some cases even exceeding 100%

However, if the PR is measured at moments in time where there is an important difference in weather conditions, for example between summer and winter, or between instants with a large temperature difference, substantially different values may be obtained, making this metric insufficient to use as a basis to measure the performance of a PV device when precise confidence intervals are needed [37]. Most notably, weather affects the PR mostly by affecting the module operating temperature, making this metric to be strongly dependent on temperature and implying that lower PR values may be expected at locations with warm climates or during summer months, and higher ones at colder locations or winter months. In fact, the seasonal variation in PR can be as large as ± 10% [37]. An example of these effects are illustrated in *Figure 3*, showing that the PR metric by its own (in blue) is not consistent throughout the year.

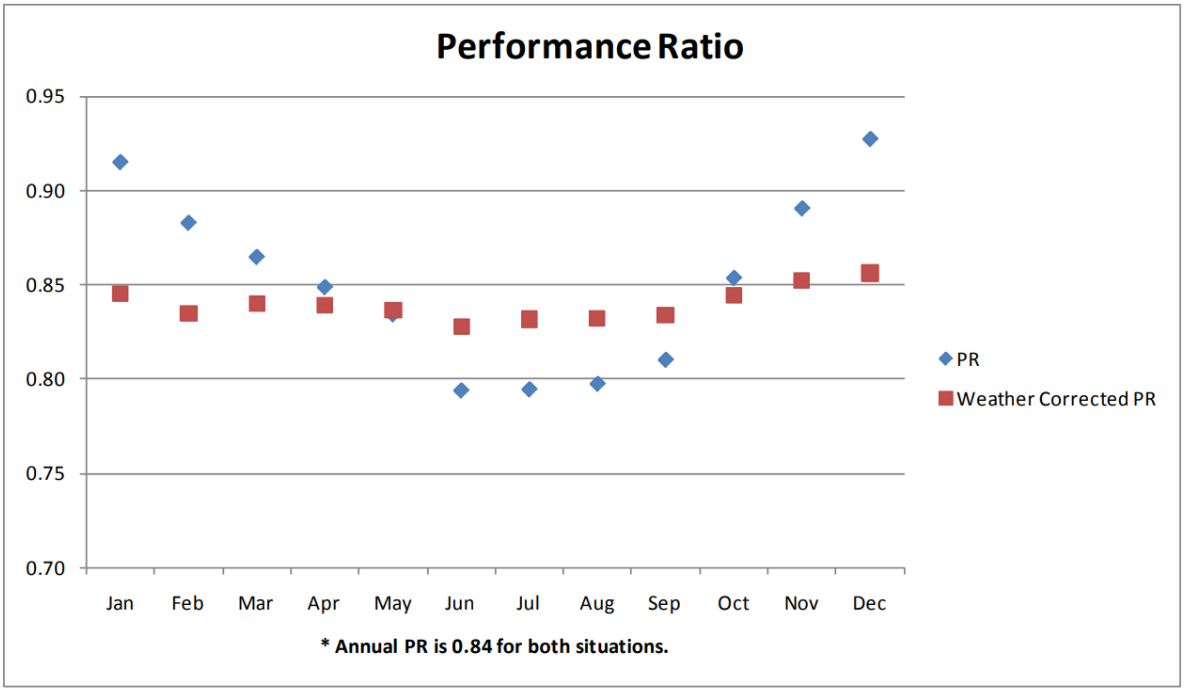

Figure 3: (in blue) PR and TCPR (in read) from simulated results where the annual PR is 0.84 for both simulations. Source: [37].

This is why it is necessary to modify the PR calculation to neutralize biases that may be introduced by weather variations and obtain a metric that gives more consistent values throughout the year while retaining the familiarity this metric brings to the PV industry. The modified PR metric accounting for PV module operating temperature (which accounts for the effects of the ambient temperature, wind speed and irradiance heating) is known as the (monofacial) weather-corrected performance ratio or (monofacial) temperature-corrected performance ratio (TCPR), which example of its application are represented by the red datapoints in *Figure 3* and its instantaneous equation can be defined as follows:

$$TCPR_{monofacial} = \frac{P_{meas,front}}{\left(P_{STC,front} \cdot \frac{G_{POA}}{G_{STC}}\right) \cdot \left(1 - \frac{\delta}{100} \cdot (T_{ref} - T_{cell})\right)} \cdot 100\%$$

where T_{ref} is the reference temperature at STC (25 °C), T_{cell} is the operating cell temperature (in °C) and δ is the power temperature coefficient of the PV device (in %/°C). By using the equation described above, the PR metric is adjusted taking into account the on-site irradiance conditions and the operating temperature of the PV cells, minimizing as much as possible the effect of these two weather variables and turning this metric into a reliable parameter used to compare the performance of a PV generation unit at moments with different weather conditions, such as

within a short timeframe (for example, between different times of a day) or between larger periods of time (for example, between different seasons).

It is worth mentioning that correcting the PR to a common temperature of 25 °C usually results in higher PR values, as PV devices usually operate at higher temperatures. Thus, while a correction to 25 °C essentially tries to solve the problem of seasonal variation as much as possible, it may still slightly overestimate the actual performance of the PV generation unit. Even with this effect, the TCPR constitutes a metric that effectively addresses the limitations proper of the traditional PR metric by minimizing the influence of fluctuating irradiance intensity and cell operation temperature in the performance assessment of a PV generation unit. By adjusting this metric for local irradiance conditions and correcting it for the real operating cell temperature, the TCPR valuable tool for consistently comparing the performance of PV devices and ensuring that weather-related biases are minimized as much as possible, and providing a more stable and reliable parameter to quantify the performance of PV devices across different times of the year and varying weather conditions.

2.5. bPV simulation software *BIGEYE*

BIGEYE (which stands for Bifacial Gain in Energy Yield) is a MATLAB based simulation software specifically designed to model and simulate the electrical performance of bPV devices. It was first developed by ECN and TNO back in 2017, at a time in which bPV technology was increasingly becoming more popular due to its surpassing performance in relation to mPV and was gaining each time more attention from consumers and manufacturers. The commercial simulation software packages for PV applications that were available at that moment were still not able to model the electrical performance of bPV devices, thus there was an urgent need for an accurate simulation software for energy yield demonstrations and performance simulations of bPV devices.

The term 'EYE' in the software's name alludes to the inclusion of increasingly sophisticated view factor models. *BIGEYE* was first developed integrating a simple, extended 2-dimensional view factor model, which slowly evolved to a 3-dimensional one as newer versions of the software were released. With each newer version, the calculation engine was also improved, keeping always a balance between accuracy and computational resources and making it possible to handle larger and more complicated simulations each time. The results of the software have been validated against the performance of real bPV facilities different in size and complexity, showing small variations between simulation results and real-life performance measurements.

The use of *BIGEYE* becomes really attractive when it comes to the simulation of XIPV devices, since it offers a wide range of modelling possibilities. In the specific case of buildings (BIPV), *BIGEYE* offers the possibility of modelling the devices at a completely vertical placement, which was not supported by other software packages in the past, such as *PVsyst*, even for mPV applications. In the case of vehicle applications (VIPV), it is possible to model non-planar modules and cut-cells that match the curvature and shape of a vehicle body. Its use for the simulation of bPV devices in other infrastructure applications results also very convenient, as it allows to model curved PV strings or additional mounting frames. All these features make

BIGEYE a good choice when it comes to the simulation of unconventional bPV devices with a wide range of particularities.

One of the merits of *BIGEYE* is that minimal inputs are required to simulate the performance of bPV devices [39]. These inputs must be loaded in the graphical user interface (GUI) of the software by means of two excel (.xlsx) files: one comprising the geometrical, optical, thermal and electrical properties all the objects that are part of a simulation model (referred to as the 'geometry file'), and another one comprising a set of time-dependent meteorological data containing information of at least the Global Horizontal Irradiance (GHI) and the ambient temperature (referred to as the 'meteo file').

In the geometry file, several instances of objects can be specified to add different structures to a model. In particular, bPV arrays, consisting of one or more bPV modules can be inserted and their geometrical, optical, thermal and electrical properties can be specified. In this file, it is also possible to specify the properties (mainly geometrical and optical) of the ground and of different shade-causing objects (beside the bPV modules), which can mimic real-life structures, such as poles, beams, walls, mounting structures, etc. In the meteo file, Diffuse Horizontal Irradiance (DHI) and windspeed data can also be optionally supplied. If the DHI data is not provided, it will then be calculated using the Perez model [39] [40]. If windspeed data is included, it will be considered in the calculation of the thermal model. A diagram of the simulation process in *BIGEYE* is illustrated in *Figure 4*.

Figure 4: diagram of the BIGEYE simulation process.

In *BIGEYE*, the necessary view factors of the bPV module's front and rear sides to the sky and to the ground are fully 3D and numerically calculated (therefore, by means of a sky view factor approach). Since the view factor is calculated numerically for both planes of array (POAs) (front and rear) of every bPV module in an array, finite array lengths with different separation distances between them and at different tilt angles can be modelled. The thermal model of *BIGEYE* [23] is calculated by means of a simple stationary heat balance, while the electric model is based on the single-diode model. The temperature dependance of the photogeneration current, I_L, is user-supplied and is proportional to the front-side irradiance increased with the

rear-side irradiance multiplied by the bifaciality factor the power, i.e., the equivalent or compensated current method [42]. The temperature diode dependence on the diode ideality, as well as the dark saturation current, I_0, are calculated as outlined by [43]. More information on the *BIGEYE* simulation tool with additional description of its mathematical models and calculation methods can be found in literature [22] [38] [43].

Finally, it is possible to define an albedo coefficient value for reflecting objects in *BIGEYE*. The albedo coefficient represents the fraction of incident light that is reflected by a surface. For instance, a high albedo coefficient should be used to model high-reflective materials, such as metals, glass, bright colored paints, polished surfaces, etc. On the contrary, low albedo coefficients should be used to model low-reflective surfaces, such as non-metallic materials, objects with dark or matte color surfaces, or objects that are not polished or have a texturized finish. This allows to mimic a wide variety of materials and to give a better estimate on the total irradiance incident on the bPV setup on both of its sides, contributing to a better simulation accuracy.

3. The *ZIEZO* testbed: facility overview and experimental setup

3.1. The *SolarBEAT* outdoor research facility

SolarBEAT, which stands for Solar Building Elements Application Testing, is the TNO and TU/e's outdoor research facility for BIPV, in which building-integrated and solar energy products and systems are tested on-site at all times, all year round, both for electricity and heat production. In this way, *SolarBEAT* plays a crucial role in solar energy research for the Dutch and European energy transition.

The facility was founded back in 2014. It is located on the lower section of the Vertigo building rooftop at the TU/e campus in Eindhoven, The Netherlands. An important characteristic of its ground surface (and of the building orientation itself) is that it is accurately oriented towards South, which makes it very convenient for testing the performance of solar energy systems and products under ideal orientation conditions. *Figure 5* shows a top view of the *SolarBEAT* facility.

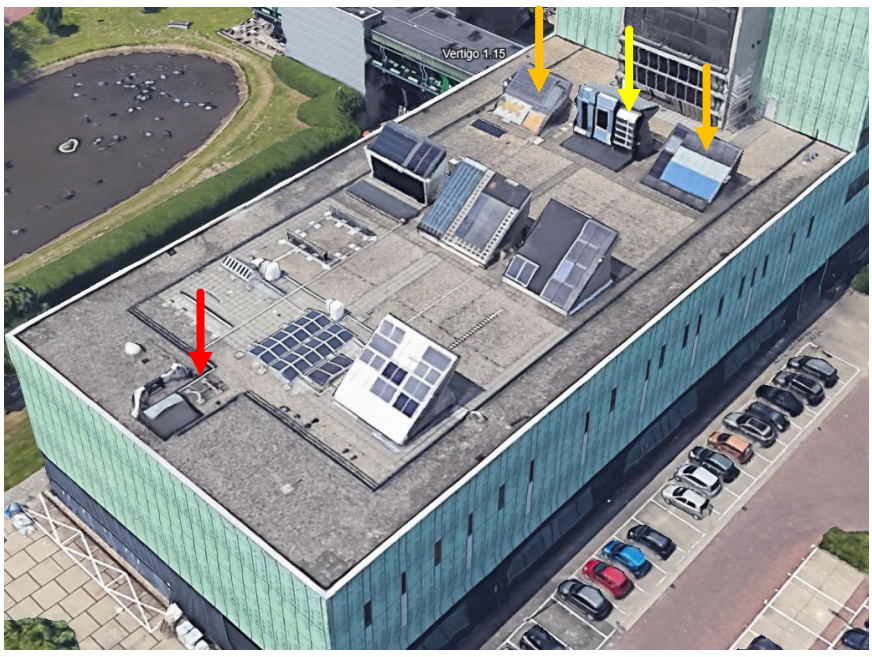

Figure 5: top view of the SolarBEAT facility. Source: Google Earth.

The research cabin at which the 12 bPV window demonstrators have been mounted simulates the structure of a building (further referred to as the 'dummy building') and is indicated by the yellow arrow in the figure. It is also important to mention that the surrounding research cabins (pointed by the orange arrows in the figure) were responsible of causing some partial shading over the bPV window demonstrators at some periods of the year, especially during the early morning and late afternoon, which effects can be visible in the electrical measurements as will

later be shown in section *4.5 Validation of the electrical model*. A better view of these surrounding cabins can be seen in *Figure 6*. Finally, the meteorological measurement station of the research facility is pointed out by the red arrow in the figure. As it implies, not all meteorological measurements are taken at the exact same position of the 12 bPV window demonstrators, but some meters farther away. This is an important aspect to keep in mind, which will later be explained in more detail in section *3.7 Sensors and measured parameters*.

As can be seen in *Figure 5*, other solar systems and devices have also been deployed at the facility for testing purposes. Most of these projects undergo a testing cycle of at least one full year, involving an in-depth analysis of the physical performance of full-scale systems in real operational conditions in different seasons and different weathers. In this way, the design and control of the tested demonstrators can be further finetuned based on the research findings, observations and simulation studies [45]. Among these prototypes, many types of BIPV devices and applications are under testing, including solar windows, solar facades, balcony fences, solar roof tiles, among others. Since testing is done in real outdoor conditions, *SolarBEAT* plays an important role in the improvement of innovative BIPV prototypes and in the development of new ones, which is usually done in collaboration with architects, construction companies, developers and installers. This makes *SolarBEAT* an important research center that fosters the collaboration between industry and academia for the development and refinement of BIPV technologies.

Figure 6: view of the bPV window research cabin and surrounding cabins at SolarBEAT. Source: TNO internal.

3.2. bPV window demonstrator test setup

Figure 7 shows a closer view of the dummy cabin at *SolarBEAT* in which the 12 bPV window demonstrators have been installed for testing purposes. Other test setups belonging to different research projects for BIPV applications can also be seen at the center and left side of the cabin.

Figure 7: (left) the dummy building at SolarBEAT, in which the 12 bPV window demonstrators have been installed (at the right side). (Right): numbering of the bPV window demonstrators for identification purposes. Source: TNO internal.

Just as the Vertigo building itself, the dummy building at which the 12 bPV window demonstrators have been installed is also accurately oriented towards the South, which makes it very convenient for testing the performance of the bPV window demonstrators under ideal orientation conditions. The reason behind the fact that 12 bPV window demonstrators have been manufactured and installed at the *SolarBEAT* facility is because each one of the 12 bPV window demonstrators has been designed and manufactured with a different unique combination of PV technology (among two different types), CR (among two different CR values) and type of Venetian blinds (among three different types of Venetian blinds). This was done in order to be able to individually assess the influence of each feature in the window performance during the course of one full year. During this period of time, different measurement campaigns were followed, in which the position of the Venetian blinds was changed in terms of their tilt angle to assess differences in window performance due to different PV technologies, CR values, Venetian blind types and positions, weather conditions, time of the year, etc. The results from these experiments can be found in literature [7].

Furthermore, a black cloth was placed at the back of the bPV window demonstrators to isolate the reflective effect of the blinds as much as possible and to minimize the contribution of artificial illumination coming from the inner side of the dummy building. In this way, it was

assured that the total rear-side illumination was mostly provided by the blinds and not from other sources, which would lead to overestimated reflection results. For the same reason, the inner sides of the dummy building were covered with black-colored paper. However, in reality still some parts remained uncovered and had some of its wooden surface exposed, as can be seen in *Figure 8*. This consideration is important, as it influenced the decision of which albedo coefficient value to use for modelling the inner side walls of the dummy building, as will later be detailed in section *4.3 Dummy building and PV field's modelling*.

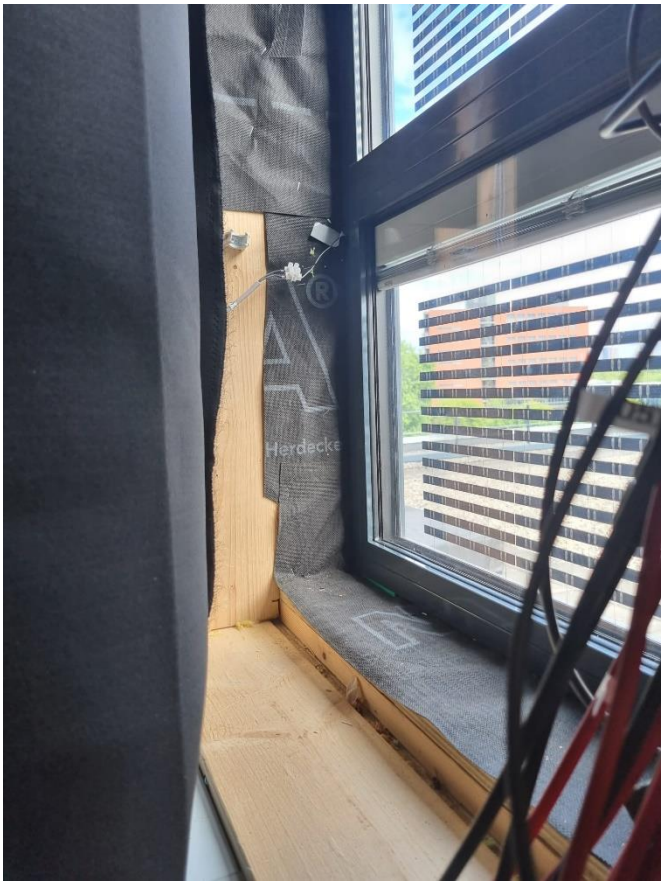

Figure 8: bPV window view from the inner side of the dummy building, where a wooden exposed surface can be seen. Source: TNO internal.

3.3. The innovative bPV window concept

Figure 9 shows a schematic depiction of the innovative and multifunctional *ZIEZO* bPV window, designed and manufactured by the partners collaborating in this project.

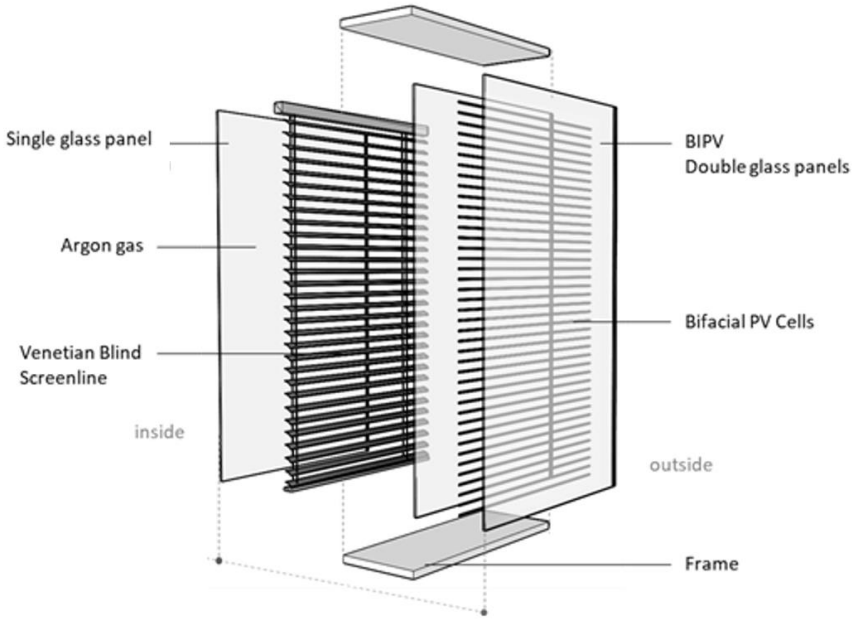

Figure 9: schematic depiction of the ZIEZO bPV window. Source: TNO internal.

As can be seen from the figure, going in the inside to the outside direction, the back side of the bPV window consists of a unique insulating glazing unit (IGU), which is a spacer formed between two insulating glass panes provided by *Pilkington* and filled out with argon gas. Important to realize is that the glass pane that separates the inner of a building and the IGU (the one at the very back) has a low-emissivity coating, which gives the bPV window its insulating properties. The insulating properties of this bPV window are one of the main advantages of this BIPV window product, as it helps to keep an overall low SHG of a building by blocking a great portion of incoming near-infrared (NIR) irradiance, reducing its heating and cooling demands and therefore, further improving its energy performance. Embedded inside of the IGU, a set of reflective Venetian blinds is embedded. In practice, the position of the Venetian blinds (in terms of height and tilt angle) can be adjusted by the users of a building to achieve visual comfort according to their preferences.

The front side of the window consists of thin bPV c-Si cell strips laminated between the intermediate and the outer glass panes and vertically separated between them. Depending on the size of the bPV cell strips and the separation between them, different levels of transparency can be achieved for the window, and thus, different rated power outputs and illumination levels.

The whole idea behind the power output boosting effect provided by the deployment of the reflective Venetian blinds is that, when partially or fully deployed, they will act as back reflectors and will reflect part of the incoming sunlight to the rear side of the bPV cell strips, further boosting the power output of the window. The rest of the sunlight that is not reflected by the slats can freely pass through the window and contribute to the illumination of the inner space of a building. *Figure 10* shows a visual representation of this effect.

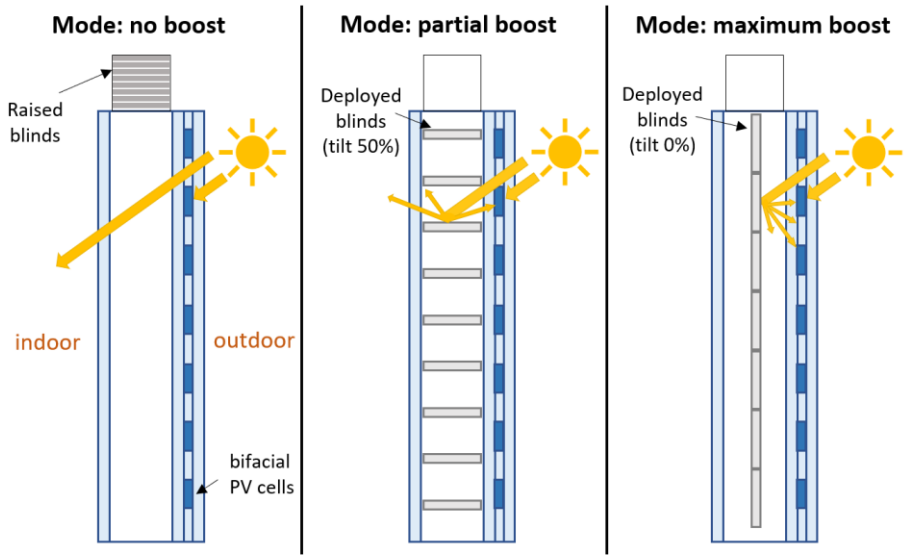

Figure 10: visual representation of how the power output boosting effect of the ZIEZO bPV windows is achieved when the set of reflective Venetian blind is deployed. Source: TNO internal.

As can be seen in *Figure 10 a)*, in no-boosting mode (i.e., when the reflective Venetian blinds are completely retracted, the sunlight that is not directly absorbed by the front side of the opaque bPV cell strips can freely pass through the window and illuminate the inner space of the building. In *Figure 10 b)* an example of partial boosting mode is represented, in which the blinds are partially deployed in terms of height and tilt angle. In this situation, part of the incoming sunlight that is not directly absorbed by the front side of the opaque bPV cell strips is transmitted to the inner space of the building in some part, and the rest is reflected toward to the rear side of the bPV cell strips, achieving a partial boosting in power production. Finally, when the Venetian blinds are fully deployed (almost totally closed) as shown in *Figure 10 c)*, almost all of the incoming sunlight that is not directly absorbed by the front side of the bPV cell strips is reflected to their rear side, maximizing the power output boosting effect of the Venetian blinds and the power output of the window itself.

3.4. bPV window's geometrical and electrical properties

Since the goal of this particular research project is to investigate the effect of using different blind configurations in the overall performance of the *ZIEZO* bPV window, the window number 1 (see *Figure 7*) has been chosen for conducting the PV modelling and window performance simulations that are part of this research project. In this way, any future reference to the 'bPV window' will refer to this particular bPV window demonstrator. Furthermore, the three types of

Venetian blinds under test are also part of this research project. In this way, the investigation here conducted will focus on the bPV window demonstrator labeled with the number 1, but varying its type of Venetian blinds between the three different ones. More information regarding the bPV cell technology, the CR and the three types of Venetian blinds that were investigated as part of this research project will be described in the following section. The dimensions of this chosen bPV window demonstrator are next detailed in *Figure 11*.

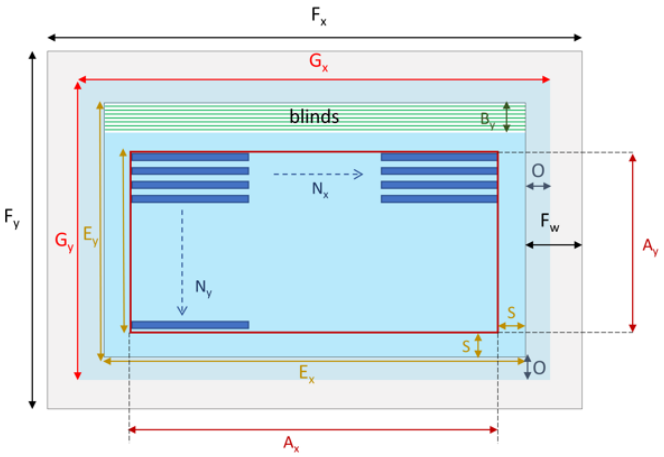

- **Cell area: 166 mm x 10 mm**
- **Vertical cell spacing: 7 mm**
- **Cell block spacing: 1.5 mm**
- **33 blinds when fully deployed**

Frame length	Fx	600 mm
Frame height	Fy	529 mm
Frame width	Fw	68 mm
Glass length	Gx	494 mm
Glass height	Gy	423 mm
Overlap glass/frame	O (=Ox=Oy)	15 mm
Safety gap	Sx Sy,up Sy,down	60 mm 48.5 mm 12 mm
Blinds height (when not deployed)	By	57 mm
Exposed glass length	Ex	455 mm
Exposed glass length	Ey	390 mm
Max PV active area length	**Ax**	333 mm
Max PV active area height	**Ay**	265 mm

Figure 11: dimensions of the bPV window demonstrator number 1. This demonstrator was chosen as the bPV window sample for which three different types of Venetian blinds were tested as part of this research project.

The electrical parameters of this bPV window are next detailed in *Table 1* and *Table 2* for the front and rear of its sides, respectively.

Table 1: Electrical parameters of the front side of the bPV window chosen for this research project.

Electrical parameter	Value	Units
Front-side peak power	10.09	W_p
Front-side efficiency at STC	19.0	%
Front-side efficiency at STC	11.4	%
Bifaciality	82.0	%
Front-side I_{sc}	0.64	A
Front-side V_{oc}	21.16	V
Front-side I_{mpp}	0.59	A
Front-side V_{mpp}	17.11	V
Front-side FF	74.5	%

Table 2: Electrical parameters of the rear side of the bPV window chosen for this research project.

Parameter	Value	Units
Rear-side peak power	8.27	W_p
Rear-side efficiency at STC	15.6	%
Rear-side efficiency at STC	9.4	%
Bifaciality	82.0	%
Rear-side I_{sc}	0.53	A
Rear-side V_{oc}	20.95	V
Rear-side I_{mpp}	0.49	A
Rear-side V_{mpp}	16.95	V
Rear-side FF	74.4	%

3.5. bPV window's PV technology and Coverage Ratio (CR)

The front side of the bPV window consists of thin bPV c-Si IBC zebra cell stripes manufactured by *SPIC Solar*, which technical specifications can be consulted in *Appendix A: bPV cell specifications*. The cells have been laser-cut in thin cell stripes, and TNO has used them to manufacture the bPV window by laminating them between the middle and the outer glass panes of the window (see *Figure 9*) and vertically separating them by a distance of 7 mm from each other. In practice, depending on the size of the bifacial c-Si PV cell strips and the separation distance between them, different levels of window transparency can be achieved, and thus, different bPV window peak power and window illumination levels.

The relationship between the PV cell area and the total window area (comprised by the sum of the PV cell area and the area of the empty spaces between them) is defined by means of a parameter called the 'coverage ratio' (CR), which value is calculated just as the ratio between these two areas (CR = PV cell area / total window area). The CR of the bPV window that was modelled as part of this research project was of 0.6 (or 60%), meaning that the bPV cells cover 60% of the total bPV window area and implying that this bPV window has a transparency of 40%. *Figure 12* shows a real-life front-view picture of a bPV window demonstrator and illustrates the previous definition of the bPV window's CR.

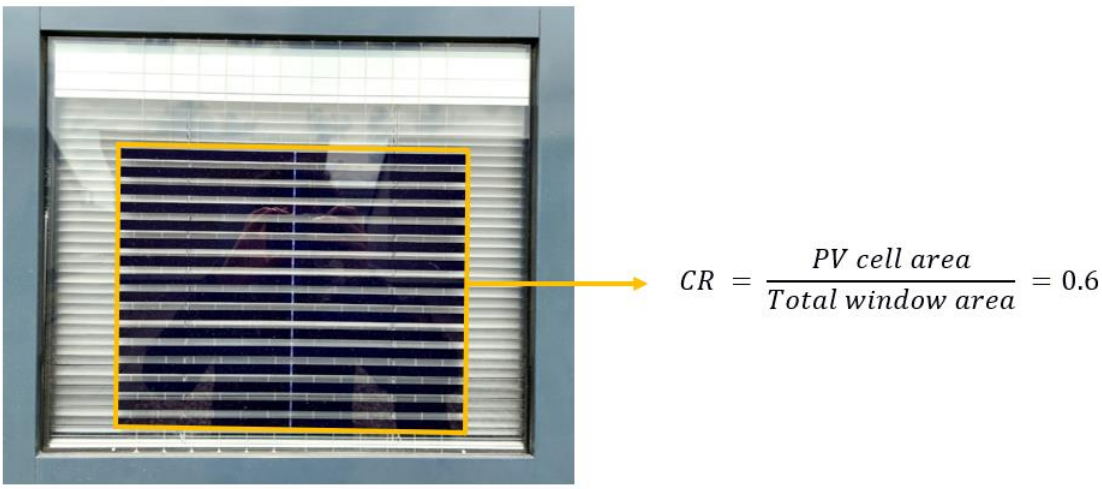

Figure 12: a real-life picture of the bPV window demonstrator that was chosen for this research project. It's cell coverage ratio (CR) is defined as the ratio between the PV cell area and the total window area and is equal to 0.6.

As can be seen from *Figure 12 (left)*, the bPV window in real life is comprised by two vertical blocks of thin bPV cell stripes, which are electrically connected in series between each other and have been framed in orange color in the figure. Each block of bPV cells is comprised by 16 individual bPV cell stripes, which are electrically connected in series between each other as well. In this way, the 32 bPV cells of the window are all electrically connected in series. A description of how these bPV cells were modelled in *BIGEYE* will later be described in section *4.1 bPV cell stripes' modelling*. Finally, the bPV window has then two junction boxes at its left side, each one having one by-pass diode that bypasses the current of a whole block of bPV cells in case of partial shading.

3.6. Types of Venetian blinds under test

As previously described in section *3.3 The innovative bPV window concept*, a set of slightly curved Venetian blinds are located at the cavity of the IGU and their position in terms of height and tilt can be freely adjusted. This will cause different kinds of interactions between the blinds and incident sunlight, which will change the intensity of the sunlight that is being reflected at the rear side of the bPV cells and ultimately will affect the power output of the bPV window. The three types of Venetian blinds that were tested a part of this research project were manufactured by *Pellini* [46] and will be described in detail in this section.

The three types of Venetian blinds that were tested as part of this research project differ from each other in terms of color and coating type. These three blind types are: *a)* the S157 blinds, which have a grey colored coating and is the most sold blind type of *Pellini*; *b)* the S102 blinds, which have a white colored coating; and c) the V95 blinds, which have a silver colored coating. In order to better describe the optical properties of the Venetian blinds that were tested as part

of this research project, *Figure 13* shows the spectral reflectance of the three blind types that were tested. In this figure, the absorption range of c-Si cells and the spectral range of visible light are also indicated. As can be seen from the figure, the reflectance of these types of Venetian blinds is not constant, but wavelength dependent, and in reality, it also varies along the curvature of the slats.

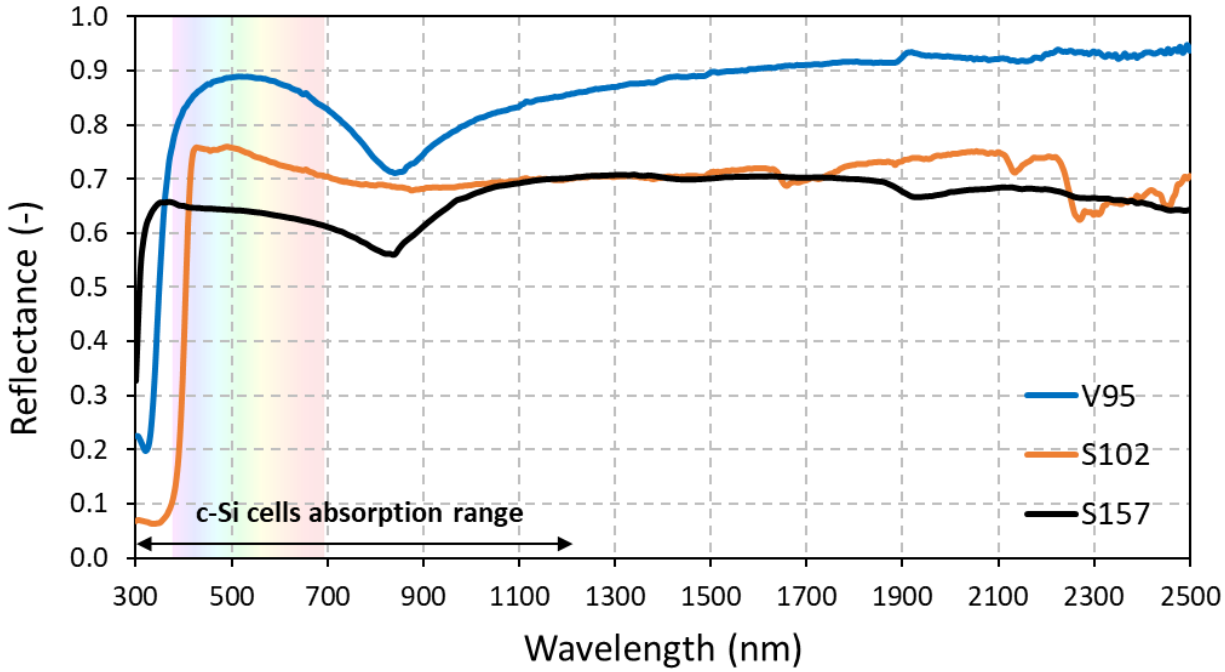

Figure 13: spectral reflectance of the three blind types tested as part of this research project. The absorption range of c-Si cells and the spectral range of visible light are indicated in the plot.

The previous figure shows that the S157 blinds (grey colored, represented by the black curve) have the overall lower spectral reflectance, especially in the visible light range and in the c-Si absorption range, followed by that of the S102 (white colored, represented by the orange curve) blinds and finally, the V95 (silver colored, represented by the blue curve) blinds. Important to notice is that this last type of blinds has been coated with a special constructive interference film specially designed to reflect the most critical solar radiation. This is why a high reflectance peak can be observed for this type of blinds in the visible light spectral range. This coating also results in low emissivity slats, thus effectively reflecting the long wave infra-red radiation, as can be seen in *Figure 13*.

In reality, the diffuse and specular reflectance components of each type of blinds is wavelength dependent, and also varies across its curved shape. For the sake of simplicity, their reflectance components at three different points across the slats have been measured experimentally and averaged along the visible light spectrum. Therefore, they can be approximated as presented next in *Figure 14*.

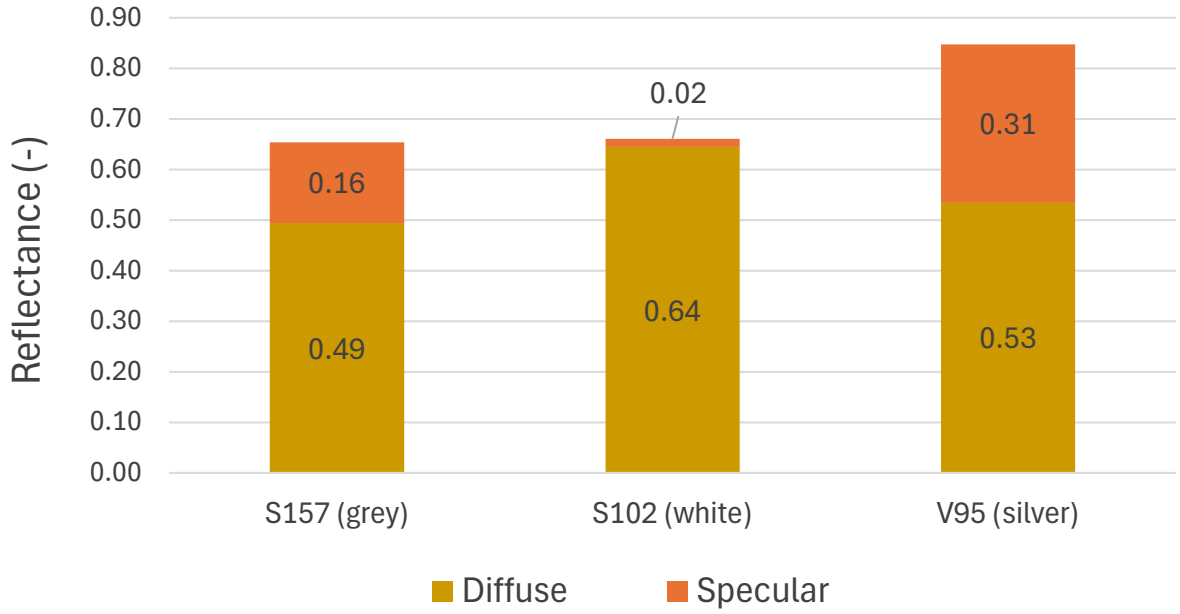

Figure 14: average diffuse and specular reflectance components of each type of blinds that were tested as part of this research project.

As can be seen from the figure, the total reflectance of the S157 blinds (grey colored) is of around 0.65, with its diffuse and specular components being of 75% and 25%, respectively. The total reflectance of the S102 blinds (white colored) is just slightly higher (of around 0.66) than that of the S157 (grey colored), and its reflectance is almost fully diffuse, which means that they can scatter light almost equally in all directions. Finally, V95 blinds (silver colored) have the highest total reflectance of the three blind types (or around 0.84), being the specular component an important part of it, as it accounts for around 37% of its total reflectance, while the diffuse component makes up the remaining 63%.

In this way, the real-life properties of the three types of blinds under test can be summarized as follows:

- S157: grey colored, highly diffuse reflectance and most sold commercially.
- S102: white colored, almost completely diffuse reflectance.
- V95: silver colored, highly specular reflectance.

In this section, the real-life properties of the three blind types under test have been described, but it is important to mention that not all these properties were successfully modelled in the bPV window simulation models that were created as part of this research project. This difference between the measured and modelled properties of the blinds is mostly attributed to limitations in the *BIGEYE* simulation software. More information about the measured and modelled blind's properties will be explained in detail in section *4.2 Venetian blinds' modelling*.

3.7. Sensors and measured parameters

At *SolarBEAT*, both, the outside of the dummy building and the dummy building itself contain various high-tech sensors. Regarding the ones inside of the dummy building, *Figure 15* shows two of the bPV window demonstrators as seen from inside of it. As can be seen from the figure, several sensors have been coupled to the bPV window demonstrators to track their thermal and electrical performance at all times.

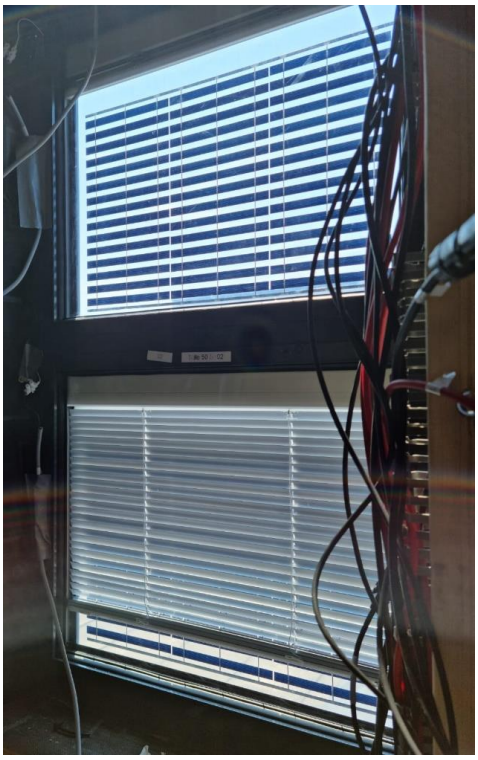

Figure 15: bPV window demonstrators seen from the back (from inside of the dummy building). The black cloth has been removed to take the picture. The monitoring sensors of the bPV demonstrators can be appreciated at both of their sides.

It is important to mention that the bPV window demonstrators are not electrically connected to each other as part of a common PV system, but individually monitored. Therefore, each bPV window demonstrator can be interpreted as an independent PV module which performance has been assessed individually. The electrical performance of each bPV window demonstrator was measured independently by means of an I-V tracer (EKO MP-160), which is a device used to measure the full I-V curve of a bPV window and record all its relevant external parameters, such as the P_{mpp}, V_{mpp}, I_{mpp}, V_{oc}, I_{sc}, etc. Worth noticing is that between the I-V sweeps measuring these parameters, the bPV windows were kept in open-circuit conditions, as they are not connected to an inverter or to a power optimizer. Typically, a PV module that is operating in open-circuit conditions tend to have a higher operating temperature than if it is kept at the maximum power point (MPP).

The monitoring of the 12 bPV window demonstrators stared on 08/09/2023 and it was conducted during a full single year to assess their electrical performance in real-life outdoor

conditions, under different seasons and weathers, and to the use of different types of Venetian blinds at different tilt angles. In this way, several measurement campaigns were conducted, in which the position of the blinds was systematically changed to observe differences in the bPV window performance.

It is important to mention an undesirable effect of the I-V tracers, which consists on the recording of noisy or spiky measurements at low irradiance levels, which mainly affected the I_{mpp} and V_{mpp} measurements. During the measurement campaigns, it was noted that notorious spikes were presented in the I_{mpp} and V_{mpp} measurements (and therefore, in the P_{mpp} measurements as well). As this effect occurred at moments of low irradiance levels, it mostly took place in the early morning and late afternoon, but it was also present in totally overcast moments, causing the measurements at these moments to be unreliable. A visualization of this undesired effect was made visible (highlighted in yellow) in plots *a)*, *c)* and *d)* of Figure 24, Figure 25 and *Figure 26*.

Furthermore, the operational temperature of the bPV cells of every bPV window demonstrator is not directly measured, but approximated by means of a temperature sensor that has been embedded within the IGU spacer of every demonstrator, just as can be seen in *Figure 16*.

Figure 16: Temperature sensor embedded in the IGU spacer. Its recorded data is an approximation to the operational temperature of the bPV cells.

On the external part of the dummy building, a vertically mounted pyranometer has been installed completely aligned with the POA of the bPV window demonstrators, just as can be seen in *Figure 17*.

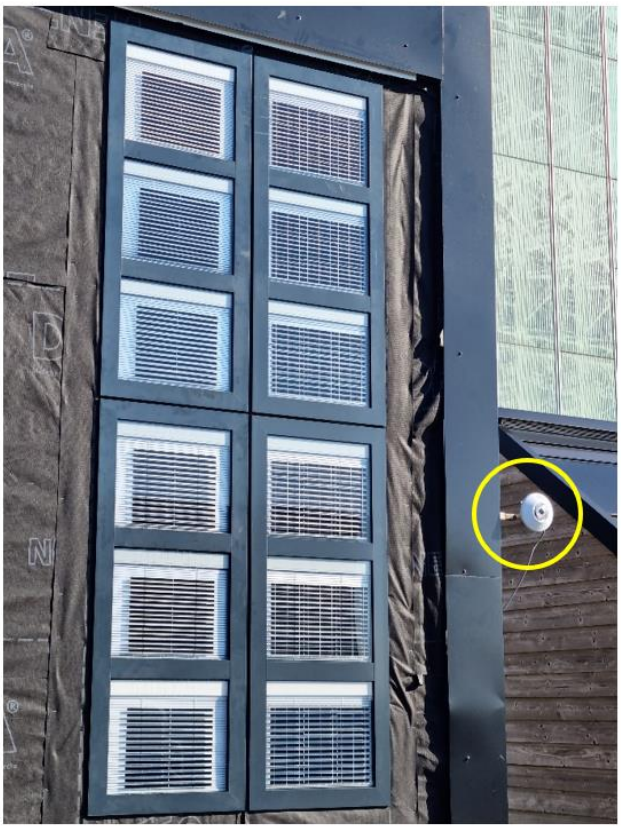

Figure 17: facade of the dummy building at SolarBEAT, at which the 12 bPV window demonstrators have been installed. On the right and pointed by a yellow circle, a vertically mounted pyranometer aligned with the bPV window's POA can be seen.

As can be noted, this vertically-mounted pyranometer is at the same height of the bPV window demonstrators labeled with numbers 4 and 10 in *Figure* 7 and is not positioned at the same height of the bPV window demonstrator number 1, which is the one that has been chosen to develop the bPV window models that are part of this research project. In this way, it is possible that the total irradiance measured by this pyranometer (total front-side irradiance on the bPV window POA) is not the same as that one received by the bPV window demonstrator number 1.This differences may be mainly caused by an increased reflected irradiance at the position of the pyranometer (at a lower position) due to its closer proximity to the ground, or an increased diffuse irradiance at the bPV window demonstrator number 1 (at a higher position) due to an increased sky view factor. Even if there might be some differences of the total irradiance at these two positions, the irradiance measured by this pyranometer is a good approximation of the irradiance received at the front-side of the bPV window demonstrator number 1's POA.

Moreover, as previously pointed by the red arrow in *Figure 5*, *SolarBEAT* hosts a calibrated, high-quality weather station for accurate characterization of irradiance, temperature and wind conditions [45]. At this station, more than 1000 sensors are constantly monitoring weather and meteorological conditions at the facility, which were key for the modelling work conducted as part of this research project. At this weather station, several parameters are constantly being

monitored, such as the GHI, DHI, Direct Normal Irradiance (DNI), ambient temperature, windspeed, etc.

It's important to note that both, the GHI and the DHI being measured at the weather station are referenced to the horizontal plane, rather than to the bPV window demonstrator's POA, which is completely vertical (tilt angle of 90°). This distinction is crucial, especially as later in chapter *5 Results and* discussion, the concept of diffuse fraction, k_d, will be introduced, which is simply the ratio of the DHI to the GHI.

Understanding this difference helps to clarify how the diffuse fraction, k_d, behaves differently depending on the POA of reference. For instance, during a very sunny moment with a low k_d value (e.g., 0.2), if the sun has moved behind the dummy building, every bPV window will only receive diffuse irradiance at the front side. Even though k_d on the horizontal plane is low, a much higher k_d on the window plane can be expected, as the diffuse component on this plane is way higher. It is also important to keep in mind that only the total irradiance on the vertical POA is measured, and not their direct and diffuse components on the same POA. Therefore, the k_d described here and for the rest of this research project is defined using DHI and GHI referenced to the horizontal plane, as only these ones were experimentally measured at *SolarBEAT*.

4. bPV window modelling methodology

This chapter presents a detailed description of the approach followed to create the bPV window simulation models. By describing the modelling approach, some of the software's limitations, and consequently, the simplifications and assumptions made during the modeling process are addressed. In this way, section 4.1 is dedicated to describe the approach followed to model the window's thin bPV cell stripes. In section 4.2, the process for modelling the reflective Venetian blinds of this bPV window is described in detail, while section 4.3 provide a brief description of the modelling process of the dummy building and the PV field where it lies. In this way, sections 4.1 through 4.3 are focused on achieving Objective 1: (O1: create a set of PV simulation models that describe the performance of this BIPV window when different types of reflective Venetian blinds are used).

Finally, sections 4.4 and 4.5 are dedicated to describe the validation process for the optical and electrical models of this bPV window, respectively. These validations were key for creating a simulation models that are able to accurately simulate the electrical performance of the bPV window. In this way, the combined focus of these sections aims to achieve Objective 2 (O2: validate the created models with experimental data to test their accuracy and reliability) of this research project.

4.1.bPV cell stripes' modelling

The first step in the bPV window modelling process consisted of modelling the thin bPV cell stripes of the bPV window that were previously described in section *3.5 bPV window's PV technology and Coverage Ratio (CR)*. To this end, each one of the 32 bPV cells of this bPV window were not modelled individually, but as part of a single homogeneous semi-transparent bPV module. *Figure 18* illustrates this modelling approach.

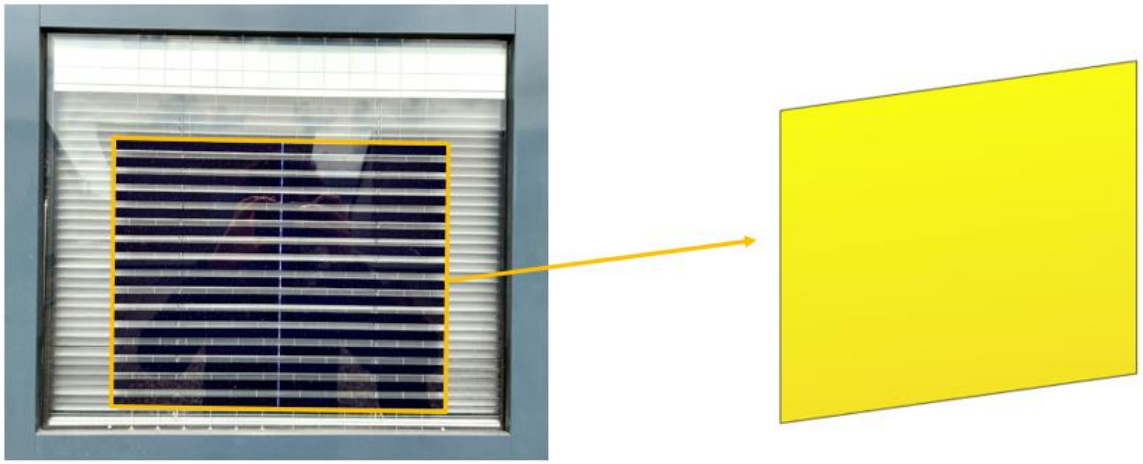

Figure 18: (left) a picture of a bPV window demonstrator in real life, where the two blocks of bPV cells are framed in orange. This area has a cell CR of 60%. (right) the two blocks of bPV cells modelled in BIGEYE as a single homogeneous semi-transparent bPV module.

As the cell CR of this bPV is of 60%, a transparency level of 40% was defined for this homogeneous bPV module to account for the empty spaces between the thin bPV cell stripes that the bPV window demonstrator hold in reality.

The reason behind choosing this modelling approach was mainly influenced by limitations in the computational power of the *BIGEYE* software calculation engine, since practical experience using the simulation software showed that each additional object inserted in the bPV window model significantly increased the computational time of the simulations. As a result, this modelling approach allowed to just add one single object to the bPV model, instead of the 32 objects that would have to be inserted if each bPV cell was modelled individually. In this way, this modelling approach allowed to optimize the amount of inserted objects into the bPV window model, while still getting a high degree of accuracy in performance simulations, as will later be shown in section *4.5 Validation of the electrical model*.

Additionally, if each one of the 32 bPV cells would have been modelled individually, they would have to be modelled as very small bPV modules, and not exactly as bPV cells as they are in real life. This is because *BIGEYE* was specially designed for modelling and simulating the performance of bPV modules, hence the insertion of individual bPV cells is not supported in the current software version.

Finally, internal discussions with *BIGEYE* developers and employees at TNO who previously used this software indicated this to be the most appropriate approach to model the thin bPV cell stripes.

In this way, this bPV module was modelled with the same azimuth and tilt angle than those of the bPV window demonstrator in real life, namely oriented toward the South and with a tilt angle of 90° (completely vertical). Some of the most relevant parameter values that were used to model this bPV module are described in *Table 3*:

Table 3: most relevant input parameters used in BIGEYE to model the bPV module that was used to model the thin bPV cell stripes of the bPV window.

Parameter	Value	Units
Module size (long side)	0.333	m
Module size (small side)	0.265	m
Number of cells along long side	2	-
Number of cells along short side	16	-
Transparency factor	0.40	-
Module bifaciality factor	0.82	-
Module efficiency at STC	0.16	-
Heat transfer coefficient for conduction	20	$W/(K*m^2)$
Heat transfer coefficient for convection	0	$W/((K*m^2)*(m/s))$
Module's absorption at the front side	0.95	-
Module's absorption at the rear side	0.95	-
Temperature coefficient for Isc	0.000269	A/K
Energy bandgap	1.05	eV
Energy bandgap temperature coefficient	-0.000135	eV/K
bPV cell area	16.6	cm^2
Module ideality factor	1.0	-
Module's I_{sc}	0.64	A
Module's saturation current, I_0	4.2E-12	A
Module's series resistance, R_s	3	Ohm
Module's shunt resistance, R_{sh}	1598	Ohm
Module's thermal halftime	20	min

4.2. Venetian blinds' modelling

Previously in section *3.6 Types of Venetian blinds under test*, a detailed description of the real-life properties of the different types of Venetian blinds under test was given. In this section, the approach followed to model them in *BIGEYE* is explained in detail

an explanation of the different tilt angles of the blinds that were tested as part of this research project will be presented. Furthermore, an explanation on the Venetian blind's modelling approach, including and input parameters will be covered

The modelling approach that was followed to model the Venetian blinds in *BIGEYE* was to model the slats as completely flat reflectors, instead of modelling the slightly curved shape they have in real life. Similarly as in the case of the thin bPV cell stripes modelling, this modelling approach was chosen mostly due to *BIGEYE* limitations to model curved objects. The current version of *BIGEYE* only supports the insertion of totally flat objects. Therefore, modelling the curvature of the Venetian blinds was not done. An initial approach consisted of modelling the curvature of the blinds as a series of smaller tilted flat surfaces placed consecutively to each

other to approximate a curved structure, but this approach was not implemented, as it would be quite complicated to model and would also add too much complexity to the bPV window model itself. Moreover, this approach would also considerably increase the number of inserted objects, which, as explained in the previous section, would be computationally expensive.

Important to mention is that when the Venetian blinds were modelled in *BIGEYE* at different tilt angles, their reflective properties were added only for one of their sides, namely the one which would be facing toward the bPV module (consequently, the other side of the slat, pointing toward the inside of the dummy building, did not have any defined reflective properties). Again, this simplification relies in the limitations of the current *BIGEYE* version to define an albedo coefficient applicable for both sides of a reflector object. A possible approach to overcome this limitation is to place two objects with their non-reflective sides together, allowing the reflective sides to face outward. Tests were conducted to assess the feasibility of this approach, showing it to have a minor effect in improving the accuracy of the bPV window model, while substantially increasing its complexity and computational time, as the number of blinds objects was doubled from 33 to 66. Therefore, this approach was discarded.

As part of this research project, four different blinds' positions were tested to assess their effect in boosting the bPV window performance. The tilt angles of these blinds' positions are detailed in *Table 4*. Additionally, a schematic illustrating the blind's inclination (with respect to an horizontal plane) is included, in which the yellow arrows represent the side of the modelled blinds for which the reflective properties were defined. Lastly, schematics of the blinds' alignment within the bPV window are also shown.

Table 4: Venetian blinds' tilt angles that were tested on the bPV window model. A description of the different tilt angles, blinds' schematics and bPV window's schematics are included.

Blinds' tilt angle [°]*	**Description**	**Blind's schematics**	**bPV window's schematics**
No blinds	Blinds are not deployed (reference case)	n.a.	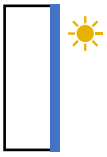
10°	Blinds are completely deployed and slightly tilted from the horizontal plane towards the bPV cells	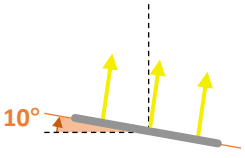	
60°	Blinds are completely deployed and almost closed (reflective side facing to the bPV cells and upward)	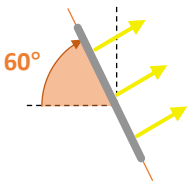	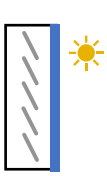

120°	Blinds are completely deployed and almost closed (reflective side facing to the bPV cells and downward)	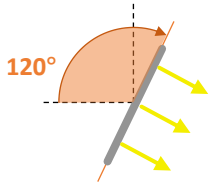	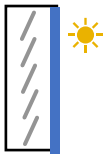

*With respect to the horizontal plane (perpendicular to the window's POA).

In this way, a set of 33 reflector objects simulating the Venetian blinds of this bPV window was vertically aligned behind the bPV module. *Figure 19 (left)* shows a view of the bPV module with the reflective slats incorporated behind it, as modelled in *BIGEYE*. *Figure 19 (right)* shows a side view of both bPV window components. As can be appreciated, all the Venetian blinds are all vertically aligned, just as in real life.

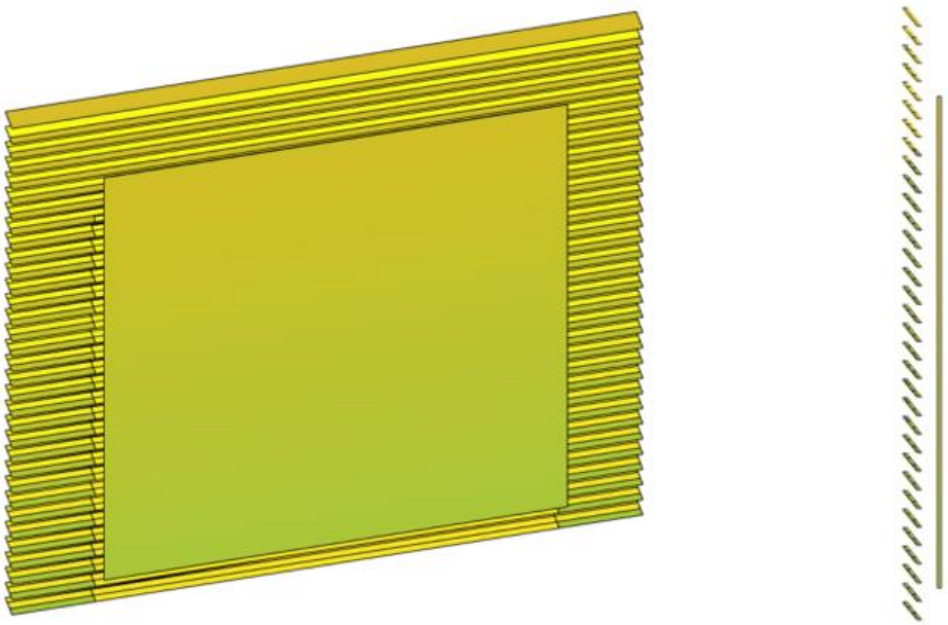

Figure 19: (left) set of Venetian blinds incorporated behind the bPV module, as modelled in BIGEYE. (right) side view of both bPV window components (slats and bPV module).

Due to limitations in the *BIGEYE* software, it was not possible to model the spectral reflectance of the Venetian blinds (previously shown in *Figure 13)*, nor their average proportion of specular and diffuse reflectance components (shown in *Figure 14*). Instead, the reflective slats that simulate the Venetian blinds were modelled as fully diffuse reflectors (which can scatter light with an equal distribution in all directions). To compensate this effect, suitable albedo coefficient values for the Venetian blinds in the model were chosen as part of the validation work conducted to create the bPV window models (see sections *4.4 Validation of the optical model: the total front-side irradiance* and *4.5 Validation of the electrical model)* and in line

with the experimental measurements what were conducted in parallel. In this sense, the validation process consisted on making sure that the different combinations of simulated blinds' tilt angles and albedo coefficient values caused a similar effect in the simulated electrical performance as the one observed in real life from the measurement campaigns that were conducted.

In this way, the albedo coefficient values for the different types of blinds were defined in *BIGEYE* as follows:

- S157 (grey colored, highly diffuse reflectance and most sold commercially): albedo = 0.55
- S102 (white colored, almost completely diffuse reflectance): albedo = 0.66
- V95 (silver colored, highly specular reflectance): albedo = 0.8

4.3. Dummy building and PV field's modelling

The final step in the creation of the bPV window models consisted in modelling the dummy building in which the bPV window is embedded, and the rest of the PV field over which this dummy building lies. These structures have been illustrated in *Figure 20*.

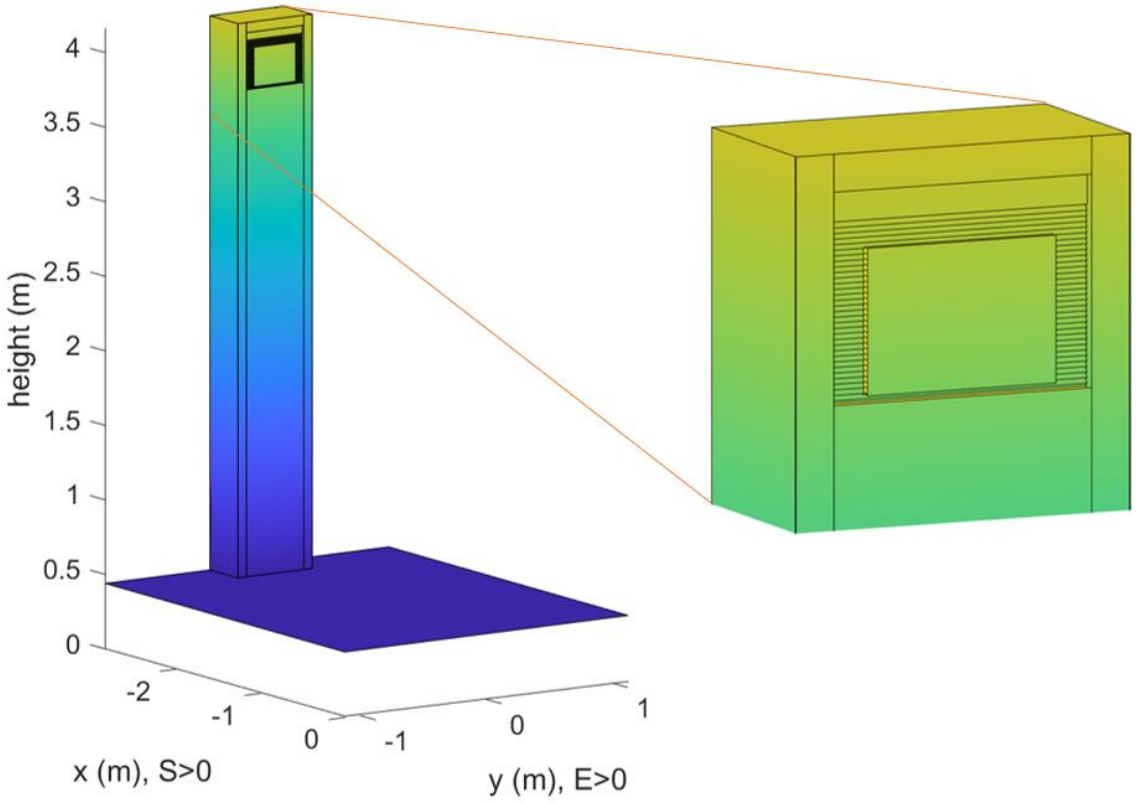

Figure 20: (left) finalized structure of the bPV window model, showing a dark platform (in dark blue color) with the dummy building on top, in which the bPV window with integrated Venetian blinds have been installed (right).

As can be seen from the figure, the dummy building has been modelled by adding several reflector objects together to form a rectangular structure. Similarly as mentioned in the previous section for the blinds, the reflective properties of these reflector objects are situated at that side facing to the inside of the dummy building, as in real life these surfaces slightly reflect sunlight (see *Figure 8*) and can contribute with some reflection toward the rear side of the bPV cells. The albedo coefficient value of all these reflector objects was equally defined (albedo = 0.35) to account for both, the wooden surface and the surface wrapped with black-colored paper seen in *Figure 8*. The only exception was the albedo coefficient value defined for the reflector object at the back side of the dummy cabin, as this one represents a black cloth that was placed in real life right behind the bPV window demonstrators to isolate the reflective effect of the blinds as much as possible and to minimize the contribution of artificial illumination coming from the inner side of the dummy building, just as previously described in section *3.2 bPV window demonstrator test setup*. For this particular reflector object, the albedo coefficient was defined with a value of 0.15. It is important to realize that in real applications, this cloth is of course not used, and the bPV windows can receive an extra light contribution on their rear side mainly due to artificial light illuminating the inner spaces. As a consequence, their power output in real applications could be slightly increased from this effect.

Finally, the black platform in which the dummy building stands (see *Figure 7*) was also included in the model (albedo = 0.05), which has some important effect in the reflected irradiance. Similarly, by specifying a ground entry, the properties of the ground surface in which the whole bPV facility stands can be set. This entry contains information about the size of the ground surface (corresponding to the size of the ground surface in front of the dummy building at *SolarBEAT*), its meshpoint granularity (number of sections in which the ground surface will be divided for performing the calculations in the simulation procedure) and other relevant ground parameters. The albedo coefficient value of the ground surface was defined as 0.2 to account for the dark pebbles laying on the ground at *SolarBEAT* (see *Figure 6*).

4.4. Validation of the optical model: the total front-side irradiance

Initial simulation efforts were focused on validating the results from the simulated irradiance on the front side of the window plane. This first validation step consisted on making sure that the simulated total irradiance on the front side of the window plane was consistent with experimental measurements. This was a key step in developing a model that will later be used to accurately simulate the electrical performance of this bPV window, as correctly inputting its electrical parameters would be pointless if the simulated irradiance would not consistent with real data, since this would lead to important deviations in performance estimations. The irradiance validation process was carried out across all seasons and under different weather conditions, namely sunny, partially cloudy, and completely overcast days, in order to test the model's robustness and reliability in simulating incoming irradiance under different operational scenarios.

Figure 21 presents an example of these validations for a fully sunny day (08/09/2023). As shown in this figure, the simulated front-side irradiance, represented by the orange curve,

closely follows the measured front-side irradiance, depicted by the blue curve, with minimal deviation. The agreement between the simulated and measured data demonstrates that the model is effective in simulating both, the magnitude and the trend of the real-world irradiance measurements. This close agreement between measured and simulated data across different weather and seasonal conditions demonstrated that the created model is able to simulate the front-side irradiance on the window plane with a high degree of accuracy, which is a crucial step before proceeding with the electrical validation of the model, which will be discussed in the following section. The other three curves in the figure, shown in gold, green, and grey, represent the simulated irradiance gain on the rear side of the window's plane when the V95, S102, and S157 blinds are used at a tilt angle of 60°, respectively. Finally, the purple curve represent the simulated irradiance gain on the rear side of the window's plane when no blinds are used. A detailed analysis of these curves will be presented in section *5.1 Influence of type of blinds*.

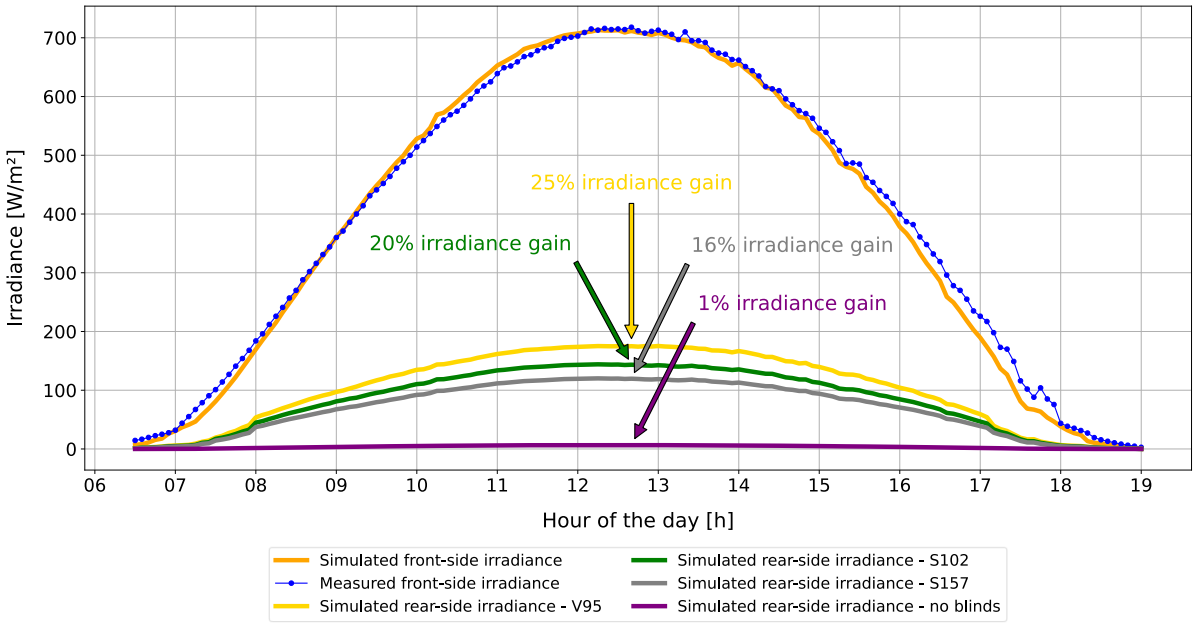

Figure 21: comparison between measured (blue) and simulated (orange) irradiance on the front-side of the window plane in a fully sunny day (08/09/2023). The simulated irradiance gain on the rear-side of the window plane when the V95, S102 and S157 blinds are used at a tilt angle of 60°, and when no blinds are used at all, is also shown.

Additional examples of similar plots as the one shown in *Figure 21* are shown in *Figure 22* and *Figure 23* for a partially cloudy day (03/04/2024) and a totally overcast day (26/05/2024), respectively.

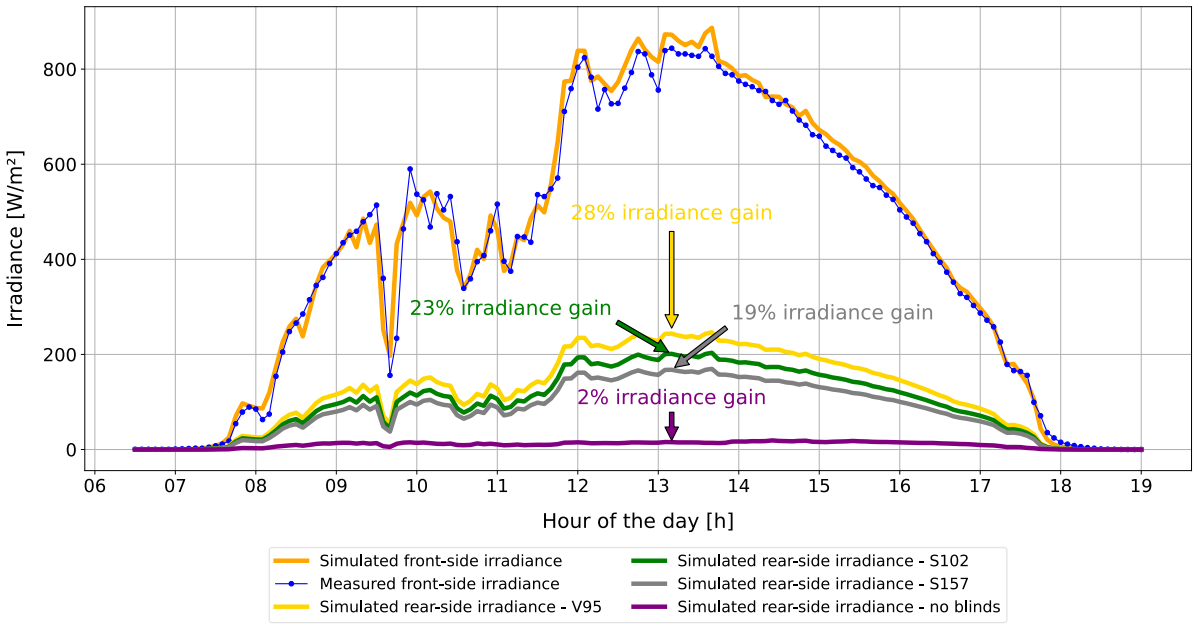

Figure 22: comparison between measured (blue) and simulated (orange) irradiance on the front-side of the window plane in a partially cloudy day (03/04/2024). The simulated irradiance gain on the rear-side of the window plane when the V95, S102 and S157 blinds are used at a tilt angle of 60°, and when no blinds are used at all, is also shown.

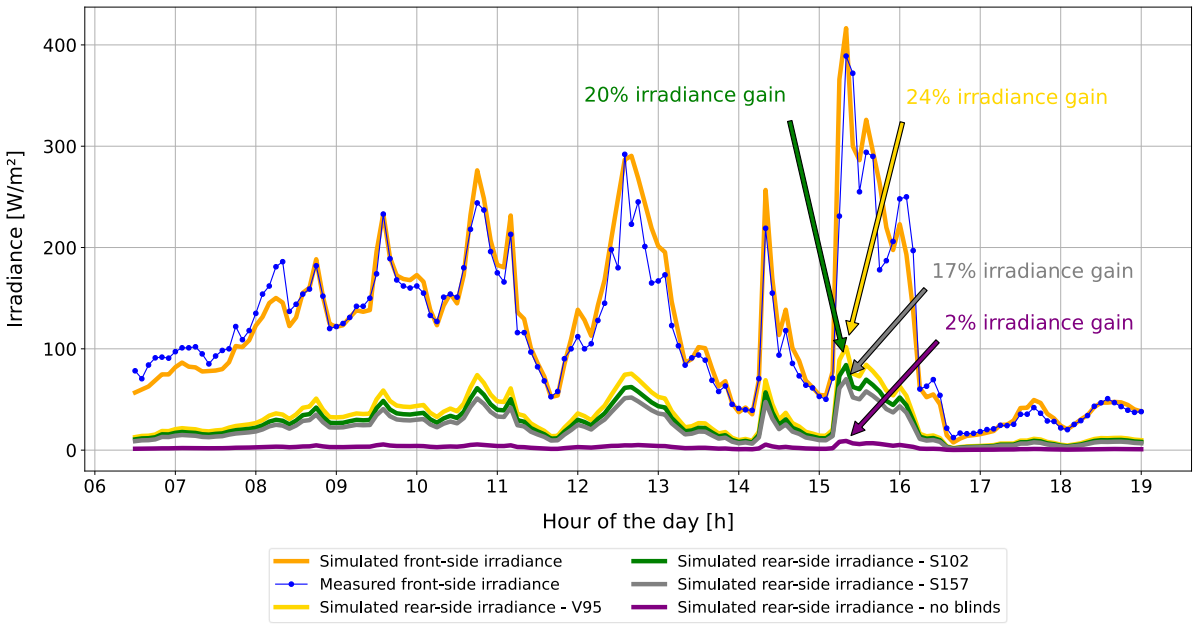

Figure 23: comparison between measured (blue) and simulated (orange) irradiance on the front-side of the window plane in a totally overcast day (26/05/2024). The simulated irradiance gain on the rear-side of the window plane when the V95, S102 and S157 blinds are used at a tilt angle of 60°, and when no blinds are used at all, is also shown.

4.5. Validation of the electrical model

The next step in the model's validation process consisted on verifying its capability to accurately simulate the electrical behavior of the windows. This was done by comparing the results of the simulated electrical performance with experimental outdoor measurements, and this validations were conducted for all seasons, in different weather conditions and with different blind positions to test the accuracy and reliability of the model in different operational scenarios. *Figure 24* shows an example of this kind of validations, which corresponds to a fully sunny day (29/07/2024) with S102 blinds deployed at a tilt angle of 60°.

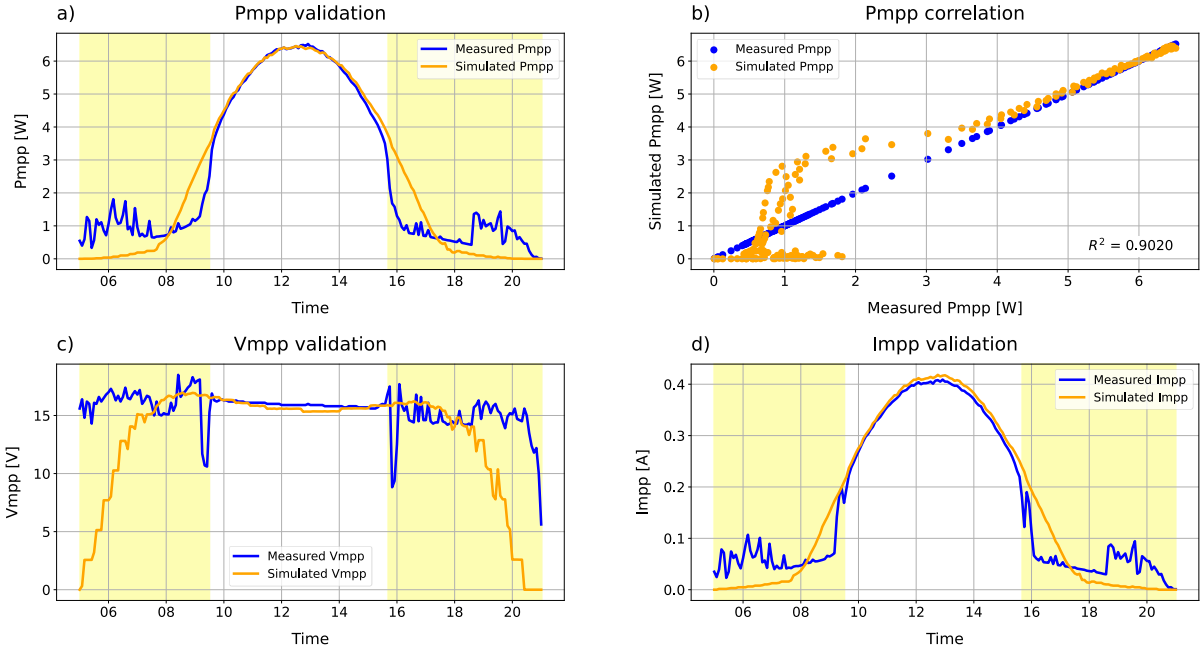

Figure 24: example of electrical validation of a fully sunny day (29/07/2024). On this day, the S102 (diffuse) blinds were deployed at a tilt angle of 60 °.

Figure 24 a) shows the comparison between the measured and simulated power at the maximum power point (P_{mpp}) on this particular day. Although the model can accurately simulate the power output of the window demonstrators for most of the day, there are two underlying effects that cause an important mismatch between both curves for the rest of the time, which have been highlighted in yellow. Firstly, it is possible to observe some peaks in the measured P_{mpp} at the first and last hours of the day. These peaks in the measured power does not correspond to actual power being produced by the window, but are noisy, unreal measurements from the I-V tracer that are always present at low irradiance levels and that affect the V_{mpp} and I_{mpp} measurements, at these moments, making them not reliable. Secondly, next to these noisy measurements there is also an important mismatch between measured and simulated P_{mpp}, where the latter is considerably overestimated. This difference can be explained by the fact that the experimental setup experiences some shading caused by surrounding cabins at the research facility (visible in *Figure 6*), which were not included in the simulation model. This turns the simulated P_{mpp} as a reliable estimation of the real performance of the windows, as both undesired effects were

excluded from the model. Excluding both effects was also necessary to assess the real potential of the blinds to boost the power output of the windows, which will be further analyzed in the upcoming sections.

Figure 24 b) shows the correlation between measured and simulated P_{mpp}. On this plot, measured P_{mpp} has been plotted on both axes, so that measured datapoints form a straight line (x=y). In this way, the alignment of simulated P_{mpp} to this straight line can provide information on how accurate are the results from the simulations compared to the experimental measurements. As can be seen from this figure, both undesired effects discussed for *Figure 24 a)* are visible for P_{mpp} values below 3.5 W. However, at higher P_{mpp} levels, simulated P_{mpp} align quite well with measured P_{mpp}. Even if both undesired effects of measured P_{mpp} are taken into account, the R^2 coefficient is still high (of around 0.9 on this particular day), with the potential of being even higher if these affects (datapoints) are discarded, showing that there is a strong correlation between the simulated and measured P_{mpp} and indicating that the simulated values can accurately explain the variability of the measured ones.

Similarly as in *Figure 24 a)*, *Figure 24 c)* shows the comparison between measured and simulated V_{mpp}. It is possible to observe that simulated V_{mpp} aligns quite well with experimental measurements for most of the day and also shows less noise, which indicates that the model can accurately simulate the operational voltage of the windows. An important effect highlighted in yellow can also be seen in this plot, which consists on the measured V_{mpp} starting earlier in the day and decaying later than the simulated V_{mpp}. This effect in the measured operational voltage is also caused by the noisy measurements of this particular measurement equipment at low irradiance levels (as explained for *Figure 24 a*). This is a feature that is not accounted for by the model, which allows to isolate this undesired effect and simulate the actual V_{mpp} of this bPV window solution. In this way, it can be said that the simulated V_{mpp} is representative of the operational voltage of the windows under real operation conditions.

Finally and similar to the case of *Figure 24 a)*, *Figure 24 d)* shows the comparison between measured and simulated I_{mpp} on this particular day. It is possible to observe the simulated I_{mpp} following quite closely the behavior of the experimental measurements, showing the capability of the model to accurately simulate the current production of the windows thanks to both, their accurate electrical modelling and a thorough irradiance modelling. Both undesirable effects on the experimental measurement that were previously described for *Figure 24 a)* can also be seen highlighted in yellow on this plot, as they primarily have an effect on this electrical parameter (and, consequently, on the P_{mpp}).

Additional examples of similar validation plots as those shown in *Figure 24* are presented in *Figure 25* and *Figure 26* for a partially cloudy day (18/10/2023) and a totally overcast day (05/04/2024), respectively. Just as in *Figure 24*, periods of time at which low irradiance levels caused measurement noise have been highlighted in yellow.

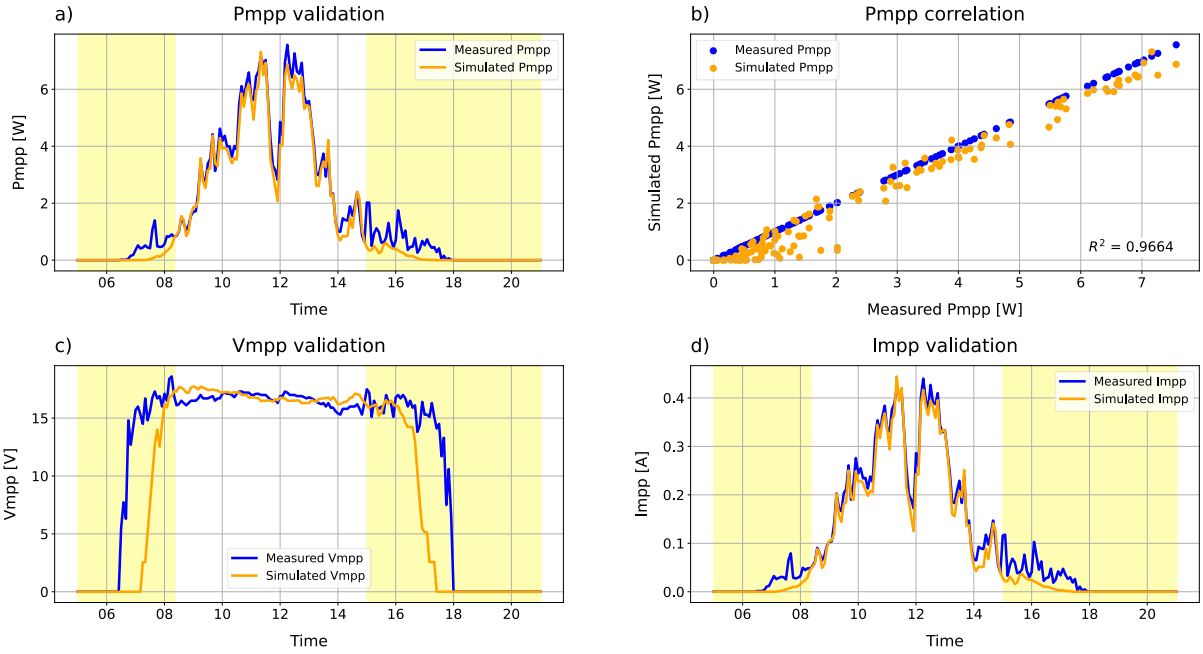

Figure 25: example of electrical validation of a partially cloudy day (18/10/2023). On this day, the S102 (diffuse) blinds were deployed at a tilt angle of 120°.

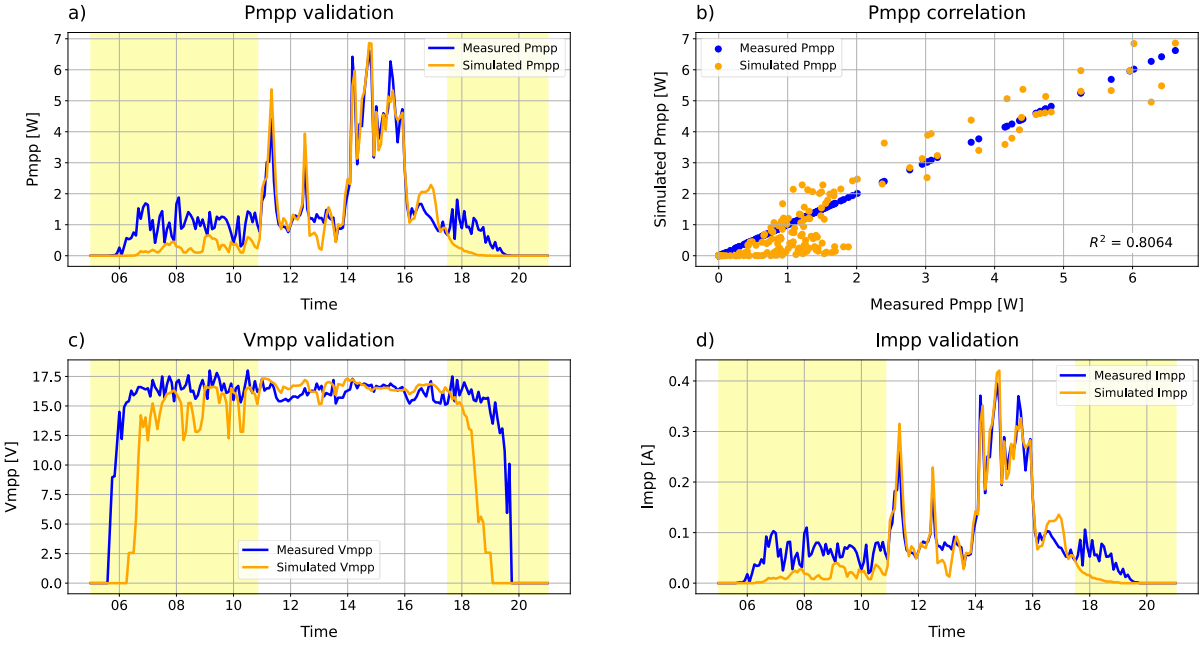

Figure 26: example of electrical validation of a totally overcast day (05/04/2024). On this day, the S102 (diffuse) blinds were deployed at a tilt angle of 60°.

In summary, section *4.1 bPV cell stripes' modelling* through section *4.3 Dummy building and PV field's modelling* presented the followed approach to model the bPV window in *BIGEYE*,

explaining the different assumptions and simplifications that were made and giving detail on the values used to describe the geometrical, optical, electrical and thermal properties of the bPV window and the PV field. In this way, the bPV window models were satisfactorily created, therefore achieving Objective 1 (O1: create a set of PV simulation models that describe the performance of this BIPV window when different types of reflective Venetian blinds are used).

Moreover, as it was previously shown in sections *4.4 Validation of the optical model: the total front-side irradiance* and *4.5 Validation of the electrical model* a set of optical and electrical validations against experimental data were conducted to make sure the created models were able to simulate the irradiance received at the front side of the window plane and to make sure that the models can accurately simulate the electrical performance of the bPV window demonstrators under real operation conditions. In this way, it was ensured that the created models were a reliable tool for accurately simulating the real performance of the experimental bPV window demonstrators, therefore achieving Objective 2 (O2: validate the created models with experimental data to test their accuracy and reliability).

5. Results and discussion

This chapter presents the results obtained from the simulation work conducted in this project, along with an analysis of these findings. In this way, the results presented in this chapter were obtained just from simulations. Measured data has only been included for comparison purposes in *Figure 33* of section 5.2.

The subsequent sections 5.1 through 5.4 are directed toward fulfilling Objective 3 (O3: use the created models to perform different simulations to assess the performance of this bPV window when different blind configurations are used). Specifically, section *5.1 Influence of type of blinds* will address Research Question 1 (RQ1: how do different types of Venetian blinds affect the electric performance of the bPV windows? What other factors influence its behavior?), while section *5.2 Influence of blind's tilt angle* covers Research Question 2 (RQ2: how does the position of the Venetian blinds affect the overall performance of the bPV windows? Can we quantify the boosting effect given by the different blind configurations and find the optimal one?). In section *5.3 Influence of blind's AOI*, Research Question 3 (RQ3: which other factors have an influence on the bPV window performance? Does it also depends on meteorological or geographical conditions?) is examined, and finally, Research Question 4 (RQ4: can we quantify the boost in yearly specific yield (YSY) given by the different blind configurations? How much can it be in other locations when the optimal blind configuration is used?) is discussed in section *5.4 Overall performance assessment*. Together, these sections provide a comprehensive evaluation of the research outcomes in line with the research questions and project's objectives.

5.1. Influence of type of blinds

The simulation model can also provide additional information on the rear-side irradiance gain due to the use of the blinds, which in real life cannot be directly measured from the experimental setup. An example of this effect was previously shown in *Figure 21*, in which the simulated rear-side irradiance contribution of the three blind types under test was quantified when fully deployed at an angle of 60° on the same day. As it is clear from this figure, thanks to the deployment of the blinds it is possible to increase the rear-side irradiance received by the bPV cell stripes by 25% (with respect to the total irradiance received on the front side of the window plane) at the time of the maximum power production of this day when the V95 blinds are used. Moreover, a contribution of an extra 20% and 16% was quantified at the same moment when the S102 and S157 blind types were used, respectively.

These simulation results can be explained by the fact that the V95 (silver colored), S102 (white colored) and S157 (grey colored) have been modelled with a progressively decreasing albedo coefficient value to account for the reflectance properties that the blinds have in reality, which were presented in section *3.6 Types of Venetian blinds under test*. Therefore, it is natural to expect the V95 blinds to provide a higher irradiance gain on the rear side of the window plane, followed by the S102 and finally, the S157. This means that the V95 blinds are more effective in reflecting and directing sunlight toward the rear side of the bPV cell stripes, followed by the

S102 and the S157 blinds. This will ultimately determine the boost in window performance that every blind type is able to provide, as will be further discussed in this section.

In real life, the previous effect of the three blind types on the irradiance gain can be explained not only by the fact that V95 blinds have an overall higher reflectance in the c-Si spectral absorption range, but also by the fact that this type of blinds reflects light in a very directed manner (like a mirror) due to its specular reflection properties; which means that most of the sunlight reaching them is mostly reflected in a specific direction rather than scattered away in many directions. With this particular blind's tilt angle, the directed reflection of the V95 blinds allows more sunlight to be effectively redirected towards the rear side of the bPV cells, and this concentration effect is what leads to a higher irradiance gain, as more sunlight is being focused onto the cells. Different is the case of S102 blinds, as they scatter incoming sunlight in many different directions due to its diffuse reflection properties. The light scattering effect taking place in this case, although still capable of redirecting some light onto the cells, is less focused towards them as in the case of the V95 blinds. As a result, S102 blinds still can increase the irradiance gain in a substantial way, but they do it less effectively compared to the V95 blinds, since part of the reflected light is scattered away from the bPV cells.

Finally, S157 blinds demonstrated to have the lowest overall reflectance in the spectral absorption range of c-Si solar cells, as previously shown in *Figure 13*. This property is what causes less of the reflected sunlight to reach the rear side of the bPV cells, making its contribution less effective to boost the irradiance gain. This is consistent with the fact that this type of blinds have been designed for shading purposes, and have not been optimized for light reflection as in the case of the other two blind types, which reflectance peak has been optimized for the most energetic sunlight spectrum range (400-700 nm).

Quantifying the contribution of the irradiance gain received on the rear side of the window plane is not trivial information. It is an important step toward developing a reliable model, as the electrical validation highly depended on this parameter as well. Moreover, it is a fundamental metric when aiming to optimize the window design, for instance, by incorporating a different type of blinds with more efficient optical properties. Furthermore, the quantification of this parameter provides an insight on the bPV window performance boosting potential of the different types of blinds under study, as both quantities are directly proportional to each other.

To evaluate the impact of using different blind types on the bPV window performance, a series of simulations for a typical meteorological year (TMY) in Eindhoven were conducted, in which, for every case, the tilt angle of the blinds was kept constant across all blind types to quantify and compare the effects of using different blinds on the bPV window performance. The goal of these simulations was to measure the absolute variation in performance with respect to a reference scenario, in which the blinds were not used. This approach allowed to get an insight on the potential of the different blind types to enhance the bPV window performance. Additionally, these simulations provided insights into other important factors that also have an influence on this outcome, such as the angle of incidence (AOI) formed between the sun and the blinds' surface normal. The monofacial temperature-corrected performance ratio (TCPR) (see section *2.4. The Performance Ratio (PR) and Temperature-Corrected Performance Ratio (TCPR) metrics*) was used as the primary performance indicator for the bPV windows in this analysis.

The results of the absolute boost in the TCPR of the windows (with respect to the case of no blinds) when different types of blinds are used and their tilt angles are kept the same are shown in *Figure 27* - *Figure 29*. In these figures, a simulated time series of the absolute boost in TCPR on a TMY in Eindhoven is plotted to observe the effects in the window performance throughout the year when different types of blinds are used at constant tilt angles of 10°, 60° and 120°, respectively. An horizontal line representing the yearly average TCPR of each blind configuration has been included in these plots.

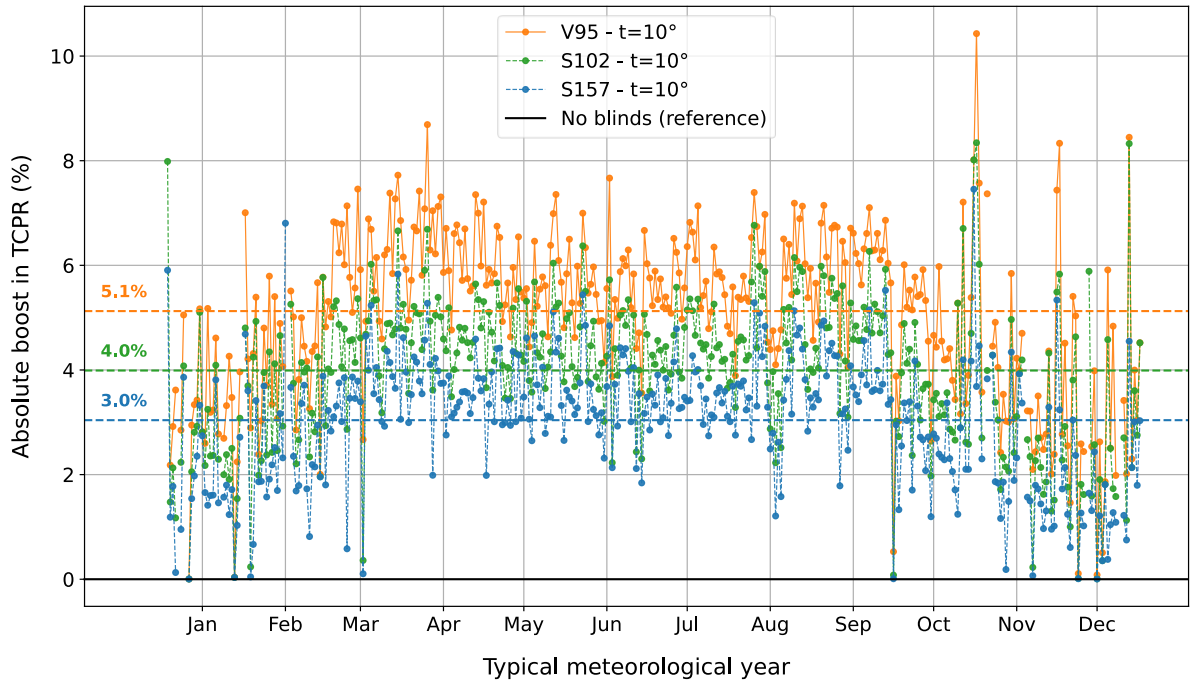

Figure 27: simulated absolute boost in daily TCPR of different blind types at a tilt angle of 10° on a TMY in Eindhoven.

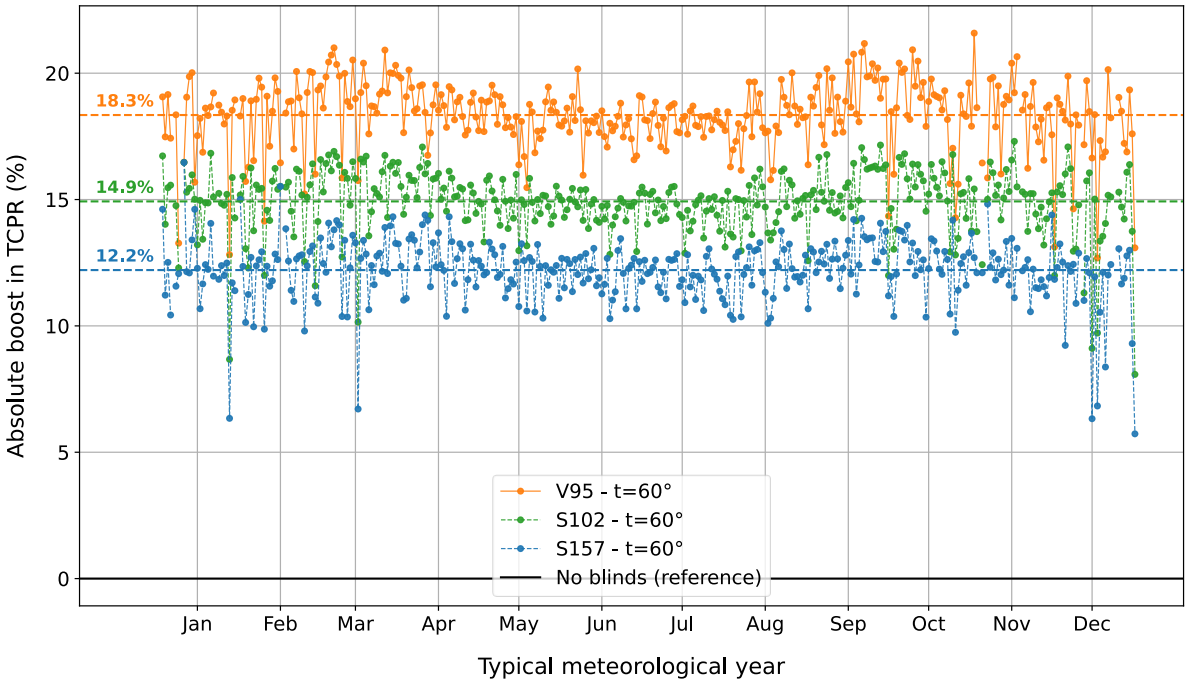

Figure 28: simulated absolute boost in daily TCPR of different blind types at a tilt angle of 60° on a TMY in Eindhoven.

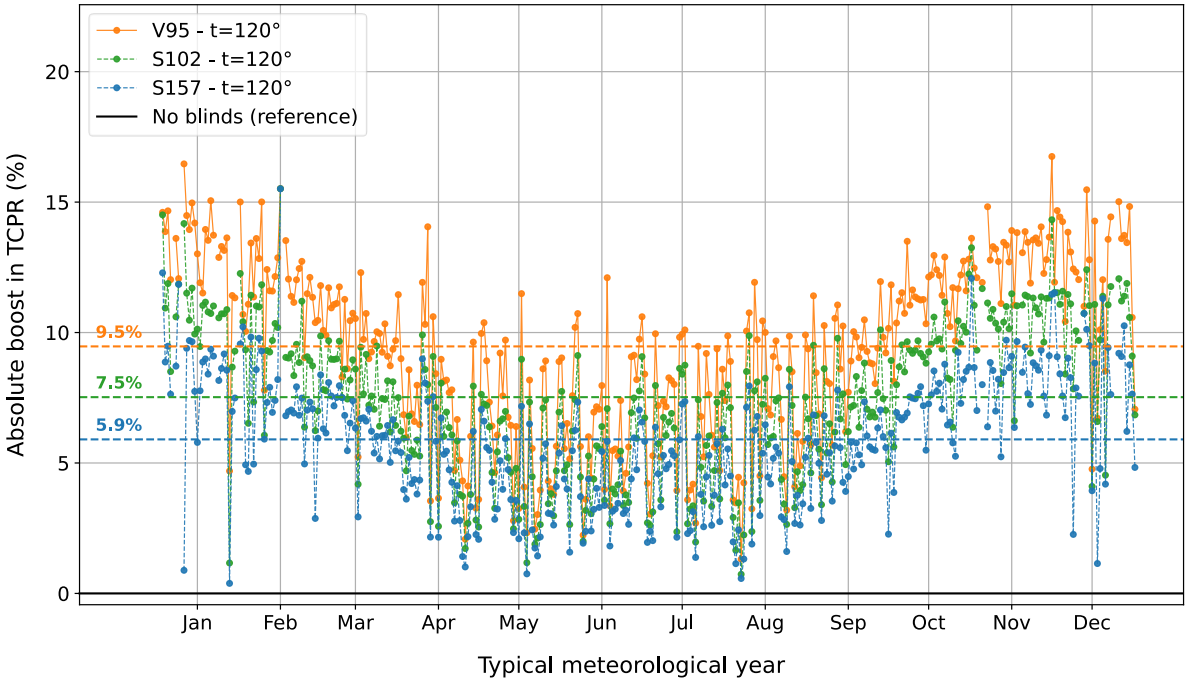

Figure 29: simulated absolute boost in daily TCPR of different blind types at a tilt angle of 120° on a TMY in Eindhoven.

From the plots shown in *Figure 27-Figure* 29, two critical observations can be made. Firstly, it is important to highlight a consistent trend observed throughout the year, in which the

performance boosting effect of the three blind types follows the same order regardless of the blind's tilt angle. Specifically, the V95 blinds consistently achieve the highest absolute boost in TCPR, followed by the S102 blinds, and finally the S157 blinds. This trend can be attributed to the fact that each blind type has been modeled as a completely diffuse reflector with a progressively lower albedo coefficient to simulate the reflectance properties that blinds have in real life, which, as previously shown in section *3.6 Types of Venetian blinds under test*, they hold the same order in reflectance properties between each other. Ultimately, this sequential reduction in the albedo coefficient value of the blinds is what causes a lower absolute boost in TCPR, as each subsequent blind type reflects and redirects sunlight toward the rear side of the bPV cells in a less effective way.

Secondly, the pattern observed in the yearly behavior of each figure, corresponding to each tilt angle under study, provides insight into an underlying effect that significantly influences the window's performance, namely, the AOI formed between the sun and blinds' surface normal. In *Figure 27*, where the blind's tilt angle was kept constant at 10°, a similar trend can be observed across all three blind types. This trend reveals a higher performance boost during the summer months and a lower boost in winter ones, giving these curves a characteristic concave shape over the annual timeframe. In summer, when the sun follows its highest trajectory across the sky, the AOI between the sun (high in the sky) and the blinds at a tilt angle of 10° (almost horizontal) is minimized. As a result, sunlight can reach the blinds more directly, allowing for more effective diffuse reflection, characterized for being scattered in all directions. In this way, more sunlight can reach the rear side of the bifacial PV cells, which maximizes the boost in power production at this time of the year when the blinds are positioned at this particular tilt angle.

In contrast, during winter months, when the sun's path is significantly lower in the sky, this AOI formed between the sun and the blinds' surface normal increases substantially for the same 10° blind's tilt angle. As a result, sunlight reaches the blinds at a much steeper angle, reducing the blinds' ability to effectively redirect light toward the rear side of the bPV cells. This less direct interaction between sunlight and the blinds diminishes their potential to enhance power production, resulting in a less pronounced TCPR boost during winter. This interplay between blind's AOI and solar path throughout the year ultimately explains the concave shape observed in the TCPR boost for this particular blind tilt angle, with peak performance occurring during the summer months and a gradual decline in winter ones.

A similar explanation can be applied to the yearly behavior of the curves shown in *Figure 28*, corresponding to blinds being set at a constant tilt angle of 60°. At this particular blind's inclination, the absolute boost in TCPR exhibits a more stable and consistent pattern throughout the year, compared to the more variable behavior observed when they were positioned at a tilt angle of 10° (*Figure 27*) or a tilt angle of 120° (*Figure 29*). During summer months in this case, a slight decrease in the TCPR boost can be noted, as the higher AOI between the sun (high in the sky) and the blinds (almost pointing to the bPV cells) causes sunlight to reach the blind's at a steeper angle, reducing their effectiveness to reflect it toward the rear side of the window. In contrast, during winter months, when this AOI is generally lower, the blinds are slightly more effective in redirecting incoming sunlight, resulting in a slightly higher TCPR absolute boost. Overall, this tilt angle allows the blinds to consistently and efficiently reflect sunlight to the rear

side of the bifacial PV cells, providing a relatively steady performance enhancement across the year.

Finally, *Figure 29* illustrates the behavior of the absolute TCPR boost when the three blind types under study are deployed at a tilt angle of 120°. In this case, an opposite effect to the one previously shown in *Figure 27* can be observed. At this blind's tilt angle, a significant reduction in the absolute TCPR boost occurs during the summer months. This reduction can be attributed to the generally increased AOI between the sun, positioned high in the sky, and the blinds' surface normal, which points downward toward the ground. As a result, sunlight struggles to reach the front side of the blinds, which is responsible for providing the irradiance gain on rear side of the bPV cells. At certain times of the day, the sunlight can only reach the rear side of the blinds when they are positioned at this inclination, to be scattered toward the inside of the building, further limiting the ability of the blinds to boost the performance of the bPV window. These combined effects lead to the notable reduction in the absolute TCPR boost that the blinds can achieve at this specific tilt angle. Conversely, the highest absolute boost in TCPR can be observed during the winter months, giving these curves their characteristic convex shape over the annual timeframe. At this time of year, the sun follows a lower trajectory across the sky, reducing the AOI between the sun and the blinds' surface normal. As a result, the blinds can more effectively redirect sunlight to the rear side of the bPV cells, leading to a higher absolute boost in TCPR.

5.2. Influence of blind's tilt angle

To evaluate the impact that changing the tilt angle of the blinds has on the bPV window performance, the same data previously shown in Figure 27, Figure 28 and *Figure 29* are presented but plotted in a different way. This time, the same blinds' type was used consistently, while only their tilt angle was changed. The objective of these visualizations was to quantify the absolute variation in TCPR (compared to a reference case in which no blinds were used) when only the tilt angle of the blinds was varied. This was done to get an insight into how different blind's tilt angles can help to enhance the bPV window's performance.

Figure 30 - *Figure 32* show the results of these simulations, presenting a time series of the absolute TCPR boost when the slats are positioned at different tilt angles, for the S157, S102, and V95 blind types, respectively. These figures illustrate the yearly behavior of the TCPR boosting potential of the blinds at different tilt angles, allowing for a clear comparison of how different blind's position can help to enhance the performance of the bPV window over the course of one full year. An horizontal line representing the yearly average TCPR absolute boost of each blind configuration has been included in these plots.

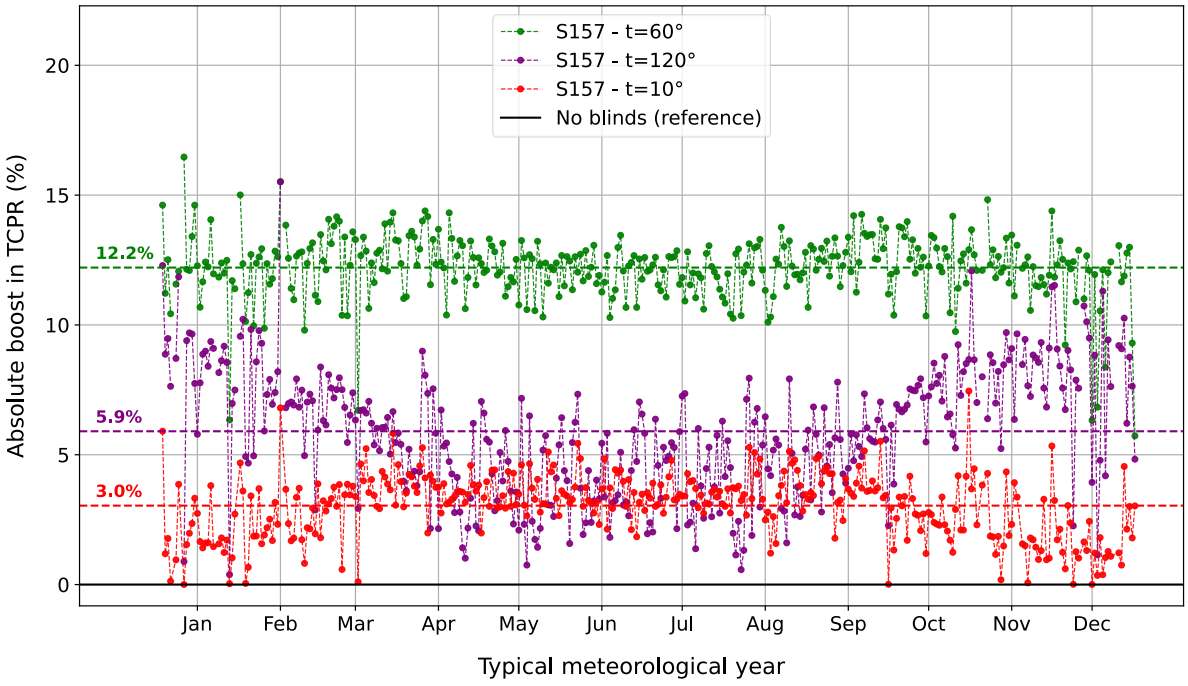

Figure 30: simulated absolute boost in daily TCPR of the S157 blinds at different tilt angles on a TMY in Eindhoven.

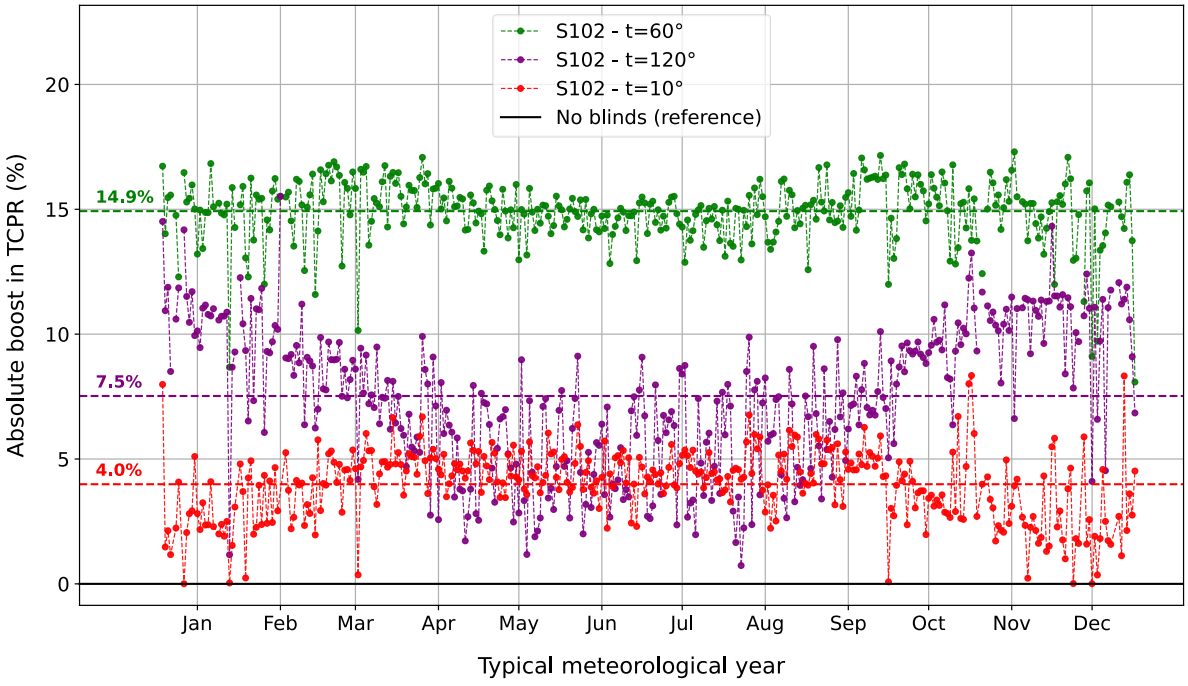

Figure 31: simulated absolute boost in daily TCPR of the S102 blinds at different tilt angles on a TMY in Eindhoven.

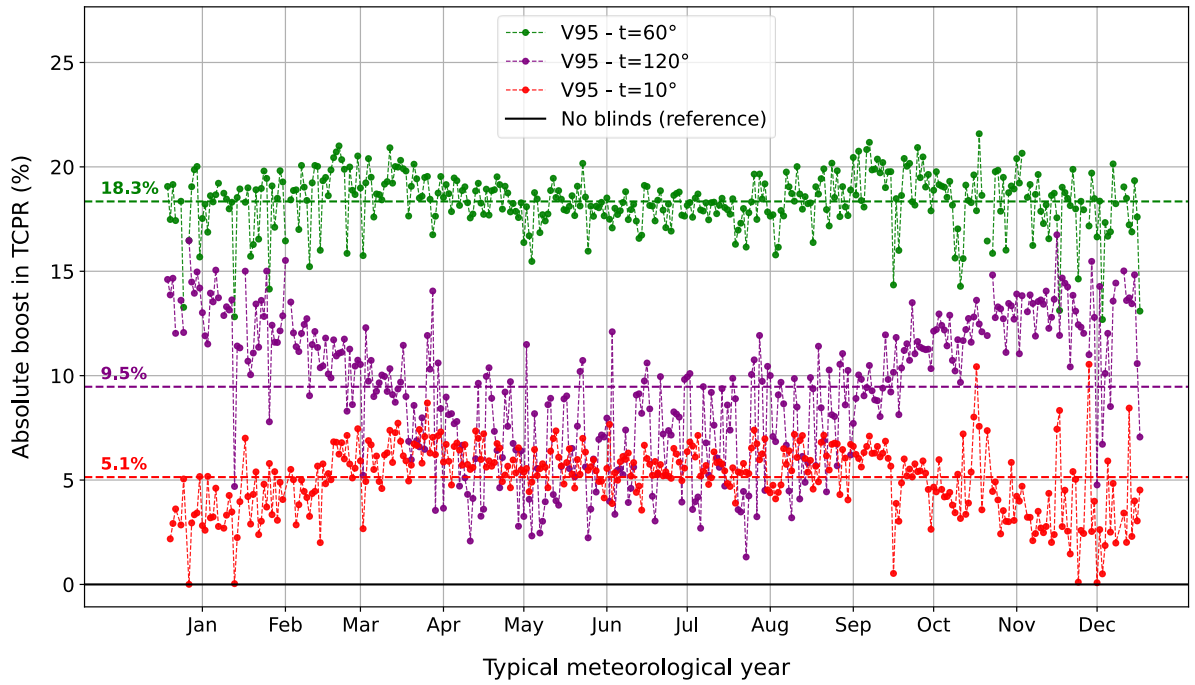

Figure 32: simulated absolute boost in daily TCPR of the V95 blinds at different tilt angles on a TMY in Eindhoven.

From *Figure 30 - Figure 32*, it is possible to observe that, regardless of the type of blinds that are used, the blinds positioned at a tilt angle of 60° not only consistently showed a more stable absolute TCPR boosting behavior throughout the year, but also demonstrated the highest overall boost in performance when compared to the other blind's tilt angles under study. This demonstrates that the 60° blind's inclination is the most optimal blind's position of the three for maximizing the performance of the bPV windows, as it consistently leads to a higher bPV window power output. Similarly, blinds positioned at a tilt angle of 120° were generally less effective at boosting the TCPR of the bPV windows compared to those at 60°, but they still outperformed the blinds set at a 10° tilt angle on a yearly basis. This highlights that while the 120° position is not ideal, it still provides a higher performance enhancement of the windows than if a 10° inclination is used, especially in the winter months (lower sun potions). Finally, the blinds positioned at a tilt angle of 10° showed to be the ones providing the smaller average boost in TCPR of the bPV windows. The explanation behind the yearly behavior of the curves plotted in these figures has already been discussed in section *5.1 Influence of type of blinds*.

It is possible to arrive at the same conclusions if the power output boosting effect achieved by the blinds positioned at different tilt angles is simulated for a single day. *Figure 33* shows an example of such simulation experiments, in which the effect of deploying the V95 blinds at different tilt angles was quantified for a fully sunny day (24/09/2023). On this day, the blinds of the corresponding bPV window demonstrator were completely kept up, and its measured P_{mpp} production is represented by the blue curve. The performance of the bPV window when no blinds were used was simulated for this day as well and is represented in the figure by the orange curve. As can be seen, this curve follows quite closely the measured data, indicating that

the model accurately simulated the real performance of the window under the real-life operation conditions. The model was also used to simulate three additional cases to show what the boost in P_{mpp} would be if the V95 blinds were at the three different tilt angles under test, namely at 10°, 60° and 120°, represented in the figure by the red, green and purple dashed lines, respectively.

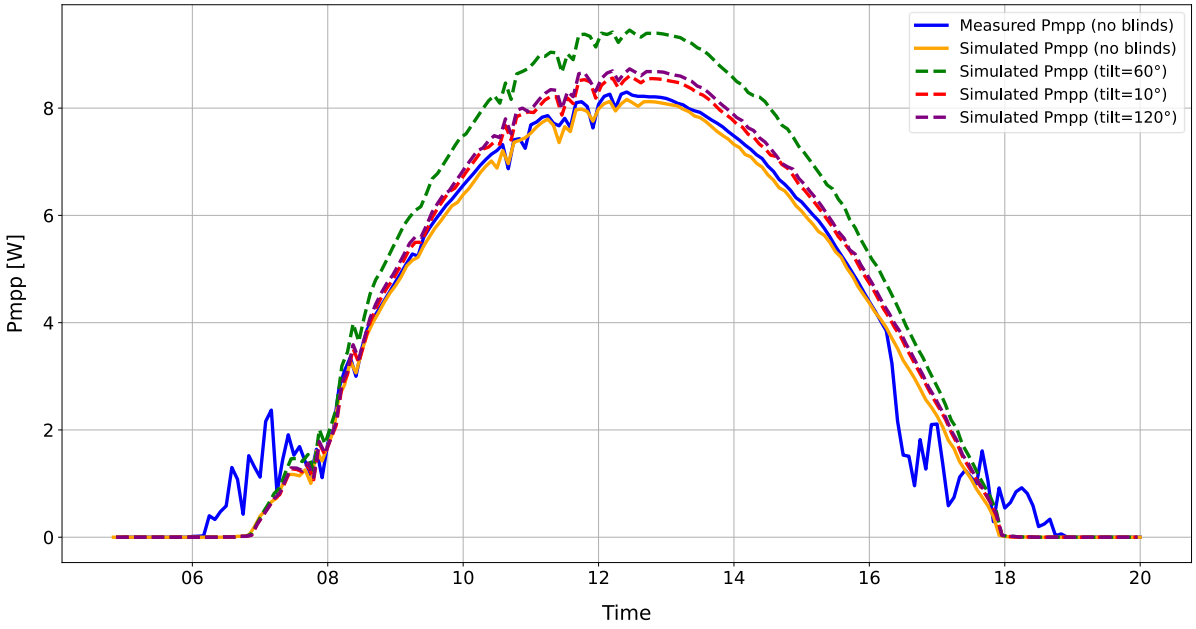

Figure 33: Boost in P_{mpp} achieved by V95 blinds at different tilt angles on a fully sunny day (24/09/2023).

As can be seen from the figure, the greatest boost in the P_{mpp} production of the window on this day was achieved when the V95 blinds were deployed at a tilt angle of 60° (depicted in green), followed by the 120° blind position (in purple), which provided only a slightly higher boost in P_{mpp} with respect to the blinds positioned at a tilt angle of 10° (in red).

As a summary of the simulation experiments presented in sections *5.1 Influence of type of blinds* and *5.2 Influence of blind's tilt angle*, *Table 5* presents the average yearly results of the plots previously shown in *Figure 30 - Figure 32*. As can be concluded from its values, the V95 blinds were consistently the ones providing the highest boost in the TCPR of the bPV windows, followed by the S102 blinds and finally, the S157. Regarding the blind's tilt angle, an inclination of 60° showed to be the optimal inclination of the three for maximizing the performance boost of the window, followed by the blinds positioned at a tilt angle of 120° and, lastly, the blinds inclined at a tilt angle of 10°.

Table 5: summary of the simulated yearly average absolute boost in TCPR achieved by the different blind configurations on a TMY in Eindhoven.

Type of blinds	tilt=10°	tilt=60°	tilt=120°
S157	+3%	+12.2%	+5.9%
S102	+4%	+14.9%	+7.5%
V95	+5.1%	+18.3%	+9.5%

5.3. Influence of blind's AOI

As the results presented in sections *5.1 Influence of type of blinds* and *5.2 Influence of blind's tilt angle* indicated that the AOI formed between the sun and the blinds' surface normal is an important factor influencing the effectiveness of the blinds to boost the bPV window's performance, a deeper analysis of this parameter and its correlation with other variables will be presented in this section.

Figure 34 shows the simulated hourly TCPR as a function of the AOI formed between the sun and the blinds' surface normal for each blind configuration over a typical meteorological year (TMY) in Eindhoven. As can be observed in the figure, regardless of the specific blind configuration, the scattered data points in every plot show a clear negative trend as the AOI between the sun and the blinds' surface normal increases. This trend indicates that a larger AOI between the sun and the blinds' surface normal has an overall effect of decreasing the performance of the bPV windows, therefore, the reflective blinds are in general terms more effective in boosting the performance of the bPV windows when sunlight reaches their surface in a more direct way. This can be explained by the fact that at higher blinds' AOI values, sunlight reaches the blinds at a steeper angle, which reduces their ability to efficiently reflect and redirect irradiance toward the rear side of the bifacial PV cells, ultimately leading to a decline in window performance.

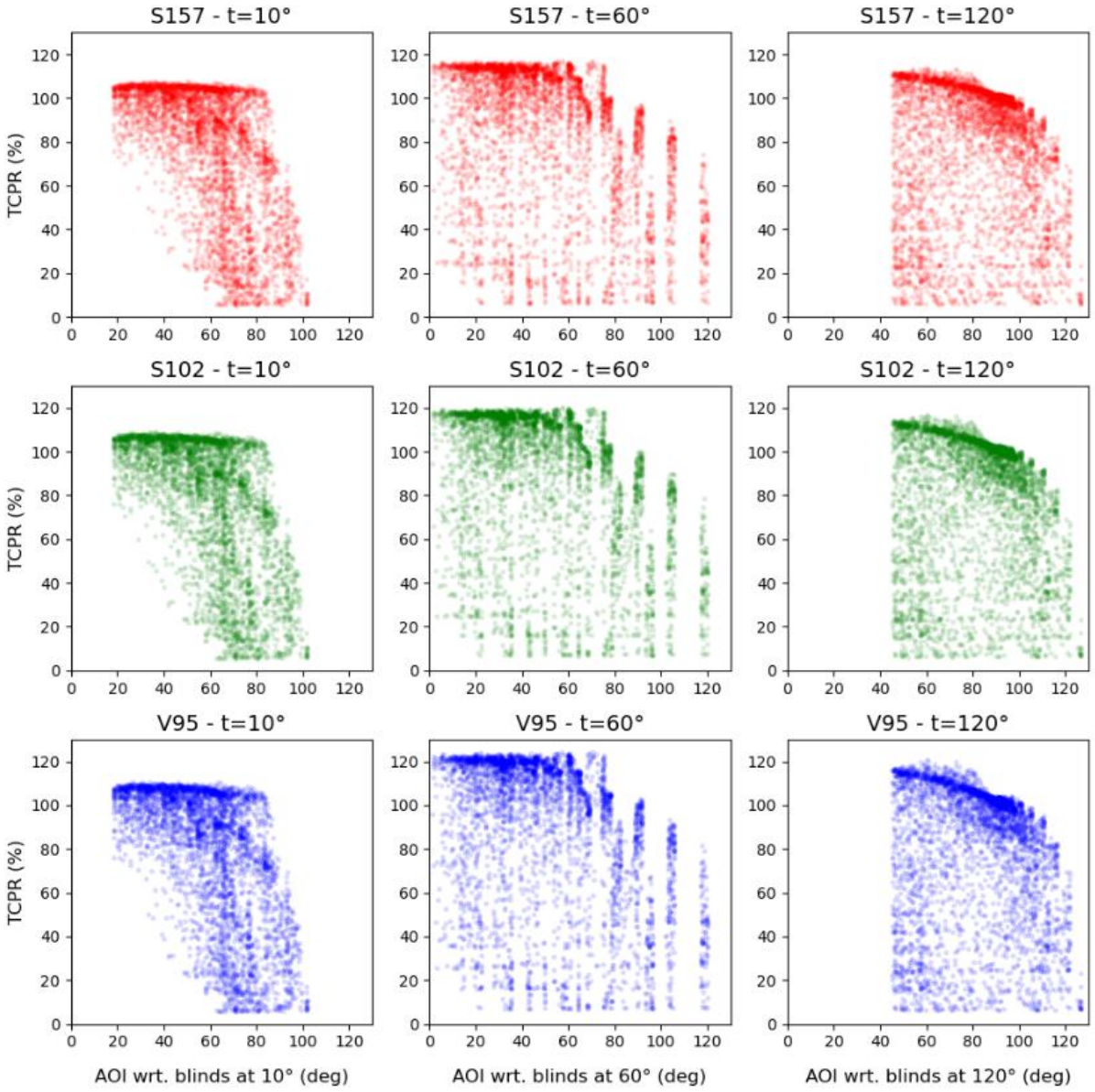

Figure 34: simulated hourly TCPR plotted as a function of the AOI formed between the sun and the blinds' surface normal on a TMY in Eindhoven for every blind configuration.

Additionally, *Figure 34* reveals that an important decline in TCPR becomes more pronounced beyond a certain threshold of AOI between the sun and the blinds' surface normal, suggesting that there is a critical AOI value for each blinds' position in which the bPV window performance starts to significantly drop as higher AOI values are reached. Identifying the critical AOI thresholds for every blind position results critical for optimizing the blind position control strategy if maximizing the window performance is desired. As can be observed from the first two columns of plots in the figure, which represent the blind's positioned at tilt angles of 10° and 60°, respectively, these blind's positions present critical AOI values of approximately 82° and 62°, respectively. This indicates that the performance of the windows tends to drop significantly when the AOI between the sun and the blinds' surface normal exceeds these angle thresholds. However, it is important to note that the window performance is not only determined

by this parameter. In practice, there are also other additional factors that play a role in the window performance, such as the available diffuse irradiance at any given time, quantified by the diffuse fraction, k_d (which is defined as the ratio between DHI and GHI and indicates the total fraction of solar irradiance that arrives as diffuse light, as opposed to direct sunlight), which influence in performance will later be discussed in this section.

In the specific case of the blinds positioned at a tilt angle of 120° (right column in *Figure 34*), the performance is reduced almost immediately as this AOI increases. This observation supports the notion discussed in the previous two sections that this blind position, characterized for having the slats pointing downward toward the ground, is specially suboptimal at higher sun altitudes (such as during the summer months), when sunlight reaches the blinds at sharper angles and only at reduced periods of time during the day. This shows that this blind position is less resilient to an increased AOI (sunlight incident at sharper angles) than others, for example, as if compared to that of the 60° blind position, which shows a more stable TCPR behavior over a wider range of AOI. In this way, it is possible to see that the performance drop for the blinds positioned at 60°, even though still present, is less pronounced than for the blinds positioned at 10° and 120°, suggesting that blinds at 60° are the most effective in maintaining a higher window performance even under less favorable sun angles.

Finally, it is also possible to notice that the first and third columns of plots, corresponding to the blinds positioned at tilt angles of 10° and 120°, respectively, exhibit a sharp cut in the distribution of their datapoints. In both cases, this effect can simply be explained by the fact that certain AOI are never reached at the respective blind positions at the specific location of Eindhoven. For instance, when the blinds are positioned at a tilt angle of 10°, only blind's AOI in the range of 20° to 102° are reached throughout the year, whereas when blinds are positioned at a tilt angle of 120°, only blind's AOI in the range of 45° to 128° are reached throughout the year. In this last case where the blinds are oriented downward toward the ground, lower AOI are never achieved because at this moments the sun is already below the horizon and the bPV windows are not generating any power, therefore not included as part of the simulated data. AOI above 90°, on the other hand, means that the sun is positioned at the rear side of the slats plane, thus no direct irradiance can reach the front side of the slats.

Similar plots as those presented in *Figure 34* have also been created to extend the previous analysis by correlating these two variables (blind's AOI and TCPR) with additional ones that also have an influence on the bPV window performance, namely the diffuse fraction (k_d), calculated as DHI/GHI, and the AOI between the sun and the window's plane normal. This was done to visualize the bPV window performance behavior with respect to the proportion between direct and diffuse irradiance and with respect to sun position to try to identify additional trends in performance. This extended analysis approach allowed to get an insight into how the combined effect of several factors play a role in the overall performance of the bPV windows, as it depends on the complex interplay between several parameters that act simultaneously. Moreover, this analysis revealed critical variable interactions that allowed to arrive to important conclusions regarding the blind's potential to enhance the bPV window's performance and provided valuable information to further optimize the blinds' control strategies. The correlation of these two variables (blind's AOI and TCPR) with the diffuse fraction (k_d) and the AOI

between the sun and the window plane's normal is presented in *Figure 35* and *Figure 36*, respectively.

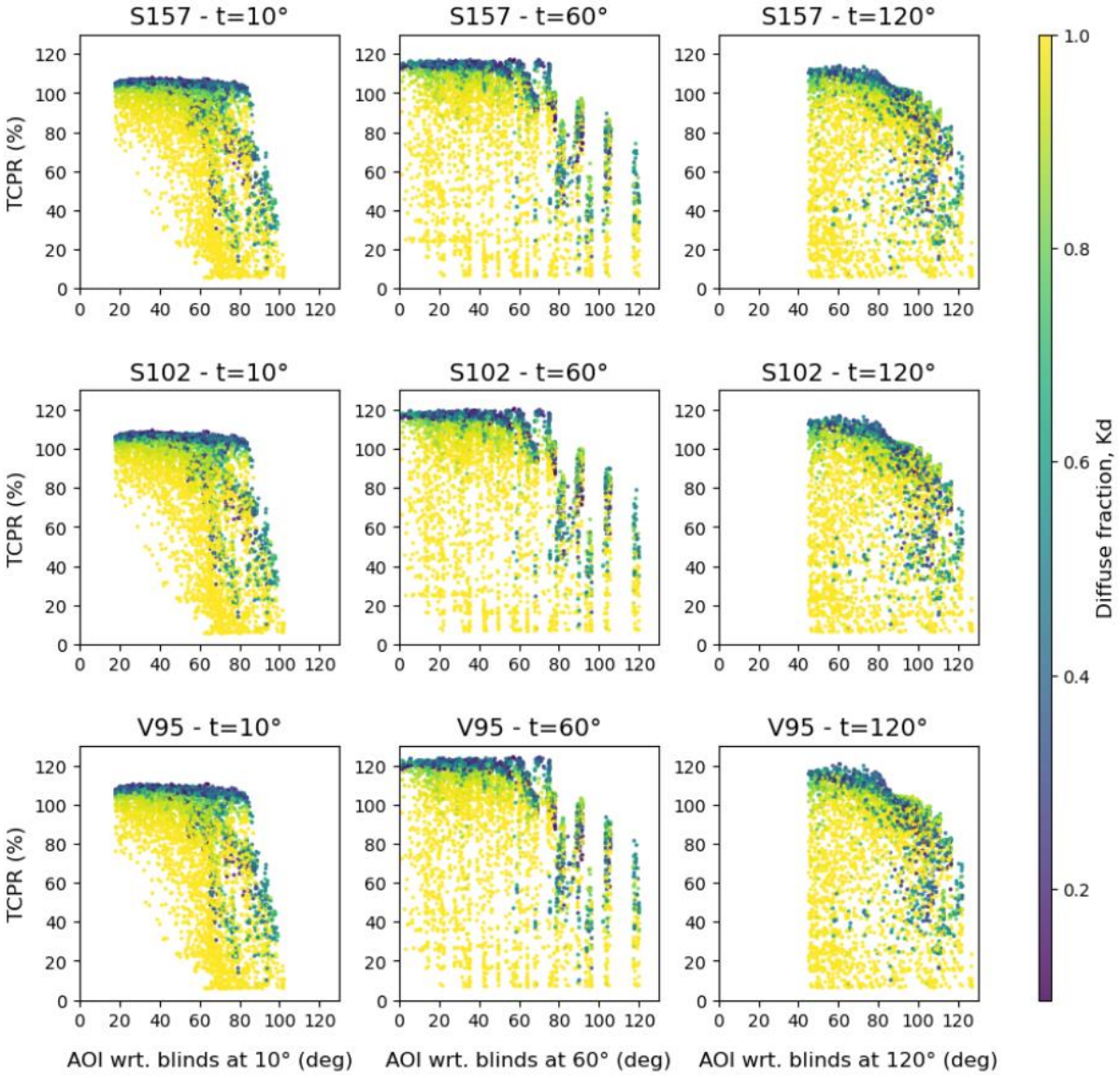

Figure 35: simulated hourly TCPR plotted as a function of the AOI formed between the sun and the blinds' surface normal on a TMY in Eindhoven for every blind configuration. Its correlation with the diffuse fraction, k_d, has been included.

As can be observed in *Figure 35*, regardless of the blind's configuration, there is a correlation between the TCPR of the bPV windows and the diffuse fraction, k_d, for any AOI formed between the sun and the blinds' surface normal. The figure shows a clear trend in which the highest TCPR values at any AOI between the sun and the blinds' surface normal are reached during periods of low diffuse fraction, meaning that the performance of the bPV windows is substantially enhanced at sunny moments when direct irradiance is the dominant component of the total front-side irradiance. This demonstrates that, irrespective of the specific blind

configuration, the slats help the windows to achieve a higher performance during moments of high direct sunlight, which is consistent with their role in reflecting and redirecting sunlight to the rear side of the bPV cells. Consequently, this behavior highlights the blinds' potential to enhance window performance under clear sky conditions.

Similarly, *Figure 36* presents the TCPR as a function of the blind's AOI correlated with the AOI between the sun and the window plane's normal to identify differences in performance due to the sun's position. From the figure, it is possible to observe that when the blinds are positioned at a tilt angle of 10° (first column of plots), the bPV window can achieve its highest performance at intermediate window's AOI. This is due to the fact that at this blind's position, the highest performance is achieved at lower AOI between the sun and the blinds' surface normal. When this AOI is close to zero, then it forms an AOI with respect to the window plane of around 80°, which coincides with the highest performance. As can be seen in these plots, at this particular blind's position, lower of higher AOI between the sun and the window plane's normal will lead to an overall decrease in performance.

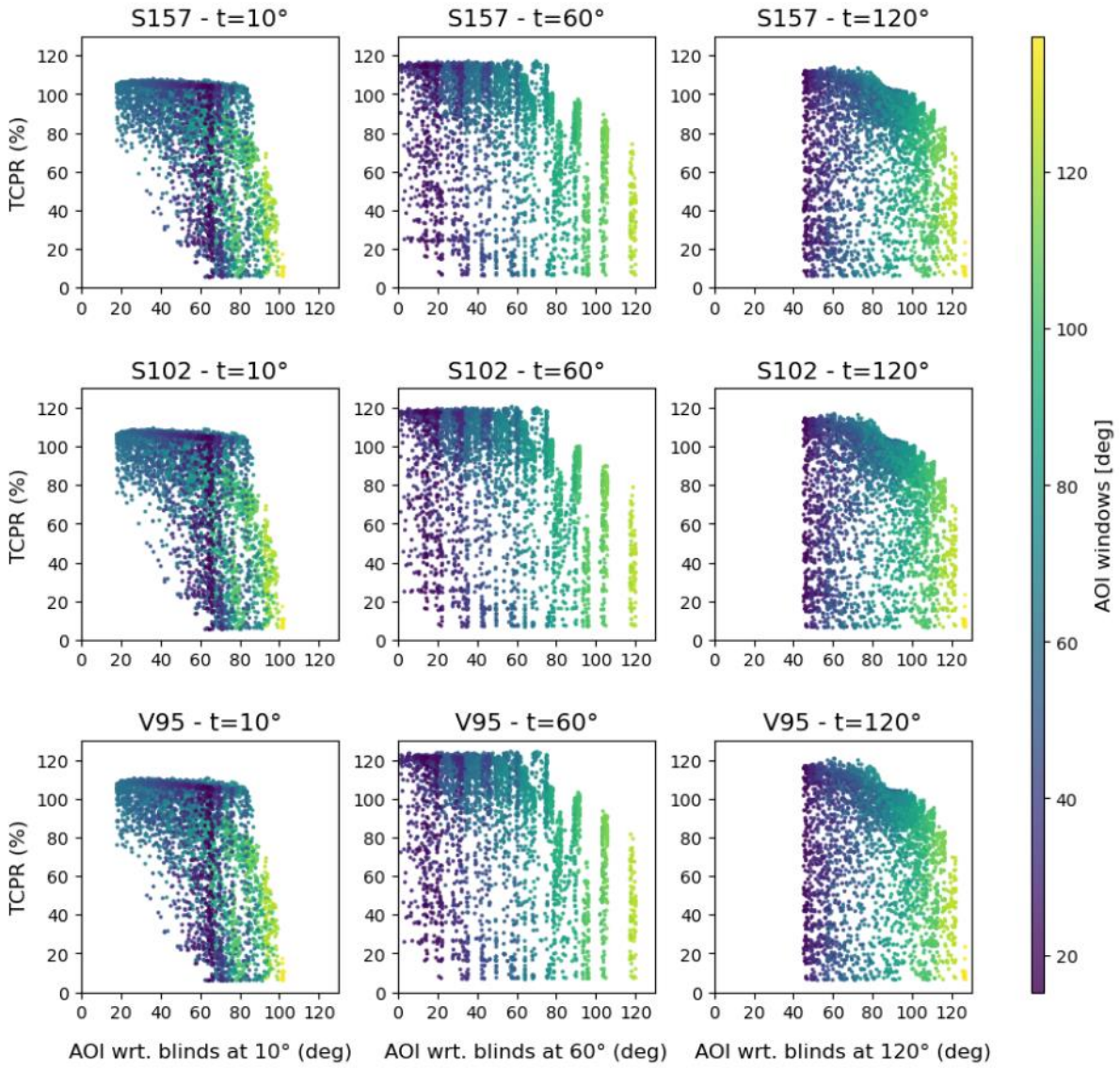

Figure 36: simulated hourly TCPR plotted as a function of the AOI formed between the sun and the blinds' surface normal on a TMY in Eindhoven for every blind configuration. Its correlation with the AOI formed between the sun and the window plane's normal has been included.

A different case can be observed when blinds are positioned at tilt angles of 60° or 120° (second and third columns of plots, respectively). In these cases, it is clear to see there is a trend indicating that the highest bPV window performance is achieved at low AOI between the sun and the window's plane. This angle coincides with a lower AOI between the sun and the blinds' surface normal, which, as previously discussed, is beneficial to achieve a high window performance. This is because at these blind's positions, the blinds are only deviated from the vertical window plane by 30°, meaning that both planes (blind's and window's surface) are more aligned to each other as in the case where blinds are positioned at a tilt angle of 10°. As a result, the relationship between these two variables is more direct, and higher window performance levels can be observed at lower AOI between the sun and the window's plane, which is less deviated from the blind's surface plane.

From the previous analysis, it can be concluded that besides the blind's configuration, there are other three additional variables that also have an influence on the bPV window performance, namely the diffuse fraction, the AOI between the sun and the blinds' surface normal and the AOI between the sun and the window plane's normal. As will be seen in the next section, these variables will play a crucial role in the bPV window performance when tested at different locations.

5.4. Overall performance assessment

Although the performance of the bPV windows was measured in real outdoor conditions over the course of one full year [7], simulation experiments were also performed to complement this analysis and obtain more representative estimates of the blind's potential to enhance the window's energy yield. This is because the weather conditions experienced during this particular year may have been atypical and not accurately reflect the long-term average weather conditions in Eindhoven. As a result, using data from this particular year could lead to skewed conclusions about the true energy performance of the product. To address this issue, a set of simulation experiments were conducted using typical meteorological year (TMY) weather data as input for the model, which represents average weather conditions in Eindhoven over a longer period of time (of around 10+ years). By using TMY weather data, it is possible to more precisely estimate the boost in energy yield provided by the different blind types under test and ensure that the findings are more reliable and representative of the expected long-term performance of this BIPV solution under normal weather conditions.

To this end, a set of simulations using TMY weather data in Eindhoven were conducted to determine the yearly specific yield (YSY, in kWh/kWp) of the window when blinds under test were deployed at different tilt angles and kept at the same position along the year except for the realistic scenario, which considerations will later be explained. The results of these simulations are presented next in *Figure 37*.

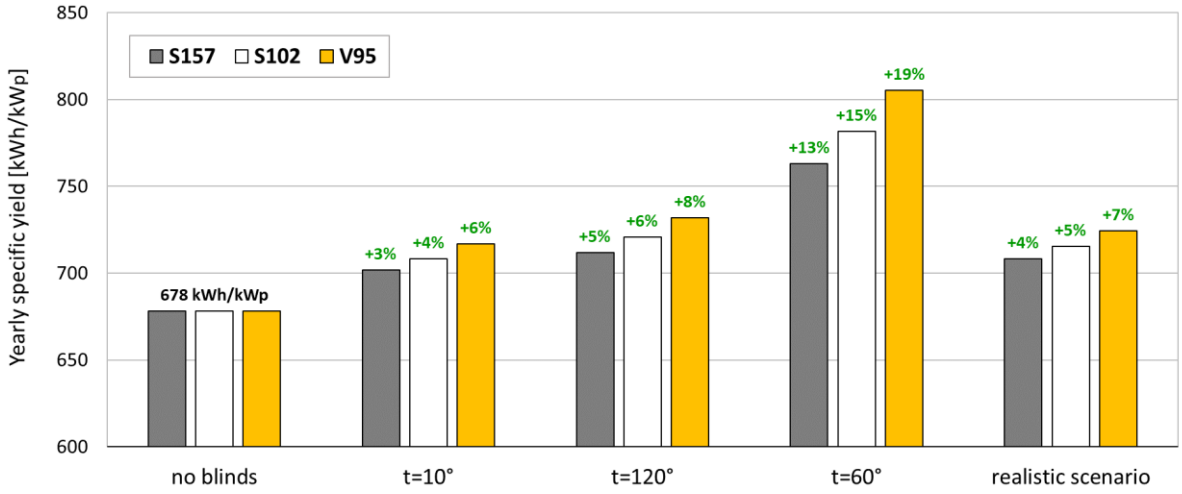

Figure 37: yearly specific yield (in kWh/kWp) of the ZIEZO window on a TMY in Eindhoven with different blind configurations.

As shown in the figure, the estimated YSY of the *ZIEZO* window when blinds are not deployed is approximately 678 kWh/kWp. While this figure is around 40% lower than the average YSY for a typical PV system installed in The Netherlands (947 kWh/kWp [47]), it is important to consider the additional benefits offered by this window solution, which were previously mentioned in section *3.2 bPV window demonstrator test setup.* This scenario was therefore taken as the baseline configuration to compare the relative increase in YSY in the rest of scenarios, with the percentages in green representing the relative boost in YSY compared to the reference case of no blinds.

From the previous figure, several important aspects can be observed. First, regardless of the tilt angle of the blinds, the V95 type consistently demonstrates to have the highest potential for increasing the YSY of the window, followed by the S102 and, lastly, the S157, as previously discussed in section *5.1 Influence of type of blinds*. This ranking aligns with their respective capabilities to enhance the irradiance gain on the window plane, as previously illustrated in *Figure 21* and discussed in section *4.4 Validation of the optical model: the total front-side irradiance.* Secondly, while a modest percentual increase in YSY can be obtained when blinds are deployed at 10° or 120° (ranging from 3 to 8%), a substantial boost in energy performance can be achieved when blinds are fully closed at a tilt angle of 60° (ranging from 13 to 19%), demonstrating to be the optimal tilt angle to boost the power output of the windows and maximizing their performance, which is consistent with the results presented in section *5.2 Influence of blind's tilt angle* and with the outdoor measurement analysis reported in [7]. Lastly, the maximum boost in energy production can be achieved when the V95 blinds are deployed at a tilt angle of 60°, which demonstrated to be the optimal blind configuration under study. At this particular position, the V95 blinds demonstrated to have a potential of increasing the YSY of the window by 19%, followed by the S102 and S157 blinds with 15% and 13%, respectively.

Since this blind configuration (in terms of blind type and tilt angle) demonstrated to have the greatest potential to boost the YSY of the window, its potential with respect to a case in which no blinds were used was also assessed for other locations in Europe. These locations were

chosen based on both, latitude (which ultimately has an influence in the AOI between the sun and the blinds' surface normal) and average meteorological conditions (to assess the influence of the diffuse fraction in the window performance). To this extent, the alternative cities of Valencia and Stockholm were chosen: Valencia being located at a lower latitude than Eindhoven (39.5 ° N, in comparison to Eindhoven's latitude of 51.4 ° N), and having an overall higher direct irradiance component (annual GHI = 1796 kWh/m^2, annual DHI = 555 kWh/m^2, k_d = GHI/DHI = 0.31, compared to Eindhoven's annual GHI = 972 kWh/m^2, annual DHI = 568 kWh/m^2, k_d = GHI/DHI = 0.58), and Stockholm being located at a higher latitude than Eindhoven (59.3 ° N) and having an overall higher direct irradiance component throughout the year (annual GHI = 975 kWh/m^2, annual DHI = 482 kWh/m^2, k_d = GHI/DHI = 0.49. The results of this simulation experiment are shown in *Figure 38*. This experiment demonstrated the V95 blinds at a tilt angle of 60° to have a YSY boosting potential of 17% (1418 kWh/kWp) and 18% (866 kWh/kWp) in Valencia and Stockholm, respectively, when compared to the case of no blinds (1210 and 732 kWh/kWp) at every respective location. In this way, both cases demonstrated to have a comparable but slightly lower potential compared to the 19% YSY boost achieved in Eindhoven with this blind configuration.

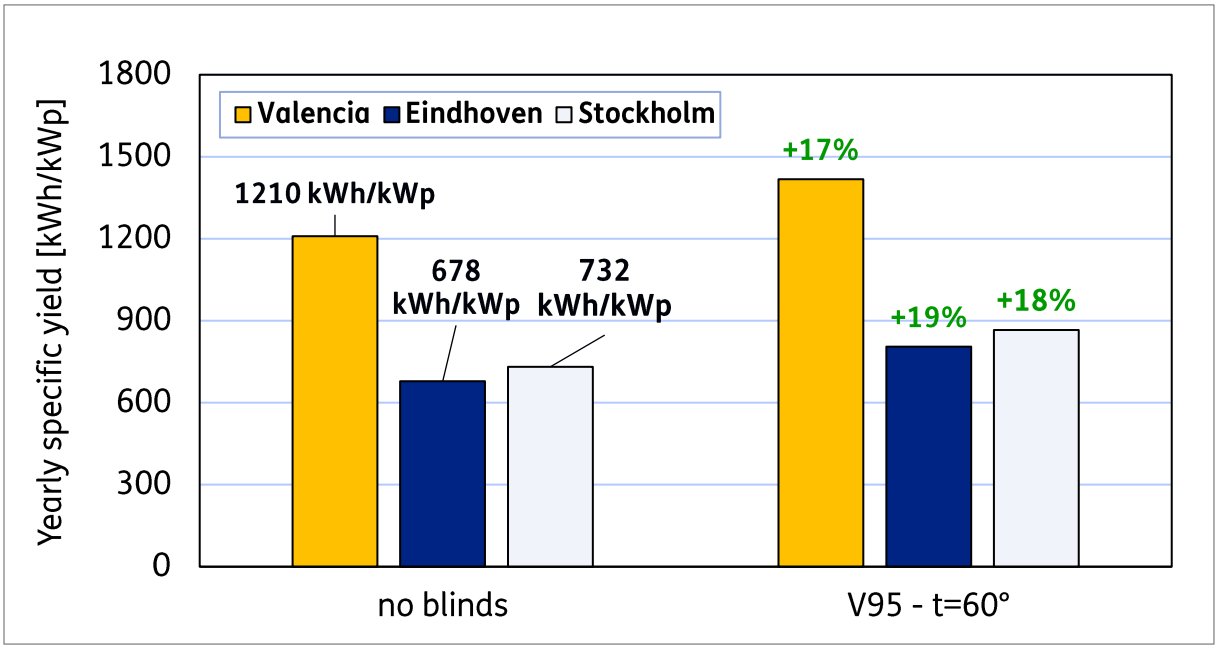

Figure 38: yearly specific yield (in kWh/kWp) of the ZIEZO window on a TMY in Valencia, Eindhoven, and Stockholm with two different blind configurations: no blinds, and V95 blinds at a tilt angle of 60°.

Intuitively, one might expect a higher YSY boosting potential at the sunniest location (Valencia). However, there are a several factors discussed in previous sections acting simultaneously, which combined effect is what explains this different outcome. First, it is crucial to consider the contribution of each irradiance component to the total front-side irradiance on the window plane at every location. As shown in *Figure 39*, the direct irradiance

component dominates in Valencia for most of the year, resulting in overall lower diffuse fraction values throughout the year than those observed in Eindhoven and Stockholm, whose proportions of irradiance components can be seen in *Figure 40* and *Figure 41*, respectively. These two last locations experience a higher proportion of diffuse irradiance throughout the year due to their higher latitudes and more frequent cloudy weather conditions, generally resulting in overall higher diffuse fraction levels. As discussed in section *5.3 Influence of blind's AOI*, a lower diffuse fraction is advantageous for maximizing the window performance, as the blinds can redirect more sunlight to the rear side of the bPV cells when the direct component proportion is greater. Therefore, in terms of diffuse fraction characteristics, Valencia is the most favorable location for achieving a high bPV window performance.

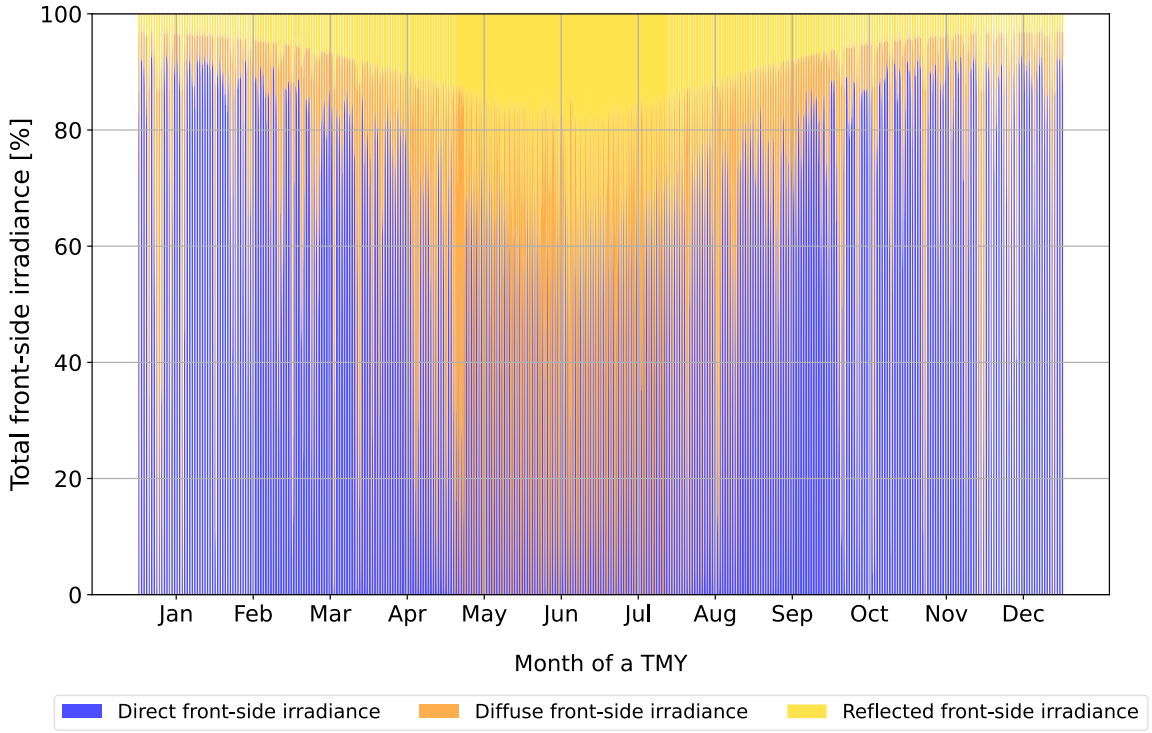

Figure 39: Contribution of each irradiance component to the total front-side irradiance on the window POA on a TMY in Valencia.

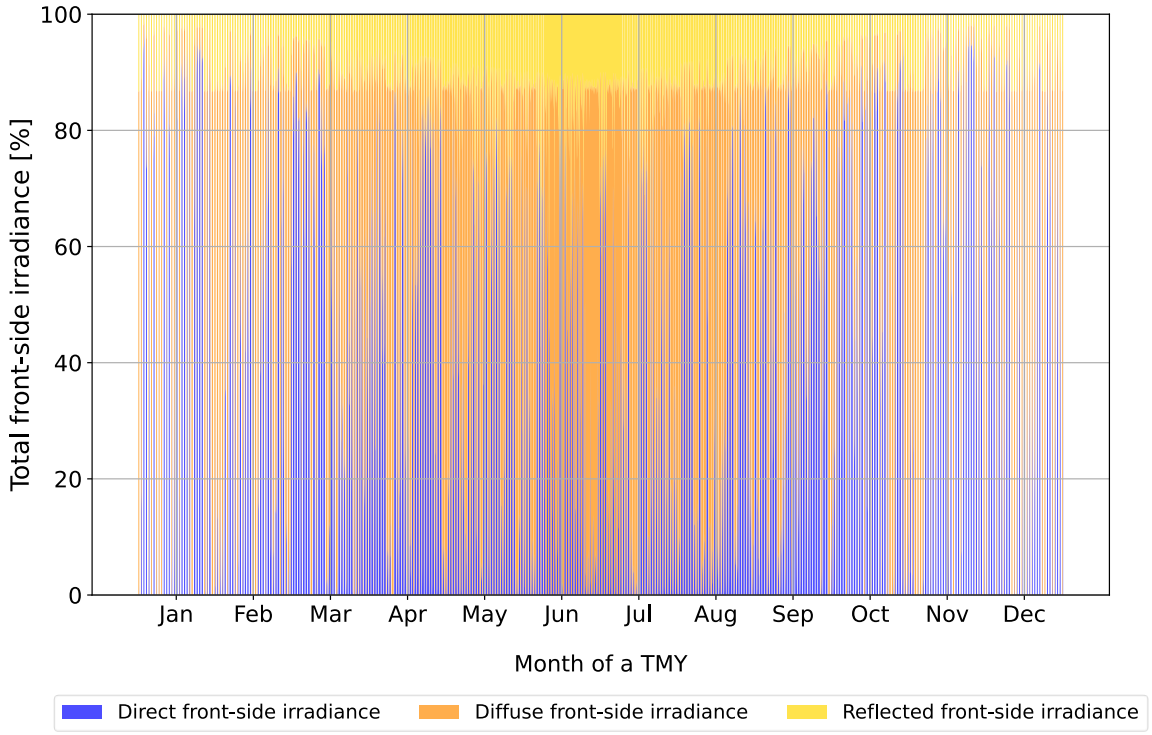

Figure 40: Contribution of each irradiance component to the total front side irradiance on a TMY in Eindhoven.

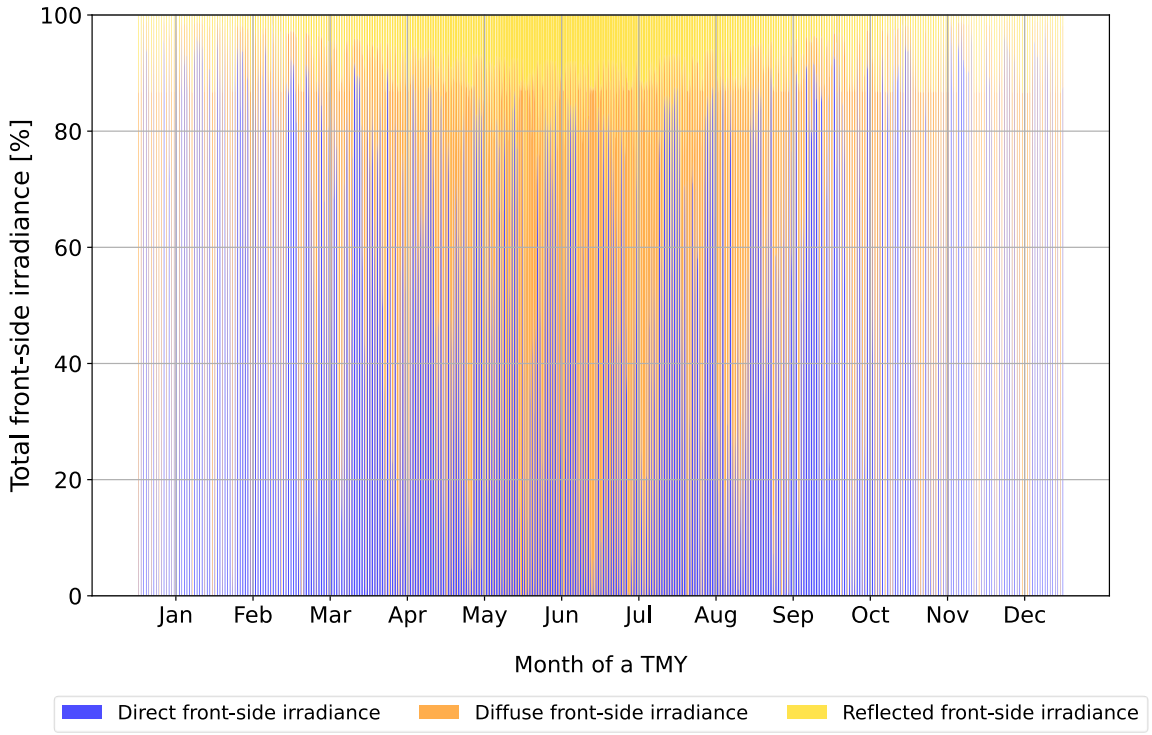

Figure 41: Contribution of each irradiance component to the total front side irradiance on a TMY in Stockholm.

Another important factor to consider is the variation of the sun altitude across the different locations, which ultimately has an influence on the AOI between the sun and the window plane's normal and on the AOI between the sun and the blinds' surface normal. *Figure 42* shows a comparison of the solar paths throughout the year followed at each location, where the green and blue lines represent the solar path in the summer and winter solstices, respectively. As illustrated, the solar path in Valencia is noticeably higher for most of the year, while in Eindhoven and Stockholm, the sun follows a much lower trajectory across the sky.

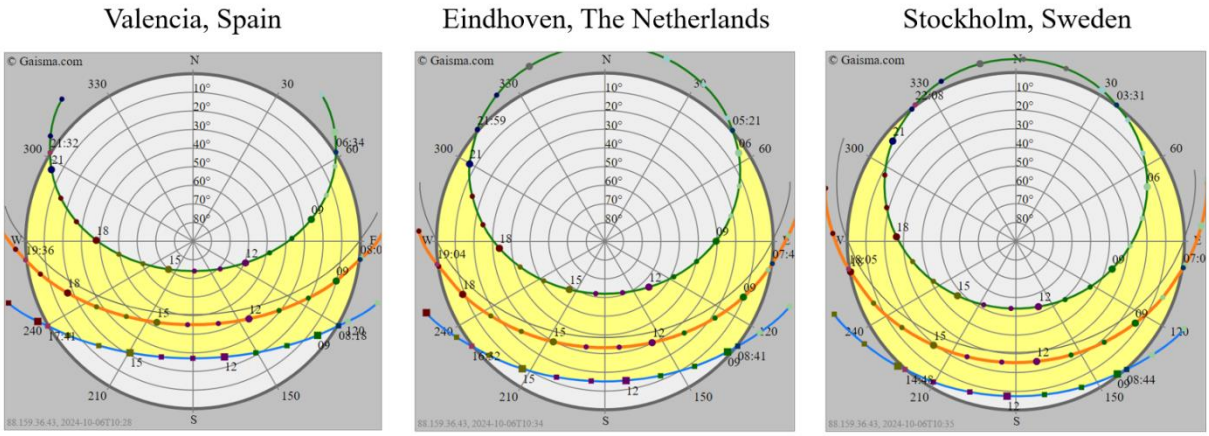

Figure 42: Solar path comparison throughout the year in Valencia (left), Eindhoven (center) and Stockholm (right) [38]-[40].

As discussed in the previous section, this variable also has an important influence in the bPV window performance, as a low sun path across the sky results in lower window's AOI values, which are correlated with a high window performance when blinds are tilted at an inclination of 60° (second column of plots in *Figure 36*, section *5.3 Influence of blind's AOI*). In higher-latitude locations, such as Eindhoven (51.4 ° N) and Stockholm (59.3 ° N), the sun follows a lower path across the sky throughout the year. This lower solar altitude experienced in Eindhoven and Stockholm is especially beneficial for the bPV windows, which are vertically installed in a south-facing facade (at a tilt angle of 90°), as sunlight can reach the windows and the blinds in a more direct way, leading to an enhanced window performance.

Another important effect to keep in mind is the AOI formed between the sun and the tilted blinds at 60°. In Eindhoven and Stockholm, the lower AOI between the blinds and the sun allows the blinds to capture and reflect the sunlight more directly. In contrast, Valencia, located at a lower latitude (39.5 ° N), experiences a higher solar altitude for most of the year, meaning the sun's rays hit the blinds at higher angles, resulting in less effective reflection toward the rear side of the window. Consequently, the higher solar path in Valencia also limits the blinds' ability to enhance the energy yield compared to locations with lower solar altitudes, such as Eindhoven and Stockholm, demonstrating that the AOI between the blinds and the sun is also an important factor that determines the performance of the blinds in boosting the power output of the

windows. In this way, locations at higher latitudes, where the sun path across the sky is lower, can be beneficial to achieve a high window performance when the blinds are positioned at a tilt angle of 60°, since both, the AOI between the sun and the window plane's normal, and the AOI between the sun and the blinds' surface normal are minimized. In this sense, both Eindhoven and Stockholm have more favorable conditions to achieve a higher boost in the YSY than Valencia.

The complex interaction between all these factors is what determines to a final extent the location at which the maximum boost in YSY can be achieved. While it is true that Valencia's higher irradiance levels and higher proportion of direct irradiance lead to a higher absolute YSY, the lower sun path across the sky experienced in Eindhoven and Stockholm causes lower AOI between both, the sun and the window plane's normal, and between the sun and the blinds' surface normal, leading to a higher relative YSY boost at these two locations although having an absolute lower YSY.

Regardless of the location, it is important to consider that the potential of the blinds to further enhance the YSY of the windows could be even higher if more complex blind control strategies would be applied. For instance, implementing a control system capable of adjusting the blind's tilt angle according to the sun's position and in alignment with the laminated bPV cell stripes could maximize the capture of irradiance on the rear side of the bPV cells and boost their energy production even more. This dynamic adjustment would be particularly beneficial for blinds with a high specular reflection component, such as the V95, as it would direct more of the reflected light onto the cells throughout the day. In practice, however, visual comfort of the users is usually prioritized over power production. Therefore, this control strategy could be applied just in specific situations, as for example when no users are present, such as in empty rooms or during holiday seasons. Furthermore, such an approach would induce additional complexity to the product design, as well as increase the production and operational costs, which could lead to a higher LCOE of this BIPV solution. Therefore, a careful assessment of the trade-off between performance improvements and cost implications would be essential for determining the feasibility of this approach.

Naturally, the approach of keeping the blinds in a static position throughout the entire year is not realistic. In practice, window users actively adjust the blinds to achieve visual comfort, resulting in varying positions throughout the day. To create a case that more accurately reflects this reality, an alternative realistic scenario was simulated (and presented in *Figure 37*) in which the blind's tilt angles were adjusted on an hourly basis throughout the year based on the diffuse fraction k_d and according to the following control logic:

$$blind's\ tilt\ angle\ = \begin{cases} 60°, & if\quad 0 \le k_d < 0.3 \\ 10°, & if\ 0.3 \le k_d < 0.7 \\ no\ blinds, & if\ 0.7 \le k_d < 1.0 \end{cases}$$

This dynamic control logic, which better reflects real-world usage, aims to balance both, visual comfort and power production by adjusting the blinds' tilt angle to 60° when the diffuse fraction k_d is low and direct sunlight is predominant, achieving protection from it while maximizing

energy generation. At intermediate k_d values, the proportion of direct sunlight is reduced and the blinds are positioned at 10°, providing some protection from sunlight while still delivering a reasonable boost in energy production. Finally, when sunlight is primarily diffuse, the blinds remain fully retracted to allow for natural illumination and enhance visual comfort. This control logic follows the principle that when direct sunlight is more abundant, maximum protection from it is required, while simultaneously presenting a significant opportunity for power boosting and energy production maximization. In this dynamic scenario, the boost in YSY was found to be 7%, 5% and 4% for the V95, S102 and S157 blinds, respectively. These values give in fact an estimation of the potential of the blinds to boost the energy production of the windows under real-use conditions.

5.5. Summary of key findings

To conclude, section *5.1 Influence of type of blinds* demonstrated the total irradiance gain on the rear side of the bPV window can be increased by up to 25%, 20% and 16% at the time of maximum power production of a fully sunny day when the V95, S102 and S157 blinds are used at a tilt angle of 60°, respectively. These percentages demonstrated to be lower in partially cloudy and completely overcast days. Moreover, the analysis of this section showed that the V95 blinds consistently achieve the greatest absolute boost in TCPR with respect to the case of no blinds for most days of a TMY in Eindhoven, followed by the S102 and finally, the S157, when the performance of these blind types was compared for a same tilt angle. Furthermore, this section also demonstrated that the yearly behavior of the absolute boost in TCPR when different types of blinds are used is highly influenced by the AOI between the sun and the blinds' surface normal, showing this to be a crucial factor influencing the boost in the window performance that is going to be achieved by means of deploying the blinds. All these conclusions combined helped to give answer to Research Question 1 (RQ1: how do different types of Venetian blinds affect the electric performance of the bPV windows? What other factors influence its behavior?).

Furthermore, section *5.2 Influence of blind's tilt angle* revealed that blinds positioned at a 60° tilt angle consistently provided the greatest absolute boost in TCPR with respect to the case of no blinds for most days of a TMY in Eindhoven, followed by blinds positioned at 120° and finally, at 10°, when the performance of different tilt angles was compered for a same blind type. In this way, the yearly average boost on a TMY in Eindhoven was quantified and reported in *Table 5*, finding that the V95 blinds at a tilt angle of 60° is the optimal blind configuration, as it led to the highest yearly average absolute boost in the TCPR of the bPV window. In this way, Research Question 2 (RQ2: how does the position of the Venetian blinds affect the overall performance of the bPV windows? Can we quantify the boosting effect given by the different blind configurations and find the optimal one?) was given an answer.

As the AOI between the sun and the blinds' surface normal was shown to be a crucial factor influencing the boost in performance of this bPV window, a deeper analysis of this factor was conducted in section *5.3 Influence of blind's AOI*. This analysis evidenced that there is a clear inverse correlation between this factor and the TCPR of the windows, as the latter shown a tendency to decrease for an increased AOI between the sun and the blinds' surface normal,

regardless of the blind configuration. Likewise, this section brought to light that other factors, such as the diffuse fraction, k_d, and the AOI formed between the sun and the window plane's normal, also play a role in the window performance, showing that the better TCPR values are obtained at moments when the diffuse fraction, k_d, is low (i.e., sunny moments) and at low AOIs formed between the sun and the window plane's for the blinds positioned at tilt angles of 60° and 120°, and AOIs formed between the sun and the window plane's around 80° for the blinds positioned at a tilt angle of 10°. The previous analysis demonstrated that meteorological and geographical conditions, such as the diffuse fraction, k_d, and the AOI formed between the sun and the window plane's normal, also have an influence on the performance of this bPV window, thereby giving answer to Research Question 3 (RQ3: which other factors have an influence on the bPV window performance? Does it also depends on meteorological or geographical conditions?).

Finally, section *5.4 Overall performance assessment* evaluated the boost in YSY that each blind configuration can provide on a TMY in Eindhoven with respect to the case of no blinds when these are kept static throughout the year. As expected, this assessment confirmed the conclusions drawn from sections *5.1 Influence of type of blinds* and *5.2 Influence of blind's tilt angle* regarding the best performing blind types and tilt angles, and revealed that a maximum boost of 19% in the YSY can be achieved on a TMY in Eindhoven by keeping the optimal blind configuration throughout the year, namely the V95 blinds at a tilt angle of 60°. The same blind configuration showed to achieve a boost in YSY of 18% and 17% on a TMY in Stockholm and Valencia, respectively. This lower boost can be attributed to the combined effect of the previous factors influencing the performance of the bPV window mentioned in previous sections, namely an overall decreased diffuse fraction, k_d, but higher AOIs between the sun and the blinds' surface normal and between the sun and the window plane's normal in Valencia; and an overall increased diffuse fraction, k_d, but lower AOIs between the sun and the blinds' surface normal and between the sun and the window plane's normal in Stockholm. In this way, an answer to Research Question 4 (RQ4: can we quantify the boost in yearly specific yield (YSY) given by the different blind configurations? How much can it be in other locations when the optimal blind configuration is used?) has been given.

In summary, with all the previous conclusions drawn from section 5.1 through section 5.4 and their respective answers to research questions RQ1-RQ4, it can be said that Objective 3 (O3: use the created models to perform different simulations to assess the performance of this bPV window when different blind configurations are used) of this research project has successfully been achieved, therefore fulfilling the goals and expectations initially set for this research project.

6. Conclusions and recommendations

To conclude, sections *4.1* through *4.3* detailed the approach taken to model the bPV window in *BIGEYE*, outlining the assumptions, simplifications, and values used to define the geometrical, optical, electrical, and thermal properties of the model as a whole. As a result, the bPV window models were successfully developed, achieving Objective 1 (O1: create a set of PV simulation models that describe the performance of this BIPV window when different types of reflective Venetian blinds are used). Additionally, sections *4.4* and *4.5* covered the optical and electrical validations performed against experimental data to ensure that the models could accurately simulate both the front-side irradiance and the electrical performance of the bPV window under real operational conditions. This confirmed the reliability of the models, thereby fulfilling Objective 2 (O2: validate the created models with experimental data to test their accuracy and reliability).

Moreover, the research conducted as part of this MSc. thesis work successfully addressed all the research questions (RQs) and achieved Objective 3 (O3: use the created models to perform different simulations to assess the performance of this bPV window when different blind configurations are used) as initially planned. By means of the analysis presented in sections *5.1* through *5.4*, the study provided clear answers to the key research questions: RQ1 explored the impact of different types of Venetian blinds on the electrical performance of the bPV window; RQ2 assessed how the blinds' tilt angle influenced performance and identified the optimal configuration; RQ3 examined the influence of other factors such as meteorological and geographical conditions on the bPV window's performance; and RQ4 quantified the boost in yearly specific yield (YSY) provided by different blind configurations across several locations. By addressing these questions and using the simulation models to assess the bPV window's performance with different blind configurations, the project successfully met Objective 3, fulfilling the intended goals and expectations of this research project.

Additionally, several recommendations for future work on this research project can be pointed out. These recommendations are focused on: *a) making improvements to the current bPV window model*s, *b) further analysis of the results that were obtained from the current simulations*, and *c) conducting market research and back-of-the-envelope calculations*. These all recommendations are tailored to obtaining more accurate simulation results and/or additional insights on the bPV window performance.

Regarding *a) making improvements to the current bPV window models*, it is crucial to keep in mind that there should always be a balance between model accuracy and computational resources when implementing any improvement to the models. This consideration is particularly important, as computational power is always limited and any improvement in accuracy should justify the additional computational cost. Overly complex models can lead to significantly longer simulation times without necessarily offering meaningful improvements in results. Therefore, any proposed enhancement must carefully weigh the benefits of increased precision against the practical limitations of computation time and resources.

It is also important to consider that the current simulation models have already been optimized in several key areas, such as the number of objects, the number of mesh points of each object, number of light bounces, number of data points used for every simulation, among others. These adjustments have been fine-tuned to achieve an adequate level of accuracy without overwhelming computational demands. However, it may be possible in the future to add more complexity to the simulation models in the pursuit of an increased accuracy without compromising computational resources as upcoming versions of the *BIGEYE* software are released.

That said, a newer version of the *BIGEYE* software (still under test) is already exploring a new functionality for giving specular-reflecting properties to an object by means of a ray tracing approach, in contrast to the currently implemented sky view factor approach, which make objects to behave as fully diffuse reflectors and may not be suitable to model the optical properties of certain Venetian blind types, such as the V95. Therefore, further work for improving the current simulation models could be done by testing this new software functionality, which may lead to more accurate results and additional insights by better describing the optical effects that take place in real life. This could also be useful to better understand the complex optical interactions between sunlight and the reflective Venetian blinds and could also help further optimize the design of this PV window solution.

Concerning *b) further analysis of the results that were obtained from the current simulations*, further work can focus on determining the extent to which each variable influences the overall performance of the bPV windows. In particular, conducting a sensitivity analysis could be helpful to understand the degree to which parameters, such as the type of blinds, the blind's tilt angle, the diffuse fraction k_d, the AOI between the sun and the blinds' surface normal or the AOI between the sun and the front-side of the window plane, affect the overall performance of the bPV windows. Such analysis would be especially be useful in future efforts to further optimize the design of the windows. Additionally, it could serve as a foundation for developing an automated smart-blinds control algorithm, which could be integrated into the bPV window product to dynamically adjust the blinds' position to further boost the energy yield of the windows based on real-time operation conditions.

Another idea involving a simple modification in the simulation models could help to simulate the performance of the bPV window in the hypothetical case mPV cells were used in this window product, instead of bPV cells. To achieve this, the bifaciality factor should simply be changed to have a value of zero. In this way, it would be possible to quantify the boost in performance by means of integrating bPV technology in the window product, instead of using conventional mPV technology. Alternatively, It would be possible to cover the front-side of the bPV window plane with an opaque object, so that no power can be produced at the front side of the window. In this way, the power produced only at the rear side could be quantified.

Furthermore, it is also possible to conduct an in-depth comparison between the obtained simulation results and the real-life performance measurements, to further identify similarities and discrepancies between them. By reflecting on these differences, it can be possible to understand the underlying reasons for any deviations in performance, such as limitations in the simulation models. This comparison could provide valuable insights that can help to refine the simulation models and improve their accuracy, but most importantly, can help to further reflect

on the ability of the blinds to boost the window performance and better understand better their behavior.

Finally, concerning *c) conducting market research and back-of-the-envelope calculations*, additional research work and back-of-the-envelope calculations can be conducted to put into perspective this bPV solution with respect to other similar products currently available on the market. Such work would help to assess the potential of this bPV window to enhance the energy performance of buildings, particularly in urban settings. For example, some key research questions that could be explored include the following:

- What proportion of the energy consumption of a typical office building could be met if these windows covered, for example, 90% of its facade area?

- How does the performance of this integrated BIPV window solution compare to other PV windows currently available on the market, or even to conventional opaque c-Si PV modules?

- How does the LCOE of this bPV window product compare to that of other PV window solutions and conventional PV modules available in the market, and what factors contribute to its competitiveness in terms of cost-effectiveness and energy performance?

These and other questions are crucial to determine whether this solution is truly competitive and viable as a market-ready product or if additional efforts should be conducted to further optimize its design based on the current BIPV market, providing insight into both its strengths and areas for potential improvement.

List of references

[1] "Energy Performance of Buildings Directive." Accessed: Aug. 07, 2024. [Online]. Available: https://energy.ec.europa.eu/topics/energy-efficiency/energy-efficient-buildings/energy-performance-buildings-directive_en

[2] P. W. Wong, Y. Shimoda, M. Nonaka, M. Inoue, and M. Mizuno, "Semi-transparent PV: Thermal performance, power generation, daylight modelling and energy saving potential in a residential application," *Renewable Energy*, vol. 33, no. 5, pp. 1024–1036, May 2008, doi: 10.1016/j.renene.2007.06.016.

[3] "A review of transparent solar photovoltaic technologies - ScienceDirect." Accessed: Sep. 12, 2024. [Online]. Available: https://www.sciencedirect.com/science/article/pii/S1364032118304672

[4] E. Pulli, E. Rozzi, and F. Bella, "Transparent photovoltaic technologies: Current trends towards upscaling," *Energy Conversion and Management*, vol. 219, p. 112982, Sep. 2020, doi: 10.1016/j.enconman.2020.112982.

[5] C. J. Traverse, R. Pandey, M. C. Barr, and R. R. Lunt, "Emergence of highly transparent photovoltaics for distributed applications," *Nat Energy*, vol. 2, no. 11, pp. 849–860, Nov. 2017, doi: 10.1038/s41560-017-0016-9.

[6] A. A. F. Husain, W. Z. W. Hasan, S. Shafie, M. N. Hamidon, and S. S. Pandey, "A review of transparent solar photovoltaic technologies," *Renewable and Sustainable Energy Reviews*, vol. 94, pp. 779–791, Oct. 2018, doi: 10.1016/j.rser.2018.06.031.

[7] S. Villa, M. Hurtado Ellmann, and R. Valckenborg, "Outdoor performance analysis of semi-transparent PV windows with bifacial cells and integrated blinds [Unpublished manuscript]," 2024.

[8] "ZIEZO." Accessed: Feb. 08, 2024. [Online]. Available: https://projecten.topsectorenergie.nl/projecten/ziezo-36497

[9] "Pilkington Insulight™ with ScreenLine®." Accessed: Aug. 17, 2024. [Online]. Available: https://www.pilkington.com/en/global/products/product-categories/special-applications/pilkington-insulight-with-screenline

[10] "Pilkington Sunplus™ BIPV." Accessed: Apr. 29, 2024. [Online]. Available: https://www.pilkington.com/en/global/products/product-categories/solar-energy/pilkington-sunplus-bipv

[11] G. Yu, H. Yang, D. Luo, X. Cheng, and M. K. Ansah, "A review on developments and researches of building integrated photovoltaic (BIPV) windows and shading blinds," *Renewable and Sustainable Energy Reviews*, vol. 149, p. 111355, Oct. 2021, doi: 10.1016/j.rser.2021.111355.

[12] "Frontiers | Multi-performative façade systems: The case of real-time adaptive BIPV shading systems to enhance energy generation potential and visual comfort." Accessed: Aug.

17, 2024. [Online]. Available: https://www.frontiersin.org/journals/built-environment/articles/10.3389/fbuil.2023.1119696/full

[13] "SolarBEAT: unique outdoor test facility for BIPV | TNO," tno.nl/en. Accessed: Apr. 18, 2024. [Online]. Available: https://www.tno.nl/en/technology-science/labs/solarbeat/

[14] P. Heinstein, C. Ballif, and L.-E. Perret-Aebi, "Building Integrated Photovoltaics (BIPV): Review, Potentials, Barriers and Myths," *Green*, vol. 3, no. 2, pp. 125–156, Jun. 2013, doi: 10.1515/green-2013-0020.

[15] K. Khaled and U. Berardi, "Current and future coating technologies for architectural glazing applications," *Energy and Buildings*, vol. 244, p. 111022, Aug. 2021, doi: 10.1016/j.enbuild.2021.111022.

[16] "Solar panels on windows, façades, and roofs | TNO," tno.nl/en. Accessed: Apr. 29, 2024. [Online]. Available: https://www.tno.nl/en/sustainable/renewable-electricity/integrated-solar-safety/solar-panels-windows-facades-roofs/

[17] J. Sun and J. J. Jasieniak, "Semi-transparent solar cells," *J. Phys. D: Appl. Phys.*, vol. 50, no. 9, p. 093001, Feb. 2017, doi: 10.1088/1361-6463/aa53d7.

[18] W. Gu, T. Ma, S. Ahmed, Y. Zhang, and J. Peng, "A comprehensive review and outlook of bifacial photovoltaic (bPV) technology," *Energy Conversion and Management*, vol. 223, p. 113283, Nov. 2020, doi: 10.1016/j.enconman.2020.113283.

[19] X. Sun, M. R. Khan, C. Deline, and M. A. Alam, "Optimization and performance of bifacial solar modules: A global perspective," *Applied Energy*, vol. 212, pp. 1601–1610, Feb. 2018, doi: 10.1016/j.apenergy.2017.12.041.

[20] M. T. Patel, M. R. Khan, X. Sun, and M. A. Alam, "A worldwide cost-based design and optimization of tilted bifacial solar farms," *Applied Energy*, vol. 247, pp. 467–479, Aug. 2019, doi: 10.1016/j.apenergy.2019.03.150.

[21] "International Technology Roadmap for Photovoltaic (ITRPV) - vdma.org - VDMA." Accessed: May 09, 2024. [Online]. Available: https://www.vdma.org/international-technology-roadmap-photovoltaic

[22] Q. Wei *et al.*, "The Glass-glass Module Using n-type Bifacial Solar Cell with PERT Structure and its Performance," *Energy Procedia*, vol. 92, pp. 750–754, Aug. 2016, doi: 10.1016/j.egypro.2016.07.054.

[23] M. W. P. E. Lamers *et al.*, "Temperature effects of bifacial modules: Hotter or cooler?," *Solar Energy Materials and Solar Cells*, vol. 185, pp. 192–197, Oct. 2018, doi: 10.1016/j.solmat.2018.05.033.

[24] R. Guerrero-Lemus, R. Vega, T. Kim, A. Kimm, and L. E. Shephard, "Bifacial solar photovoltaics – A technology review," *Renewable and Sustainable Energy Reviews*, vol. 60, pp. 1533–1549, Jul. 2016, doi: 10.1016/j.rser.2016.03.041.

[25] T. Baumann, H. Nussbaumer, M. Klenk, A. Dreisiebner, F. Carigiet, and F. Baumgartner, "Photovoltaic systems with vertically mounted bifacial PV modules in combination with green roofs," *Solar Energy*, vol. 190, pp. 139–146, Sep. 2019, doi: 10.1016/j.solener.2019.08.014.

[26] B. Petter Jelle, C. Breivik, and H. Drolsum Røkenes, “Building integrated photovoltaic products: A state-of-the-art review and future research opportunities,” *Solar Energy Materials and Solar Cells*, vol. 100, pp. 69–96, May 2012, doi: 10.1016/j.solmat.2011.12.016.

[27] M. Biancardo *et al.*, “Characterization of microspherical semi-transparent solar cells and modules,” *Solar Energy*, vol. 81, no. 6, pp. 711–716, Jun. 2007, doi: 10.1016/j.solener.2006.10.009.

[28] K. L. Chopra, P. D. Paulson, and V. Dutta, “Thin-film solar cells: an overview,” *Progress in Photovoltaics: Research and Applications*, vol. 12, no. 2–3, pp. 69–92, 2004, doi: 10.1002/pip.541.

[29] C. W. Tang, “Two-layer organic photovoltaic cell,” *Applied Physics Letters*, vol. 48, no. 2, pp. 183–185, Jan. 1986, doi: 10.1063/1.96937.

[30] G. Yu, J. Gao, J. C. Hummelen, F. Wudl, and A. J. Heeger, “Polymer Photovoltaic Cells: Enhanced Efficiencies via a Network of Internal Donor-Acceptor Heterojunctions,” *Science*, vol. 270, no. 5243, pp. 1789–1791, Dec. 1995, doi: 10.1126/science.270.5243.1789.

[31] J. J. M. Halls *et al.*, “Efficient photodiodes from interpenetrating polymer networks,” *Nature*, vol. 376, no. 6540, pp. 498–500, Aug. 1995, doi: 10.1038/376498a0.

[32] B. O’Regan and M. Grätzel, “A low-cost, high-efficiency solar cell based on dye-sensitized colloidal TiO2 films,” *Nature*, vol. 353, no. 6346, pp. 737–740, Oct. 1991, doi: 10.1038/353737a0.

[33] M. M. Lee, J. Teuscher, T. Miyasaka, T. N. Murakami, and H. J. Snaith, “Efficient Hybrid Solar Cells Based on Meso-Superstructured Organometal Halide Perovskites,” *Science*, vol. 338, no. 6107, pp. 643–647, Nov. 2012, doi: 10.1126/science.1228604.

[34] D. Prasad and M. Snow, *Designing with Solar Power: A Source Book for Building Integrated Photovoltaics (BIPV)*. London: Routledge, 2014. doi: 10.4324/9781315065731.

[35] IEC 61724, *Photovoltaic system performance monitoring - Guidelines for measurement, data exchange and analysis*, 1998.

[36] W. van Sark, N. Reich, B. Müller, A. Armbruster, K. Kiefer, and C. Reise, *Review of PV performance ratio development*. 2012. doi: 10.13140/2.1.2138.7204.

[37] T. Dierauf, A. Growitz, S. Kurtz, J. L. B. Cruz, E. Riley, and C. Hansen, “Weather-Corrected Performance Ratio,” NREL/TP-5200-57991, 1078057, Apr. 2013. doi: 10.2172/1078057.

[38] N. H. Reich, B. Mueller, A. Armbruster, W. G. J. H. M. van Sark, K. Kiefer, and C. Reise, “Performance ratio revisited: is PR > 90% realistic?,” *Progress in Photovoltaics: Research and Applications*, vol. 20, no. 6, pp. 717–726, 2012, doi: 10.1002/pip.1219.

[39] G. Janssen *et al.*, *How to maximize the kWh/kWp ratio: simulations of single-axis tracking in bifacial systems*. 2018. doi: 10.4229/35thEUPVSEC20182018-6BO.7.5.

[40] R. Perez, R. Seals, P. Ineichen, R. Stewart, and D. Menicucci, “A new simplified version of the perez diffuse irradiance model for tilted surfaces,” *Solar Energy*, vol. 39, no. 3, pp. 221–231, Jan. 1987, doi: 10.1016/S0038-092X(87)80031-2.

[41] R. Perez, P. Ineichen, R. Seals, J. Michalsky, and R. Stewart, “Modeling daylight availability and irradiance components from direct and global irradiance,” *Solar Energy*, vol. 44, no. 5, pp. 271–289, Jan. 1990, doi: 10.1016/0038-092X(90)90055-H.

[42] G. J. M. Janssen, K. C. J. Tool, E. J. Kossen, B. B. Van Aken, A. J. Carr, and I. G. Romijn, “Aspects of bifacial cell efficiency,” *Energy Procedia*, vol. 124, pp. 76–83, Sep. 2017, doi: 10.1016/j.egypro.2017.09.334.

[43] W. De Soto, S. A. Klein, and W. A. Beckman, “Improvement and validation of a model for photovoltaic array performance,” *Solar Energy*, vol. 80, no. 1, pp. 78–88, Jan. 2006, doi: 10.1016/j.solener.2005.06.010.

[44] G. J. M. Janssen, B. B. Van Aken, A. J. Carr, and A. A. Mewe, “Outdoor Performance of Bifacial Modules by Measurements and Modelling,” *Energy Procedia*, vol. 77, pp. 364–373, Aug. 2015, doi: 10.1016/j.egypro.2015.07.051.

[45] “SolarBEAT.” Accessed: Aug. 18, 2024. [Online]. Available: https://www.tue.nl/en/research/research-labs/solarbeat

[46] “Venetian blind | Pellini.” Accessed: Oct. 22, 2024. [Online]. Available: https://www.pellini.net/en/tipologie/venetian-blind

[47] J. Schardt and H. te Heesen, “Performance of roof-top PV systems in selected European countries from 2012 to 2019,” *Solar Energy*, vol. 217, pp. 235–244, Mar. 2021, doi: 10.1016/j.solener.2021.02.001.

[48] “Valencia, Spain - Sunrise, sunset, dawn and dusk times for the whole year,” Gaisma. Accessed: Oct. 13, 2024. [Online]. Available: https://www.gaisma.com/en/location/valencia-es.html

[49] “Eindhoven, Netherlands - Sunrise, sunset, dawn and dusk times for the whole year,” Gaisma. Accessed: Oct. 13, 2024. [Online]. Available: https://www.gaisma.com/en/location/eindhoven.html

[50] “Stockholm, Sweden - Sunrise, sunset, dawn and dusk times for the whole year,” Gaisma. Accessed: Oct. 13, 2024. [Online]. Available: https://www.gaisma.com/en/location/stockholm.html

Appendix A: bPV cell specifications

- A.1. Specification sheet of c-Si n-type IBC zebra bPV cells, employed in all *TNO*'s bPV windows and manufactured by *SPIC Solar*:

About SPIC Solar

SPIC is the world's top 500 companies. Ranked the list for seven consecutive years, ranked 362th in 2019. The company has a registered capital of 35 billion RMB and total assets of 1.08 trillion RMB. The national electric power investment photovoltaic power generation has the largest installed capacity in the world. with technology research and development, planning and design, polysilicon, photovoltaic cells, component manufacturing, engineering construction, production operations, training, etc. Complete photovoltaic industry chain.

Product features

The bifacial structure and half-chip design. No light-induced degradation and excellent anti-PID performance. Excellent power generation performance. High conversion efficiency and high reliability. No finger shading in sunny-side, beautiful appearance.

尺寸设计图 (单位:mm)
Mechanical Data and Design (Units:mm)

电池正面 Front side

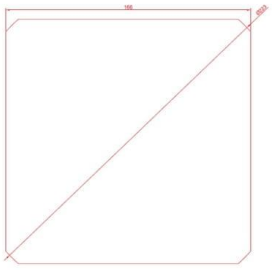

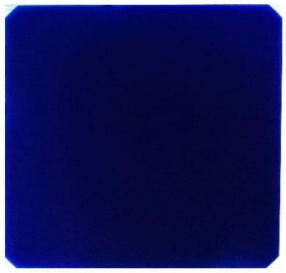

电池背面 Back side

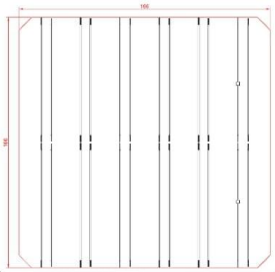

产品外观 **Product appearance**

尺寸 Dimension	(166mm±0.25mm)×(166mm±0.25mm)
厚度 Thickness	170μm±20μm
正电极 Front(+)	正面无栅线，蓝色氮化硅减反射涂层 front without grid line,blue anti-reflection coating(silicon nitride)
背电极 back(-)	0.8mm 银主栅线，蓝色氮化硅减反射涂层 0.8mm bus bars(silver),blue anti-reflection coating(silicon nitride)

ZEBRA

IBC CELL

电性能参数 **Electrical Characteristics**

转换效率	最大功率	最大功率点电压	最大功率点电流	开路电压	短路电流	填充因子
Efficiency(%)	Pmpp(Wp)	Umpp(V)	Impp(A)	Uoc(V)	Isc(A)	FF(%)
24.30-24.40	6.67	0.598	11.142	0.698	11.759	81.23
24.20-24.30	6.64	0.597	11.127	0.697	11.751	81.10
24.10-24.20	6.62	0.595	11.114	0.695	11.747	81.00
24.00-24.10	6.59	0.594	11.101	0.694	11.736	80.89
23.90-24.00	6.57	0.592	11.090	0.694	11.726	80.75
23.80-23.90	6.54	0.591	11.075	0.693	11.719	80.58
23.70-23.80	6.51	0.589	11.056	0.692	11.710	80.39
23.60-23.70	6.48	0.588	11.029	0.691	11.700	80.18
23.50-23.60	6.46	0.587	11.006	0.690	11.689	80.01
23.40-23.50	6.43	0.586	10.975	0.690	11.684	79.77
23.30-23.40	6.40	0.584	10.956	0.689	11.681	79.52
23.20-23.30	6.37	0.583	10.934	0.689	11.671	79.30

温度系数 **Temperature Coefficients**

开路电压温度系数 Voc.Temp.Coef.	-0.268%/K
短路电流温度系数 Isc.Temp.Coef.	+0.042%/K
最大功率温度系数 Pm.Temp.Coef.	-0.3%/K

光强响应 **Intensity Dependence**

光强 Intensity [W/m²]	短路电流 Isc	开路电压 Voc
1000	1	1
900	0.9	0.994
500	0.5	0.974
300	0.3	0.951
200	0.2	0.927
不同光强下的 Voc(Isc)在 1000W/m²光强下 Voc（Isc）的比率 Ratio of Voc (Isc) at reduced intensity to Voc (Isc) at 1000 W/m²		

IV 曲线 **IV Curve**

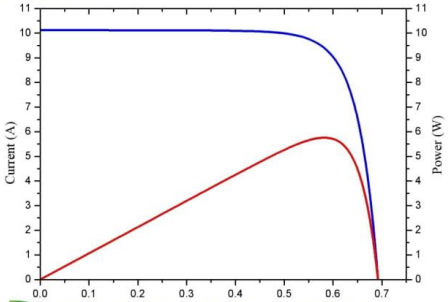

光谱响应 **Spectral Response（SR）**

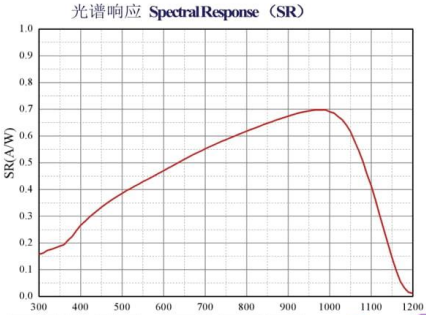

黄河水电西宁太阳能电力有限公司
HHDC XINING SOLAR POWER CO., LTD.
Add: No.4 Jinggui Road, Economic and Technological Development Zone,
Chengdong District, Xining City, Qinghai Province, China.
TEL: 0086 29 89865061 FAX: 0086 29 89865060
MAIL: spicsolar@spic.com.cn

A.2. Specification sheets of the six *TNO*'s bPV window demonstrators:

- TNO 01 bPV window (CR=60%, S102):

PASAN

Performance measurement
PASAN Tester

Operator	Lars Okel	Measurement	2023/07/17 13.12.43
PASAN Tester version	R2.4.5 / 2018/03/21 17:32:34 2.4.5 (20882)		

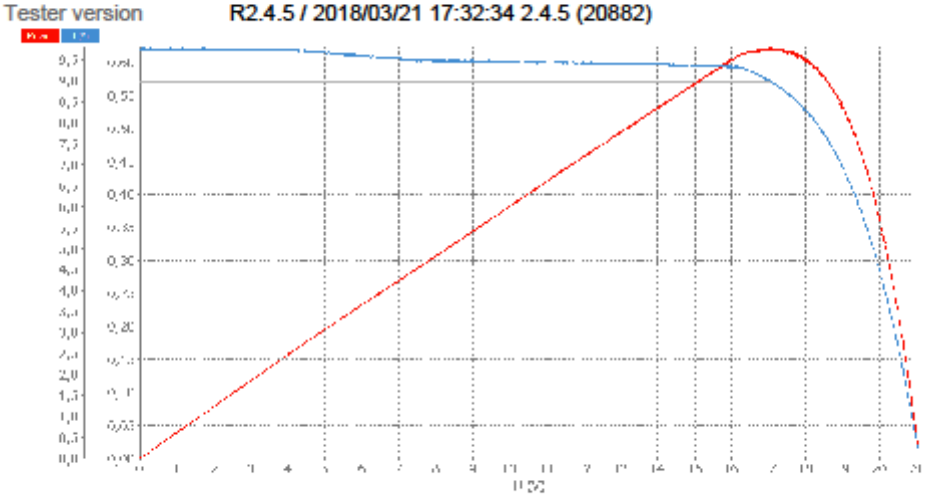

M2565 16fl IBC 1cm strip 32 cell Zebra

Manufacturer	TNO	Type	32 cells
Serial number	A7818 16fl	Configuration DUT	Module
Single cell area	16.60 cm²	DUT area	1760.00 cm²
Cells in series	32	Cells in parallel	1

Mon. for ECN021 — Irradiance Channel 1

Serial number	10115135020000293		
Sensitivity	130.390 mV/(kW/m²)	Temperature coefficient	0.04 %/°C

16 flash — Irradiance Channel 1

Monitor cell temperature	25.18 °C	Fill factor	74.51 %
DUT temperature	24.70 °C	Cell efficiency	18.37 %
Compensated	25.00 °C	DUT efficiency	5.54 %
Gavg	1000.40 W/m²		
GstdDev	0.13 W/m²		
Compensated Irradiance	1000.00 W/m²		
Voc (linear regr.)	21.096 V		
Isc (linear regr.)	0.621 A		
Regression linear for	3.491 Ω		
Rsh (linear regr.)	1598.090 Ω		
Maximum power	9.756 W		
Voltage at Maximum	17.113 V		
Current at Maximum	0.570 A		

2023/07/17 1 / 1

Appendix B: Additional result plots

- B1: Effect of different blind types on the TCPR: simulated absolute values

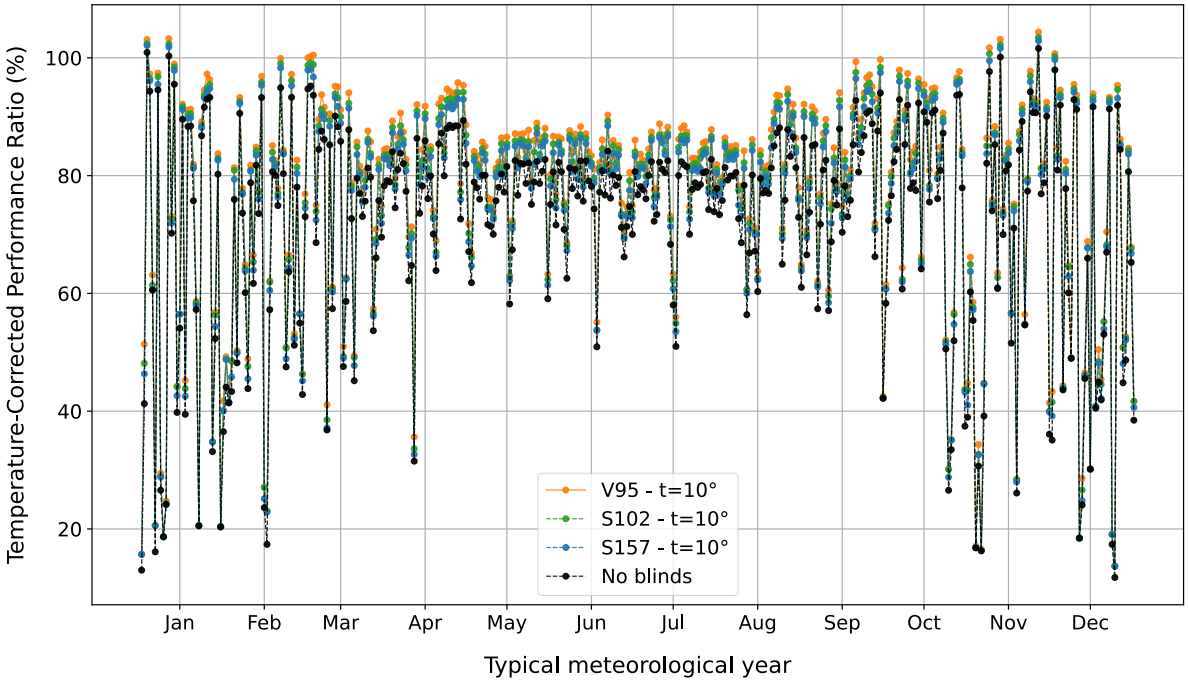

Figure 43: simulated daily TCPR of different blind types at a tilt angle of 10° on a TMY in Eindhoven.

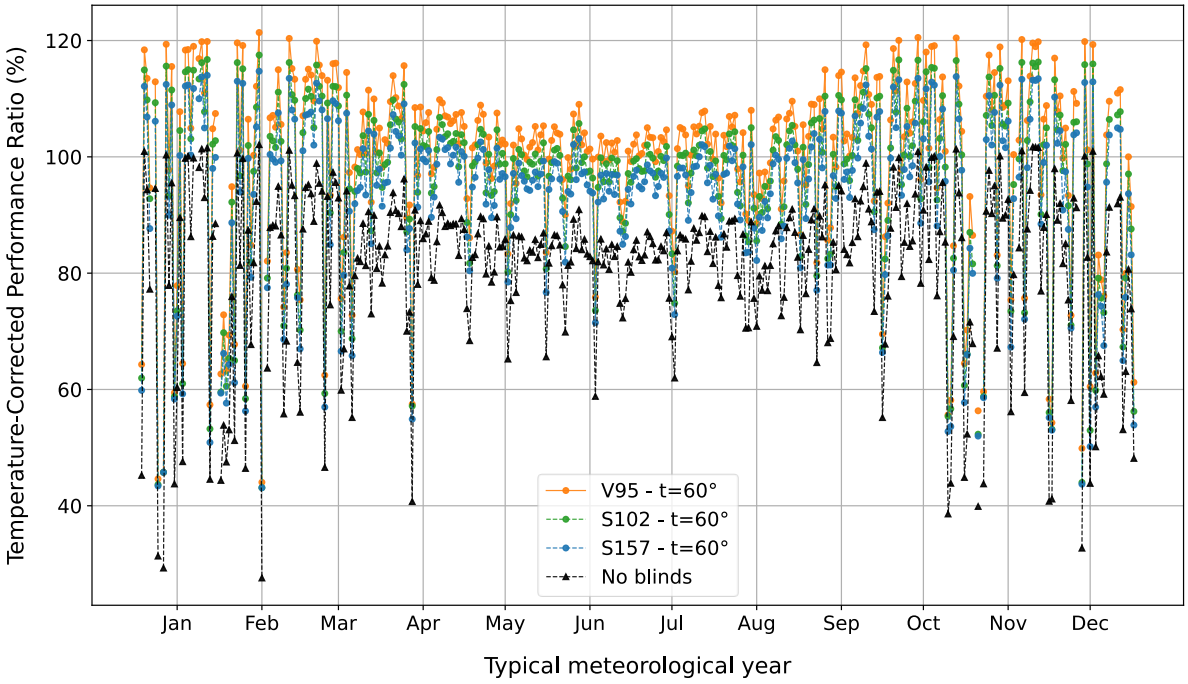

Figure 44: simulated daily TCPR of different blind types at a tilt angle of 60° on a TMY in Eindhoven.

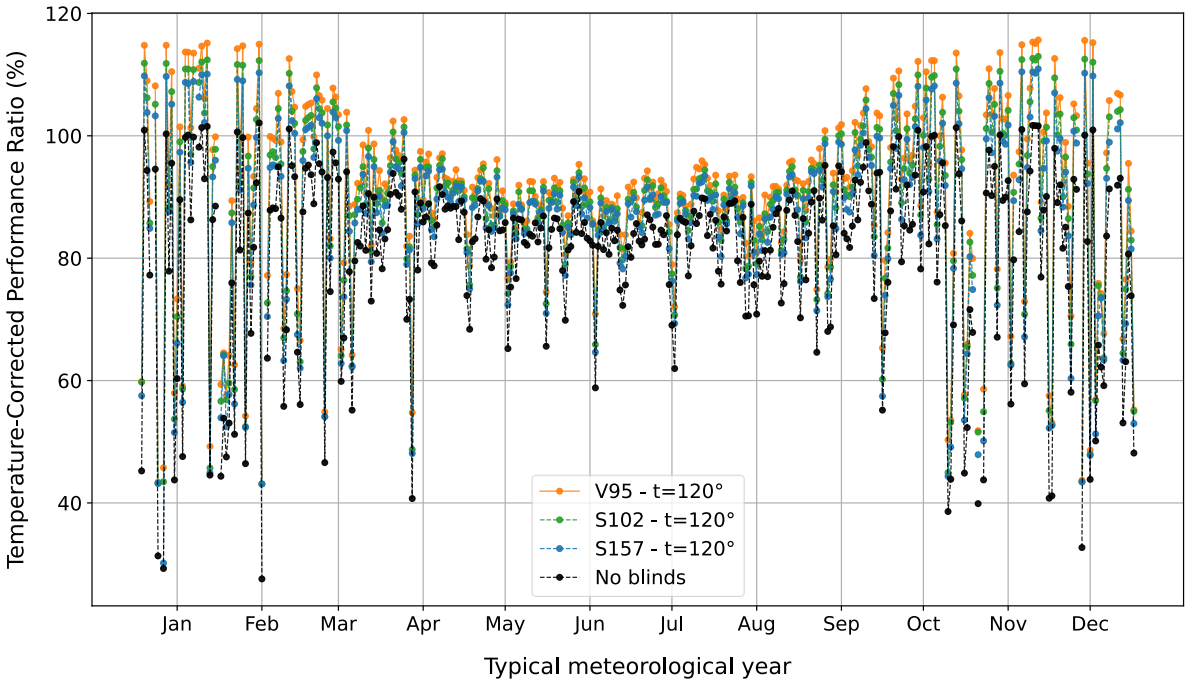

Figure 45: simulated daily TCPR of different blind types at a tilt angle of 120° on a TMY in Eindhoven.

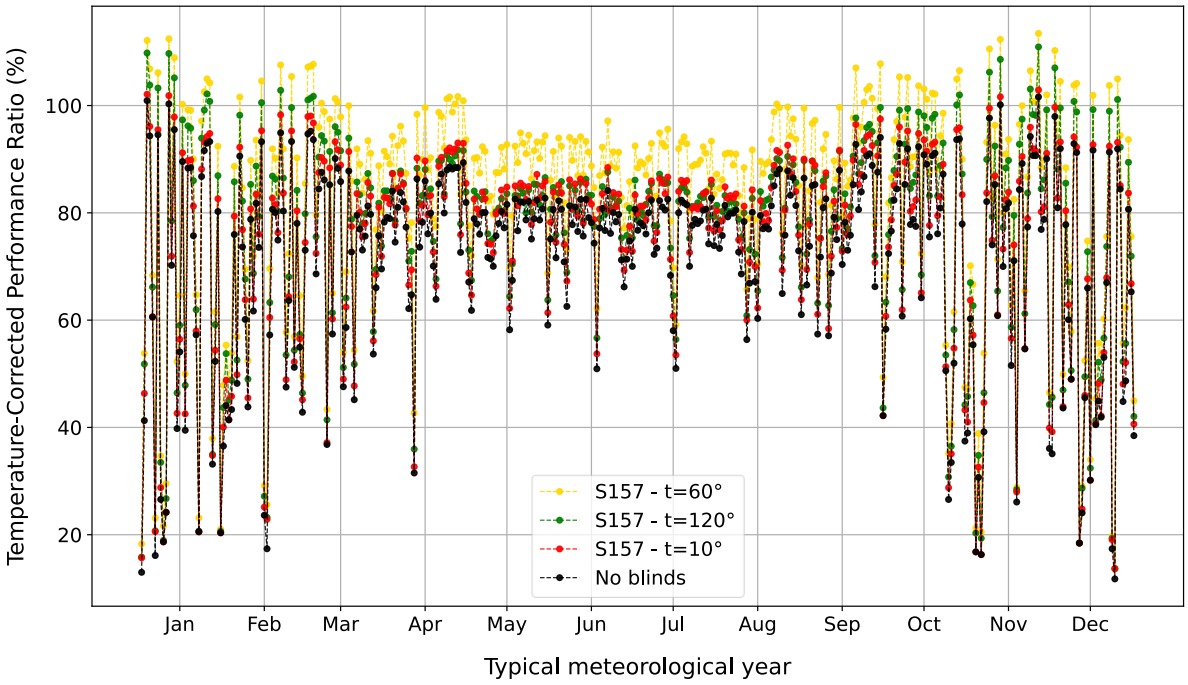

Figure 46: simulated daily TCPR of S157 blinds at different tilt angles on a TMY in Eindhoven.

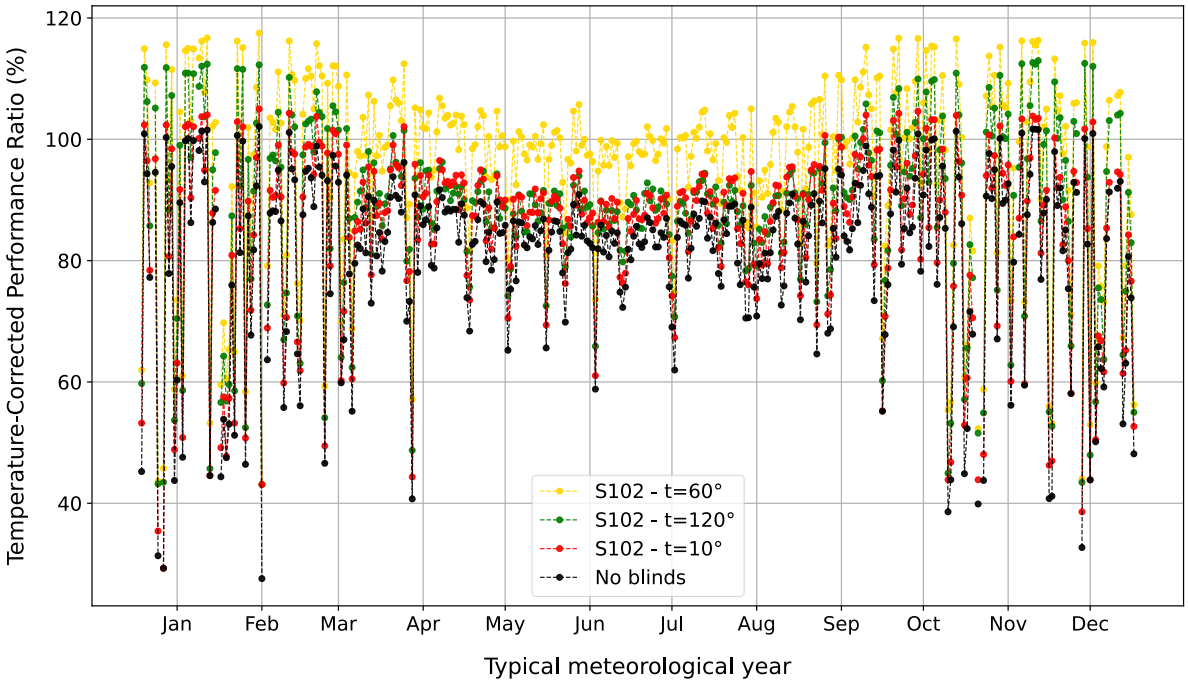

Figure 47: simulated daily TCPR of S102 blinds at different tilt angles on a TMY in Eindhoven.

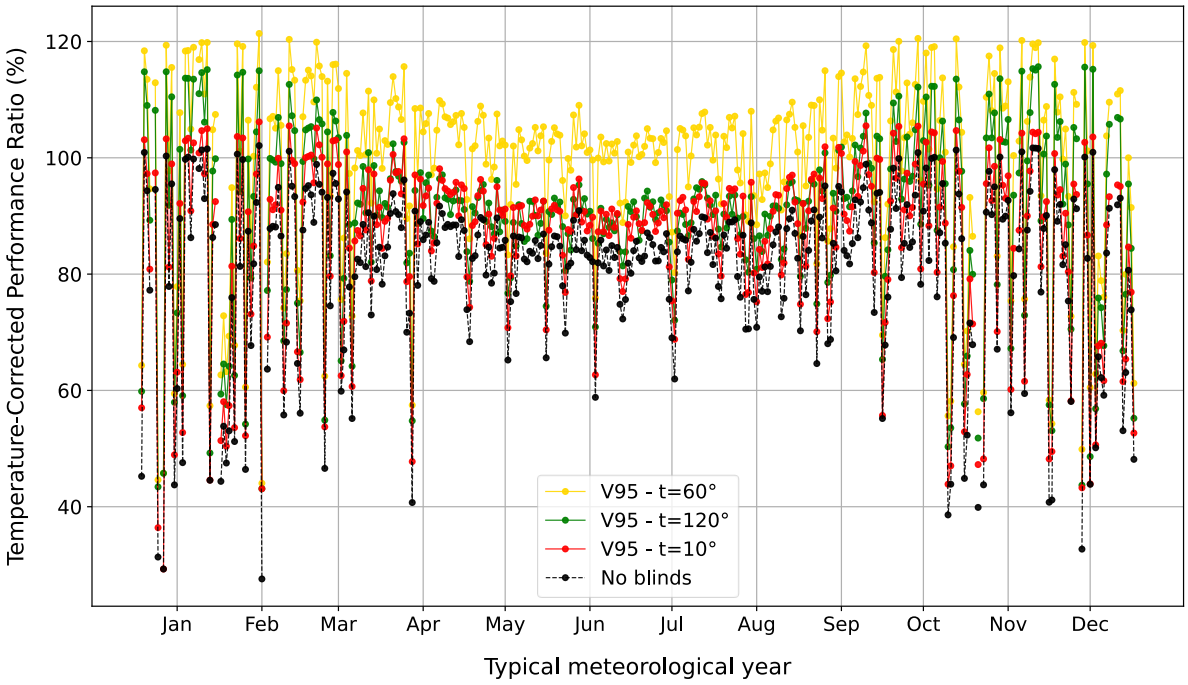

Figure 48: simulated daily TCPR of V95 blinds at different tilt angles on a TMY in Eindhoven.

- B1: TCPR as a function of blind's surface AOI correlated with other variables

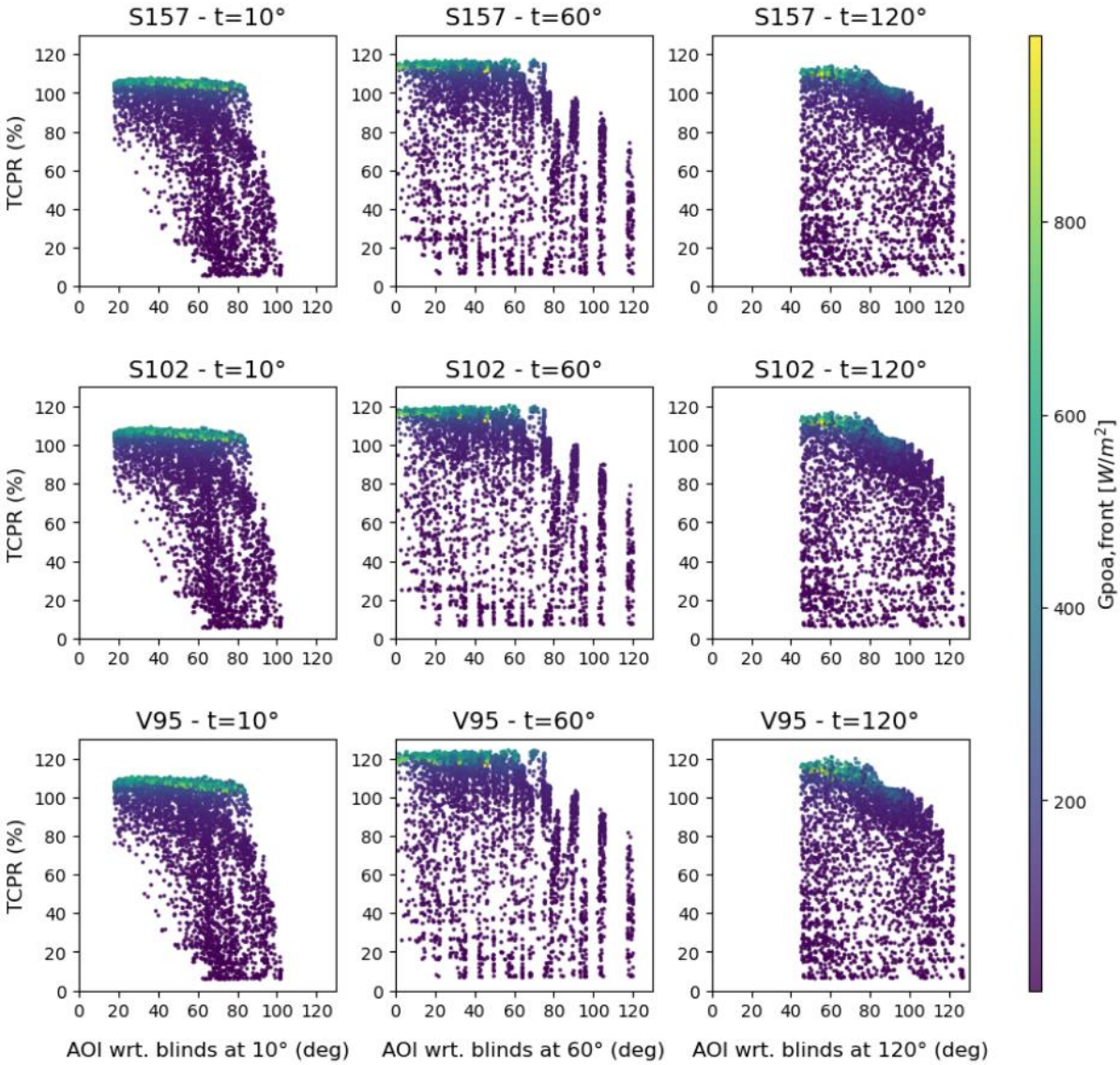

Figure 49: simulated hourly TCPR plotted as a function of the AOI formed between the sun and the blinds' surface normal on a TMY in Eindhoven for every blind configuration. Its correlation with the total irradiance incident on the front side of the window plane (G,poa,front [W/m^2]) has been included.

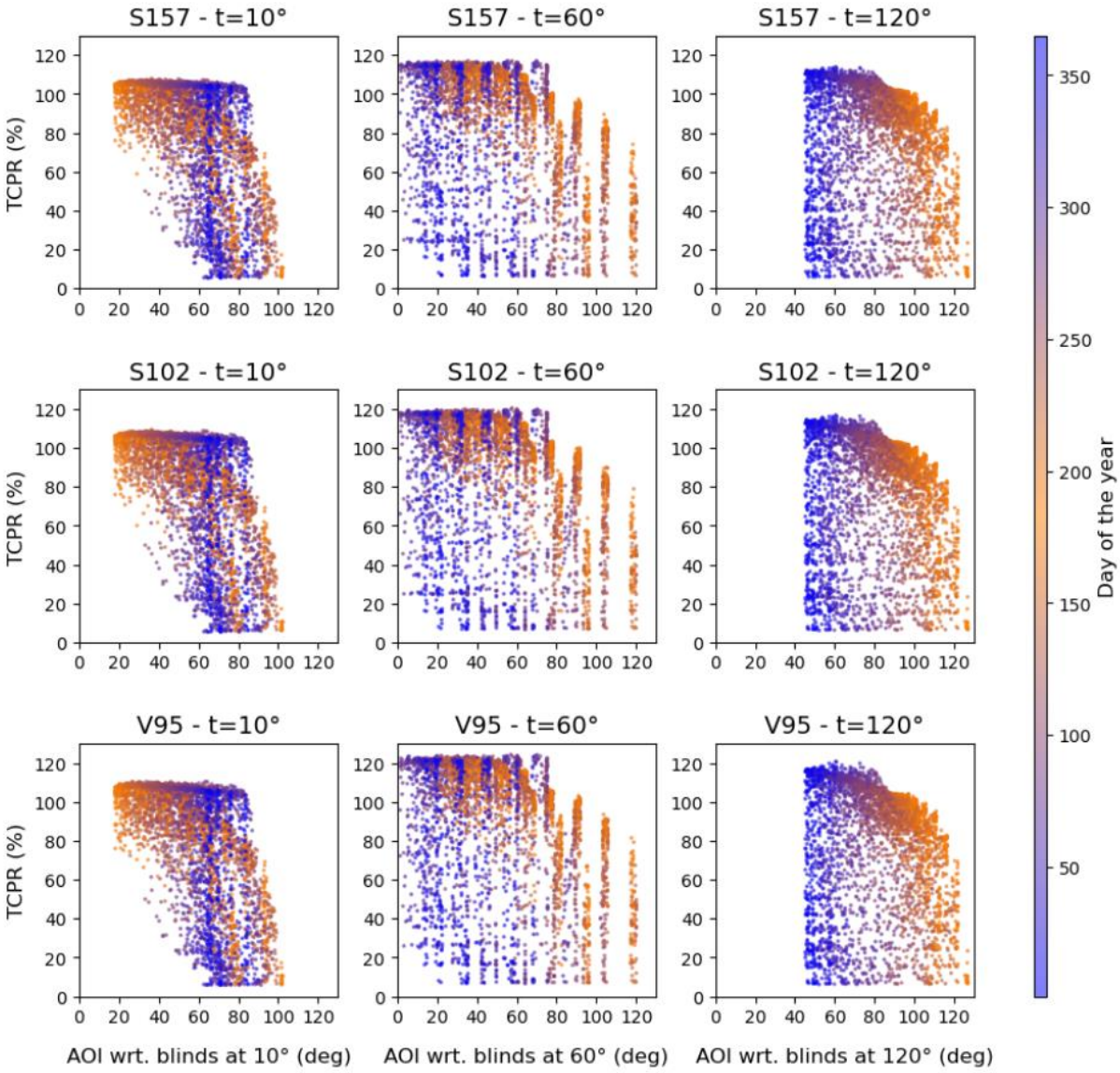

Figure 50: simulated hourly TCPR plotted as a function of the AOI formed between the sun and the blinds' surface normal on a TMY in Eindhoven for every blind configuration. Its correlation with the day of the year has been included to visualize seasonal behavior

TNO innovation for life

TU Delft

PVMD Delft University of Technology